Fall 12-2011

Physical and Electrical Properties of Trimetallic Nitride Template Endohedral Metallofullerenes and their Polymer Nanocomposites

Hanaa Mohammed Ahmed
University of Southern Mississippi

The University of Southern Mississippi

PHYSICAL AND ELECTRICAL PROPERTIES OF TRIMETALLIC NITRIDE TEMPLATE ENDOHEDRAL METALLOFULLERENES AND THEIR POLYMER NANOCOMPOSITES

by

Hanaa Mohammed Ahmed

Abstract of a Dissertation
Submitted to the Graduate School
of The University of Southern Mississippi
in Partial Fulfillment of the Requirements
for the Degree of Doctor of Philosophy

December 2011

ABSTRACT

PHYSICAL AND ELECTRICAL PROPERTIES OF TRIMETALLIC NITRIDE TEMPLATE ENDOHEDRAL METALLOFULLERENES AND THEIR POLYMER NANOCOMPOSITES

by Hanaa Mohammed Ahmed

December 2011

The main objective of this study was characterization of pure metallic nitride fullerene, MNF, and MNF containing polymers to evaluate these materials as suitable devices for tunable applications. Polymer-fullerene nanocomposites consisting of linear polyurethane (PU) segments crosslinked via polyhydroxylated fullerenes (C_{60} and $Sc_3N@C_{80}$, a metallic nitride fullerene) were prepared and characterized for their mechanical and dielectric properties using dynamic mechanical analysis (DMA) and broadband dielectric spectroscopic techniques. Polyhydroxylated fullerenes $C_{60}(OH)_{29}$ and $Sc_3N@C_{80}(OH)_{18}$ were synthesized in a high yield through a solid-state high sheer ball-milling procedure and were characterized using a verity of techniques, such as FT-IR, mass spectroscopy (MS) and thermal gravimetric analysis (TGA), to elucidate their structures. A difunctional isocyanate-terminated prepolymer was prepared from the reaction of poly(tetramethylene oxide) glycol (PTMO, ~2000 g/mol) and methylene bis(4-isocyanatobenzene) (MDI) followed by the addition of the crosslinking fullerene agent. Fullerene-polymer networks [C_{60}-PU and $Sc_3N@C_{80}$-PU] having high gel fractions and good mechanical properties and thermal stabilities were produced. Dynamic mechanical analyses of (C_{60} or $Sc_3N@C_{80}$)-PU networks indicated a glass

transition temperature, T_g, of -50 ^oC with a sub-T_g relaxation due to local chain motions. Broadband dielectric spectroscopic analyses of the nanoparticles prior to incorporation into the networks revealed one relaxation and large ε′ values in hydroxylated C_{60} relative to unfunctionalized C_{60}. The analogous hydroxylated Sc3N@C80 exhibited two relaxations, and the extra relaxation may be due to reorientations of cage-encapsulated Sc_3N clusters. Permittivity values (ε′) for $Sc_3N@C_{80}$-PU were found to be higher than the corresponding values for C_{60}-PU, likely because of the rotationally mobile dipoles. For temperature < 0 ºC there was a dielectric loss peak due to the glass transition of the PU matrix and another at a lower temperature due to short range chain motions. The loss-frequency spectra of all prepared samples were analyzed sing the Kramers-Krönig transformation and Havriliak-Negami (HN) equation to extract information about relaxation processes taken place in these samples. Capacitance-voltage characteristics of the fullerene-PUs did not show any significant change with the applied dc bias voltage in the range of our instrument window (-30 to +30 volt). A general conclusion is that this class of materials can be rendered quite polarizable.

The University of Southern Mississippi

PHYSICAL AND ELECTRICAL PROPERTIES OF TRIMETALLIC NITRIDE TEMPELATE ENDOHEDRAL METALLOFULLERENS AND THEIR POLYMER NANOCOMPOSITE

by

Hanaa Mohammed Ahmed

A Dissertation
Submitted to the Graduate School
of The University of Southern Mississippi
in Partial Fulfillment of the Requirements
for the Degree of Doctor of Philosophy

Approved:

_Janice P. Buchanan_____
Director

_Douglas Masterson_____

_Wujian Miao_____

_Jeffery Wiggins_____

_Kenneth Mauritz_____

_Susan A. Siltanen_____
Dean of the Graduate School

December 2011

DEDICATION

This dissertation is dedicated to my mother, Soad Aly, my husband, Ashraf Aly, and my kids: Mahmoud, Mena, and Maiar.

ACKNOWLEDGMENTS

My most sincere thanks go to my advisor and mentor, Dr. Paige Janice Buchanan for her support, direction and encouragement during the development of this work. I started this project with zero knowledge about fullerenes and their properties, and during my research I have learned a lot from Dr. Buchanan. I would like to acknowledge the past and present Buchanan research group members who have given me guidance, assistance and suggestions.

I am indebted to my committee members, Dr. Kenneth Mauritz, Dr. Jeffery Wiggins, Dr. Doug Masterson and Dr. Wujian Miao. They have provided, with kindness, their insight and suggestions, which are precious to me.

Special thanks are extended to Dr. Kenneth Mauritz for numerous helpful advice and inspiring discussions since my first meeting with him. Also I would like to thank Dr. Mohammad Hassan in Dr. Mauritz's research group who helped me collect and analyze the dielectric data. Dr. Mauritz and Dr. Hassan have been directly involved with many aspects of Chapter III and Chapter IV.

I would like to express my deepest gratitude to all professors and faculty members who taught and helped me during my study in the department of Chemistry and Biochemistry at the University of Southern Mississippi. Respectful thanks go to Dr. Bateman, Dr. Heinhorst, and Ms. Sharon King for all their help. Many thanks go to Dr. Stevenson for providing me with the metallic nitride fullerenes during my study.

Great thanks to my country, Egypt, for funding and giving me this great chance to study abroad. I also thank NSF CAREER Award #CHE-0847481 for financial support.

Finally and most importantly, I would like to thank my mother, my brothers and my sisters for the continuing love, support and praying. Loving thanks go to my husband, Ashraf, for his love and understanding during the most difficult times of graduate life. Special thanks to my children, Mahmoud, Mena and Maiar, for their love.

TABLE OF CONTENTS

LIST OF ILLUSTIRATIONS

Figure

Scheme

LIST OF TABLES

Table

CHAPTER I

INTRODUCTION

Fullerenes Families

Fullerenes, discovered in 1985,[1] are a family of carbon allotropes composed entirely of carbon in the form of a hollow sphere. They are typically produced by an arc discharge method using a carbon rod as one or both of the electrodes in a Kratschmer-Huffman generator,[2] see Figure 1. The reaction chamber is evacuated and an inert gas is introduced at a controlled pressure. A potential is applied between the electrodes to produce an arc discharge which forms carbon plasma, and fullerenes of various sizes are produced.

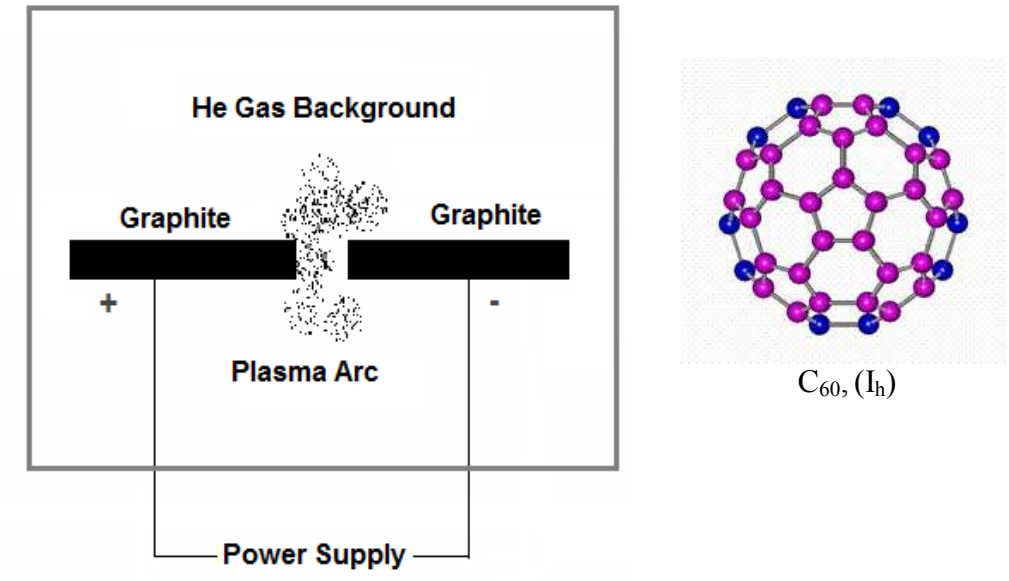

Figure 1. Schematic draw of Kratschmer-Huffman generator (left) and C_{60} (right)

There are two different families or general classes of fullerenes: classical fullerenes and endohedral fullerenes.

Classical Fullerenes

The smallest, most stable and also the most abundant fullerene is C_{60} followed by C_{70} and then higher fullerenes C_{74}, C_{76}, C_{78}, C_{80}, etc. Many studies show that C_{60} is composed of carbon atoms with predominantly sp^2-hybridization, and the arrangement of these atoms indicates an outline of 20 hexagons and 12 pentagons (which provide the curvature). The pentagonal rings sit at the vertices of an icosahedron such that no pair of adjacent pentagons exists (isolated-pentagon rule).[3,4] Furthermore, C_{60} was discovered to possess two types of double bonds: the double bonds at the [6,6] ring junctures of the cage, which are more reactive, and the double bonds at the [5,6] ring junctures.[5-7] The poor delocalization of electrons as well as the strain introduced by the curvature of the surface enhanced the reactivity of C_{60}.

The hollow space internal to the fullerenes structure varies with the size of fullerene (0.4 - 1.0 nm in diameter from C_{60} to C_{240}); [8] and in fullerenes where the void space is sufficiently large, researchers have demonstrated that it is possible to trap metal atoms, ions, or small molecules within this space producing another family of species called endohedral fullerenes. The inclusion of atoms inside the fullerene cage is difficult to accomplish once the cage has already formed, so these endohedral fullerenes must be formed as the cages are made (i.e., the cage must "wrap around" the atom as it comes together).

Endohedral Metallofullerenes

Endohedral metallofullerene is a molecule composed of one or more metal atoms trapped inside a fullerene cage. Three classes of endohedral metallofullerenes, compared

in Figure 2, are discussed here: classical endohedral metallofullerenes, metallic nitride fullerenes, and metallic nitride aza fullerenes.

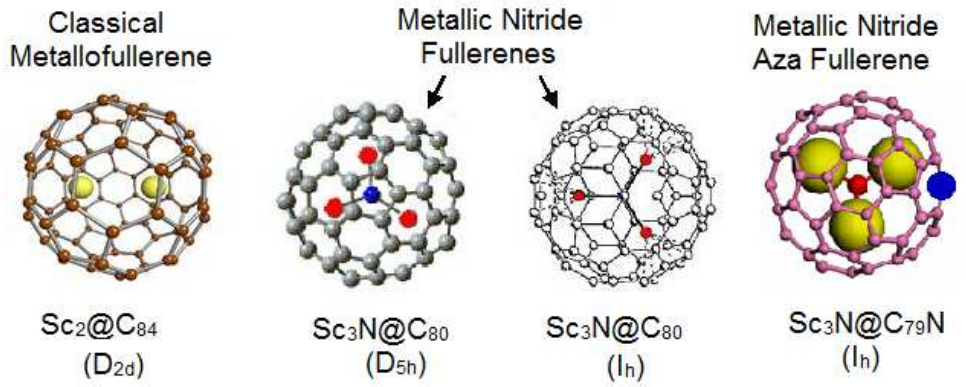

Figure 2. Comparison of endohedral metallofullerenes.

Classical endohedral metallofullerenes. This sub-family has the general formula $M@C_n$ (M is a metal and n = 60, 70, 80, 82), since the @ symbol is used for naming purposes to indicate atoms to the left are encapsulated into the carbon cage on the right.[9]

After the discovery of C_{60},[1] evidence for an encapsulation of La inside the fullerene cage was reported.[10] Laser vaporization of a $LaCl_3$-impregnated graphite rod produced an additional peak in the mass spectrum due to LaC_{60}. Evidence that endohedral complexes are so-formed came from shrink-wrap experiments showing that these complexes can lose a C_2 fragment without bursting the cluster or losing the incorporated metal.[11] For example, it was difficult to fragment past LaC_{44}^+ and impossible to go past LaC_{36}^+ without losing the trapped metal.

Macroscopic quantities of endohedral metallofullerenes were first produced using high-temperature laser vaporization of La_2O_3/graphite composite rods and the corresponding contact arc technique to produce various sizes of lanthanofullerenes.[9] Products of this technique, $La@C_{60}$, $La@C_{70}$, and $La@C_{82}$, were seen in the mass spectra

of the sublimed film from soot. Among these, the $La@C_{82}$ exhibits an enhanced stability, while the smaller lanthanum fullerenes are less stable in air and solvents.

More developments in the generation and characterization of endohedral metallofullerenes have been extensively reviewed.[8,12,13] In general, $M_n@C_{82}$ (n=1-3) are the most abundant, although empty C_{82} is not a dominant species formed under normal conditions. The fact that the unstable C_{82} efficiently encapsulates rare earth metals to form stable endohedral $M_n@C_{82}$ suggests that the electronic structure of the fullerene shell is dramatically influenced by the central metals.[8]

Most of the lanthanide metals and Group I-III metals (Li, Na, K, Cs, Ca, Sr, Ba, Sc, Y, La) have been successfully incorporated into fullerene cages to produce mono-, di-, tri-, or tetra-metallofullerenes.[14] The discovery of these materials has attracted great interest not only in physics, as a nanostructural material for electronic devices,[15] but also in biological and material science. For example, they could be applied in biomedicine as bioradical scavengers,[16] radiotracers,[17] and magnetic resonance imaging (MRI) contrast agents.[16, 18-20]

Encapsulation of metal atoms inside fullerene cages was found to significantly modify the fullerene electronic structure and produce novel materials, which hold promise in applications of charge separation, transport, and storage.[21-24] However, progress in exploring chemical and physical properties of these endohedral metallofullerenes has been hampered by their sensitivity towards molecular oxygen as well as the difficulty to scale up production to quantities greater than a few milligrams.

Metallic nitride fullerenes (MNF). Metallic nitride fullerenes (MNF), with a metal-nitride cluster (M_3N) encapsulated within the fullerene cage,[25-27] have the general

formula $A_xB_{3-x}@C_{2n}$ (x =0-3, A, B = group IIIB or rare-earth metals) with a large variety of cage sizes (C_{68}-C_{88}). Stevenson and co-workers succeeded in producing $Sc_3N@C_{80}$, the first and the most abundant member of this novel family, in a remarkably high yield and purity using the trimetallic nitride template (TNT) method.[25] In this method, a dynamic atmosphere containing nitrogen gas (in addition to the usual helium) was introduced into the Krätschmer-Huffman generator during arc vaporization of composite (metal oxide/graphite) rods producing $Sc_3N@C_{80}$ with a mass-to-charge ratio (m/z) of 1109.This preparative method opened a new field of synthetic inorganic chemistry, and this type of endohedral metallofullerene is the first containing relatively large molecules inside the carbon cage, such as $A_xSc_{3-x}N@C_{80}$, (x=0-3; A=Tm, Er, Gd, Ho, La).[25-31]

The structure of the nitride cluster is of high importance for the overall structure of the MNF. ^{13}C NMR spectrum of $Sc_3N@C_{80}$ exhibits two resolved lines with chemical shifts of 146.7 ppm and 133.2 ppm with an intensity ratio of 3:1, respectively. From these data, alongside the X-ray crystallographic studies Sc_3N unit was found to be planar inside an icosahedral (I_h symmetry) C_{80} cage.[25] In several other Sc-based MNFs, such as $Sc_3N@C_{78}$[32], the Sc_3N unit was revealed to remain planar although the cage sizes and geometries vary significantly. In contrast, the Gd_3N cluster which considered the largest cluster encaged in the fullerenes to date, was found to be pyramidal, with the nitrogen atom displaced about 0.5 Å out of the plane containing the three gadolinium ions Gd_3.[33] The differences in pyramidalization of the nitride cluster in $Gd_3N@C_{80}$, or Gd_2ScN in $Gd_2ScN@C_{80}$, were explained by the discrepancy in the ionic radius of the metals encaged.[33-35]

The ^{45}Sc NMR study indicates that, at room temperature, the Sc_3N cluster rotates freely inside the C_{80} cage to preserve the overall I_h symmetry of the cage on the NMR time scale. Furthermore, due to the small rotational barrier of the Sc_3N cluster inside the cage (~1.7 kcal/mol), it is plausible to assume that the motion of Sc_3N can be stopped at the most stable positions upon a decrease in temperature.[28]

Previous studies focused on the thermal stability of the MNFs using vibrational IR and Raman spectroscopy. The thermally stability of $Sc_3N@C_{80}$ (up to 650 K in nitrogen) reveals the strong coupling of the Sc atoms to the central N atom in addition to the Sc-cage bonds.[36] In this way, the remarkable stability of the Sc_3N cluster is amplified by encapsulation due to the charge transfer from the cluster to the cage, resulting in a significantly higher total bond energy in $Sc_3N@C_{80}$ compared to the classical metallofullerenes $La@C_{82}$ and $La_2@C_{80}$. This charge transfer has been demonstrated to alter the electronic and magnetic properties of MNF fullerenes by producing a non-disassociating salt that consists of metal cation(s) encapsulated in a fulleride anion and thus results in the mutual stabilization of the trimetallic nitride cluster structure and the icosahedral carbon cage. [37-41] Moreover, the charge transfer from the encapsulated clusters to the carbon cage helps stabilize other cages that are not available in their empty form.[31,42,43]

Metallic Nitride aza Fullerenes (MNAF). Metallic nitride aza fullerene (MNAF) is a new class of endohedral metallofullerenes in which one nitrogen atom replaces one carbon atom in the fullerene cage, so the molecular formula of this new class of material is generally written as $A_xB_{3x}@C_{2n-1}N$. The possibility to tune chemical and physical properties of fullerenes by including heteroatoms in the carbon cage has opened up a new

and very interesting research field.[44] The change in properties of fullerenes is related to the redistribution of electronic charge in the fullerene cage caused by the heteroatoms.

Efforts to synthesize larger metal atom trimetallic nitride clusters, e.g., La_3N in C_{80} cages have been unsuccessful. The difficulty in entrapping these bulky clusters in C_{80} cages has been attributed to larger ionic radii. For La_3N clusters, the preferred cage size shifts beyond C_{88}, and $La_3N@C_{96}$ becomes the dominant MNF.[45] However, La_3N clusters were successfully encapsulated inside the $C_{79}N$ cage, and the electronic stabilization of $La_3N@C_{79}N$, a molecule which represents a new class of metallic nitride azafullerenes (MNAFs), was reported [46]

In the *Ih*-C_{80}, there are two types of carbon atoms: 60 of them locate at junctions of two hexagons and one pentagon, or [665] junction, while the remaining 20 atoms are located at junctions of three hexagons, or [666] junction. Previous computational studies indicate [665] junctions for metallic nitride aza fullerenes, such as $Sc_3N@C_{79}N$, are the preferred sites for N-substitutions.[46-49] The investigation of the $C_{79}N$ cage alone by Stevenson et al. to determine which site is preferred for N-substitution, and their calculations, showed that the [665] substitution isomer of $C_{79}N$ is more stable by 13.19 kcal/mol than the [666] substitution isomer. This value is close to the 13.3 kcal/mol energy difference reported previously for the two corresponding isomers of $Y_2@C_{79}N$[49] indicating that such a preference observed in the metallofullerenes is essentially originated from the different stabilities of the two cage isomers alone.

Metallic nitride aza fullerenes are generally prepared by conducting the Krätschmer-Huffman electric-arc process under certain pressure of N_2 and He with metal oxide-doped graphite rods.[46,47] The heterofullerenes were separated from the resulting

mixture of empty cage fullerenes and endohedral fullerenes by a chemical separation and chromatographic technique.

Functionalization of Fullerenes

Endohedral metallofullerenes have attracted much attention because of their unique structures and novel properties.[8] Allowing for the incorporation of metals that possess magnetic, electro-active, and radioactive properties, MNFs are expected to show promising performance as substituent materials in diverse electronic,[50] optical[51] and biological applications.[52,53] An obvious obstacle was the complete lack of solubility of these materials in water and in common organic solvents, monomers, and polymers. One successful attempt to increase the water-solubility of fullerenes is by functionalization of their cage with carefully selected hydrophilic groups.

Chemistry of Fullerenes

Since the preparation of fullerenes in multigram amounts in 1990,[2] a wide variety of chemically modified fullerenes have been synthesized. A large number of experimental studies have been performed on the chemical derivatization of empty fullerene such as C_{60} and C_{70} to understand the basic chemical properties and obtain new derivatives with interesting electronic, catalytic, or biological properties. Moreover, it is an interesting challenge to disclose how the reactivities of empty fullerenes are modified upon endohedral metal-doping.[38] The high electron affinity of C_{60} fullerenes, investigated by cyclic voltammetry,[54] showed that C_{60} is more susceptible to nucleophilic additions[55] than electrophilic additions, and these additions produce fullerene derivatives which have attracted a great deal of interest due to their outstanding physical and chemical properties. Conversely, endohedral metallofullerenes are less reactive in nucleophilic reactions than

their classical empty-cage fullerene counterparts due to the charge transfer from the cluster to the carbon cage. In other words, characteristic redox properties of MNFs are significantly different from those of the empty-cage fullerenes. Echegoyen group[56] addressed the electrochemical redox potentials (V versus Fc/Fc^{+}) for I_h $Sc_3N@C_{80}$ relative to C_{60}; the first oxidation potential of $Sc_3N@C_{80}$ (0.59 V) was less positive than C_{60} (1.33 V), and the first reduction potential of $Sc_3N@C_{80}$ (-1.26 V) was more negative than C_{60} (-1.15 V). In other words, $Sc_3N@C_{80}$ is more easily oxidized than C_{60} fullerene and more difficult to reduce than C_{60} fullerene.

In addition to the reduced reactivity of the MNFs, the reaction sites on their carbon cage might also be different from that of the empty-cage fullerenes. Although both C_{60} and the C_{80} cage in $Sc_3N@C_{80}$ exhibit icosahedral symmetry (I_h), C_{60} possess reactive double bonds at its [6,6] junctures; however the [6,6] junctures of large empty cages are not necessarily as reactive as C_{60} due to cage shape and strain.[55,57]

Only a few reactions capable of producing functionalized MNF C_{80} adducts have been identified, and briefly these consist of hydroxylation,[58] 1,3-dipolar addition,[59-62] Diels-Alder,[63-65] and Bingel-Hirsch adducts.[59] To a large extent, chemical reactivity of metallic nitride fullerenes is believed to be controlled by the identity of the metal encapsulated, as demonstrated in a recent report by Echegoyen et al.,[59] where the $Y_3N@C_{80}$-diethyl malonate monoadduct was successfully prepared under conditions which would not produce the comparable $Sc_3N@C_{80}$ adduct. This difference in chemical reactivity was attributed to the encapsulated cluster, which affected the reactivity and the regiochemistry of the addition. Cycloadditions, such as the 1,3-dipolar addition and Diels-Alder reactions, typically yield adduct formation at a corannulene-type site, which

is a double bond located at a [5,6] ring juncture with abutting hexagons. Recently, a [6,6] monoadduct of N-ethyl pyrrolidino-$Y_3N@C_{80}$ was reported by Echegoyen, along with its isomerization to the thermodynamically favored [5,6] adduct upon heating.[66]

Hydroxylation of Fullerenes

The non-functionalized fullerene cages (empty or endohedral) are soluble only in non-polar organic solvents, making them incompatible with monomers, polymers and biological systems. Fortunately, the exterior of the fullerene carbon cage has a rich synthetic organic chemistry, which allows a wide variety of water-soluble derivatives to be prepared. One approach to increase their water solubility is to covalently modify their surface, for example by attaching hydrophilic groups as is achieved in the hydroxylation of the fullerene cage exterior. Such hydroxylation is of great importance because it is crucial in the development of new materials with potential applications in material and medical science, and in the investigation of the role that any modification of the cage plays in tuning their properties. Thus, several studies have focused on the hydroxylation of the metallofullerenes not only because of the simplicity of the synthesis, but also because of the possibility of further molecular modifications such as conjugation of the bio-reactive ligands.[16, 35]

In 1997, Zhang and co-workers[67] reported the first synthesis of the water-soluble metallofullerene derivatives, gadolinium fullerenols, by a method similar to the prior report on the preparation of poly-hydroxyl C_{60} fullerenols.[68] In this method, a toluene solution containing gadolinium fullerenes was refluxed under N_2 atmosphere with potassium. After that, the precipitates of the potassium with the fullerenes were hydrolyzed by water to give a dark brown solution of gadolinium fullerenols. The novel

synthesized gadolinium fullerenols were evaluated as a potential contrast agent for magnetic resonance imaging because they showed excellent efficiency in enhancing water proton relaxation with a relaxivity of 47.0±1.0 $mM^{-1}\cdot s^{-1}$. One year later, $Ho@C_{82}(OH)_x$, with x = 24-26, was synthesized using KOH and tetrabutylammonium hydroxide as a phase transfer catalyst following the same route for the hydroxylation of C_{60}[69], Scheme 1.[70] Then, these Ho-containing fullerenols were neutron activated and studied for use as potential radioactive tracers.[70-72]

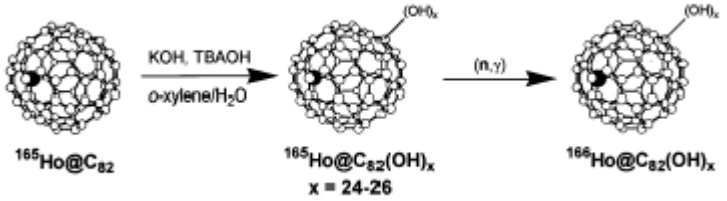

Scheme 1. Hydroxylation of $^{165}HO@C_{82}$

In 1999, Sun and coworkers[16] hydroxylated the endohedral metallofullerene by reacting the $Pr@C_{82}$ with nitric acid solution under an oxygen atmosphere similar to the previous work on hydroxylated C_{60}.[73] This exohedral hydroxylation involves the formation of NO_2 radical, that formed from the reaction of the pure endohedral metallofullerene, $Pr@C_{82}$, with a concentrated nitric acid, followed by subsequent hydrolysis process giving $Pr@C_{82}O_m(OH)_n$ (m~10, n~10). In 2000, and similar to previous methods, Kato et al.[74] reacted the $Gd@C_{82}$ with 50% aqueous NaOH containing tetrabutylammonium hydroxide as a phase transfer agent and produced $Gd@C_{82}(OH)_n$, (n= 30-40). This highly water-soluble Gd-fullerenol was suggested as a powerful contrast agent for magnetic resonance imaging, since its water proton relaxivity is 20 times higher than that of the commercial Gd-based contrast agents, currently used in clinics.[75-78]

Few articles were published about the hydroxylation of the trimetallic nitride fullerenes, MNFs. The first hydroxylated MNF, reported by Phillips and co-workers, was prepared by refluxing a toluene solution of $Sc_3N@C_{80}$ with sodium metal and then exposing solution to water and air, followed by chromatographic purification, Scheme 2.[58]

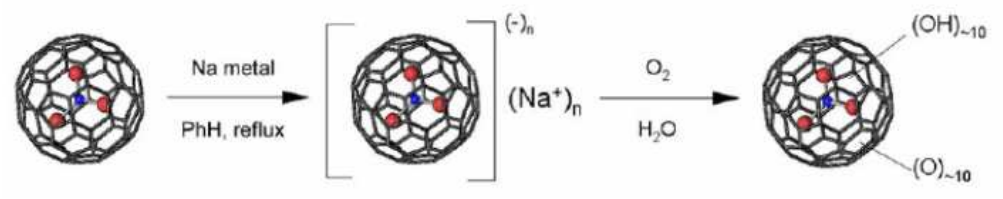

Scheme 2. Hydroxylation of $Sc_3N@C_{80}$ with sodium metal.

The XPS spectrum of the obtained hydroxylated Sc-containing MNF illustrates the different types of functionalized carbon atoms on the water-soluble cage, which suggests a metallofullerenol with the formula of $Sc_3N@C_{80}(O)_{\sim 10}(OH)_{\sim 10}$.

Since the addition of oxygen has been found to be critical to the formation of fullerenols or metallofullerenols using free radical based process, a new and green approach for the hydroxylation of C_{60}[79] and $Gd_3N@C_{80}$[80] was recently reported. In this approach, the hydroxylation was performed without solvent and under the so-called High-Speed Vibration Mill, HSVM. In this technique, for hydroxylation of C_{60}, a mixture of C_{60} and KOH was vigorously shaken under HSVM and at room temperature, and the resulting reaction mixture was readily dissolved in water, Scheme 3.[79]

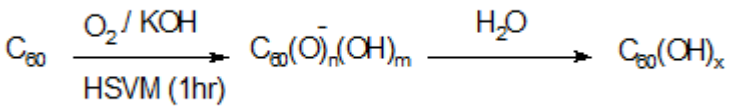

Scheme 3. Hydroxylation of C_{60} using HSVM technique

However, for the hydroxylation of $Gd_3N@C_{80}$, by this technique, a mixture of $Gd_3N@C_{80}$ and Na_2CO_3 was shaken for 14 hours, due to the low reactivity of the metallofullerene, to produce the water soluble $Gd_3N@C_{80}(OH)_m(O)_n$, Scheme 4.[80]

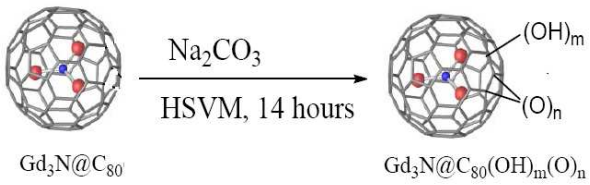

Scheme 4. Hydroxylation of $Gd_3N@C_{80}$ using HSVM technique

There are many advantages of functionalization reactions of fullerenes by using the HSVM technique over the solution reactions: overcome the low solubility problem of fullerenes, reduced pollution, low costs and simplicity in process and handling via reducing the reaction steps. Furthermore, solid-state reaction occurs more efficiently and more selectively than does the solution reaction because molecules in a crystal are arranged tightly and regularly.[81]

The ability to control functionalization of the fullerene cage surface is paramount to realize the potential of these materials in future commercial applications. Many physical and chemical properties of MNFs remain unexplored, and this project effort represents the systematic approach to synthesize MNF derivatives with enhanced solubility in common solvents, monomers, and polymers, which are suitable for direct incorporation into polymer networks using standard methods.

Fullerene-Containing Polymer Nanocomposites

Because of their original structure, three-dimensional fullerenes as well as polymers are intrinsically useful scaffolds for the construction of high molecular weight structures. The combination of both systems has led to a wide variety of new materials showing appealing features arising from the tuning of bulk properties through judicious

choice of the molecular constituents and the chemical linkage between them. Therefore, an actively developing direction of fullerene science involves the study of the synthetic procedures, properties, and application areas of fullerene-containing polymers.

Several reviews have been reported about fullerene-containing polymers,[82-87] and these have shown that this kind of composite material preserves many unusual properties of fullerenes as and may improve the properties of the original polymers. This improvement was explained by the effect of fullerene as a nanoparticle on the structure and behavior of polymers and related materials.[84-87]

Generally, fullerene-containing polymers may be divided into two major types: polymers in which the fullerene is chemically bonded to a polymer matrix and polymers modified with fullerene additives.[85,86] Furthermore, the chemically bonded fullerene-polymers may be subdivided according to the type of fullerene arrangement: in the main chain, at chain ends, and in side chains, as star-shaped where fullerene serves as a core, and as three-dimensional polymers with fullerene crosslink junctions, Scheme 5.[86]

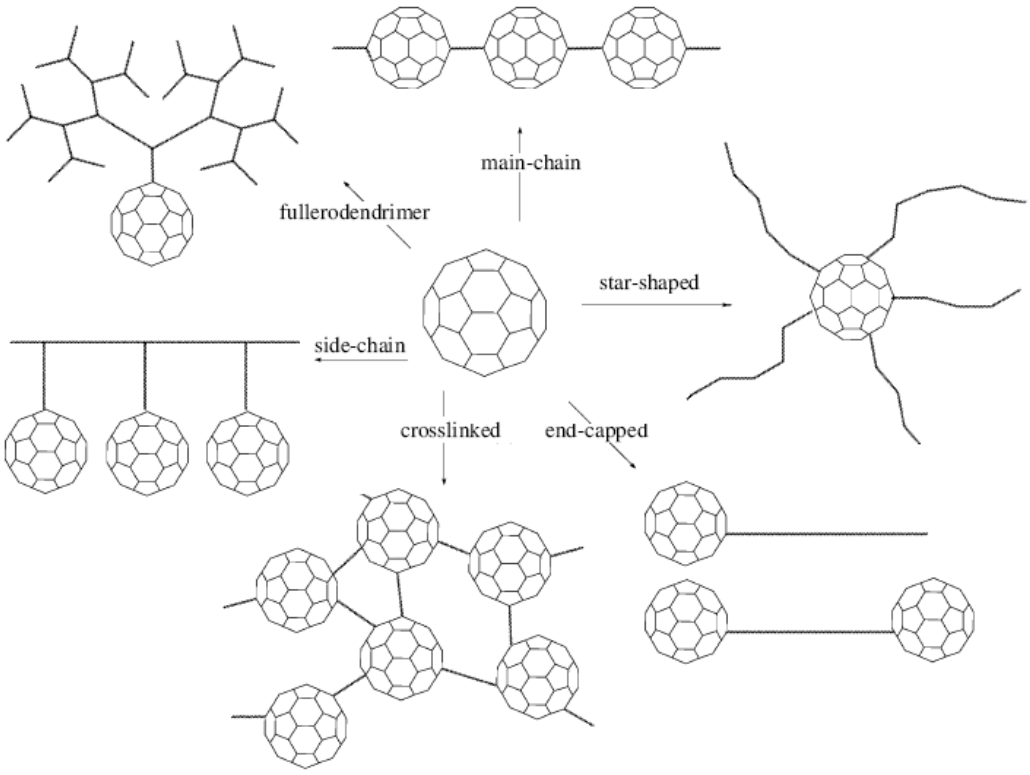

Scheme 5. Different types of fullerene-containing polymers

Fullerene-containing polymeric nanocomposites have received much attention in recent years due to their unusual properties and applications,[84-90] and a convenient and simple way to prepare this type of composite is via dispersion of fullerenes into polymeric matrices (blending). However, the poor adhesion between fullerene and polymer prevents the optimal dispersion of fullerene in the matrix.[91, 92] To enhance the compatibility and the dispersion, the fullerene is functionalized with complementary functional groups of a polymer. The specific interaction between fullerene and polymers plays an important role in the resulting mechanical performance and other properties.[89,93] Therefore, chemical modification of fullerenes with polar functionality, such as hydroxyl and amino groups, are versatile intermediates for the synthesis of esters, amides, urethane, ureas and other corresponding polymers. This chemical modification significantly broadens the scope of the science and technology of fullerenes.[83]

Highly polar polyhydroxylated fullerenes, (mainly C_{60}), resemble star-branched precursors used in fabrication of polymer networks and composites; hence, structurally, fullerenols have significant advantages over conventional hydroxylated cross-linkers due to their multiple hydroxyl functional groups. In addition, the overall ball shape of fullerenols should facilitate the synthesis of truly three-dimensionally cross-linked polymer materials with much enhanced mechanical properties.[83, 94] The chemical reactivity of tertiary fullerenolic hydroxyl functions in fullerenols is rather limited toward the nucleophilic substitution of many electron withdrawing leaving groups under basic conditions. In one exception, they are moderately reactive with isocyanate functions, forming the corresponding urethane moieties.[94-96]

Fullerene-Containing Polyurethane

The history of the polyurethanes industry started in the late 1930s with the discovery of the chemistry of the polyaddition reaction between diisocyanate and diols to form polyurethane.[97] Since that time, polyurethanes (PU) have been found in many aspects of modern life; they represent a class of polymers that have found a widespread use in the medical,[98] automotive and industrial fields.[99,100] Polyurethanes are also found in products such as furniture, coatings, adhesives, constructional materials, fibers, elastomers and synthetic skins.[101] One of their advantages is their high tensile strength and melting points that making them more durable[97], their resistance to degradation by water, oils, and solvents make them excellent for the replacement of plastics.[99]

Polyurethane is a polymer in which the repeating unit contains a urethane moiety, R-O-C-NHR', which results most readily through the reaction of an isocyanate, –NCO, with an alcohol, –OH, Scheme 6. By changing and varying the polyhydroxyl and

polyfunctional nitrogen compounds, multiple urethanes can be produced.[99-102] Furthermore, variations in the number of substitutions and the spacing between and within branch chains yield PUs ranging from linear to branched and flexible to rigid. Linear PUs are used for the manufacture of fibers and molding,[103] however, flexible PUs are used in the production of binding agents and coatings.[99] Inserting various segmental chains within the PU chain results in PUs with different degrees of tensile strength and elasticity.[104]

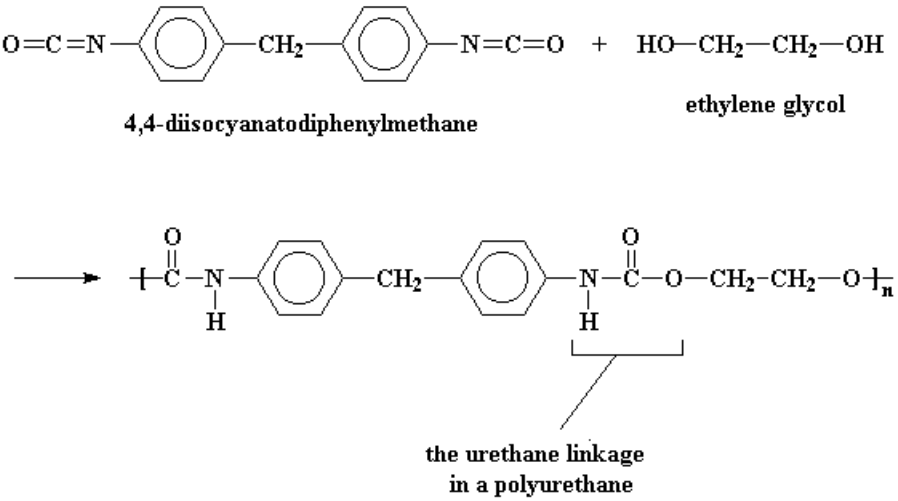

Scheme 6. Preparation of polyurethane from condensation reaction between a polyol and an isocyanate.

For the manufacture of polyurethane polymers, two groups of at least bifunctional substances are needed as reactants; compounds with isocyanate groups (isocyanate), and compounds with active hydrogen atoms (polyols). The physical and chemical properties of these compounds (structure and molecular size) affect the polymerization reaction and the final physical properties of the finished polyurethane as well. Other additives such as catalysts, surfactants, blowing agents, cross linkers, etc may be used to control and modify the reaction process and performance characteristics of the desired polymer. The

most common isocyanates, used predominantly in the manufacture of polyurethanes, are methylene diphenyl diisocyanate (MDI) and toluene diisocyanate (TDI), Scheme 7, they comprise about 90% of the total diisocyanate market.[105]

Monomeric MDI isomers

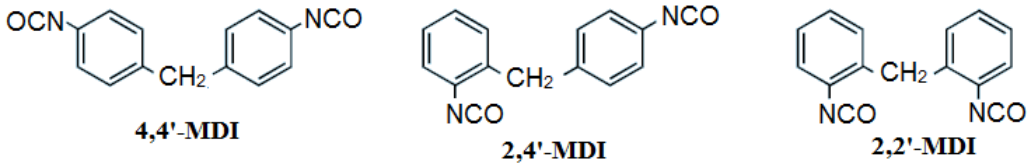

Monomeric TDI isomers

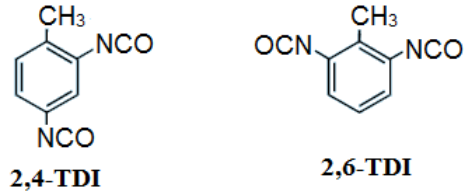

Scheme 7. Common isocyanates used in polyurethane manufacture.

Polyols , or polyether polyols, are high molecular weight polymers formed from cyclic ethers through an alkylene oxide polymerization process. They can be classified as flexible or rigid polyols depending on their molecular weight. Flexible polyols, such as polypropylene glycol and polytetramethylene glycol, have molecular weights from 2,000 to 10,000, and rigid polyols, such as sorbitol, have molecular weights from 250 to 700,[105] Scheme 8.

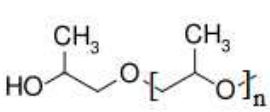

Polypropylene glycol

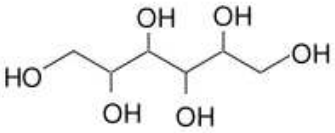

Sorbitol

Polytetramethylene oxide (PTMO)

Scheme 8. Common polyols used in polyurethane manufacture.

Numerous papers and reviews are published to describe fullerene-containing polymers:[84-87] however, little is known concerning the synthesis of fullerene-containing poly(urethanes) (PUs),[83, 94-96] although polyurethane materials (plastics, synthetic rubbers, foamed polyurethanes, dyes, and adhesives) are among the most widely employed polymer materials. In 1995, fullerene-containing PU network was first prepared from a condensation reaction between C_{60} fullerenols and a diisocyanated end-capped prepolymer. This reaction produces a high-performance elastomer with greatly enhanced tensile strength, elongation, thermal and mechanical stability, in comparison with their linear analogs or conventional polyurethane elastomers crosslinked by trihydroxylated reagents.[94]

The main objective of this research is to study the effect of fullerenes (empty and MNF) on the physical and electrical properties of fullerene-containing polyurethane networks and to evaluate these materials as suitable devices for tunable applications.

CHAPTER II

SYNTHESIS AND CHARACTERIZATION OF HYDROXYLATED FULLERENES AND FULLERENE-CONTAINING POLYURETHANE NETWORKS

Hydroxylation of Fullerenes

In this chapter, the synthesis and characterization of hydroxylated C_{60} and $Sc_3N@C_{80}$ is presented, including for the first time the hydroxylation of aza metallofullerene. In the aza hydroxylation study a well-characterized extract, containing 5% $Sc_2LaN@C_{79}N$ aza MNF and 95% mixture of fullerene (empty and MNF), was used in lieu of a pure starting material. In the development of a methodology that worked well for our study, various reported techniques were evaluated.[69, 70, 79, 80] Among those methods screened, a modified technique which performs the hydroxylation under HSVM conditions was selected [79, 80], not only because it is a green method, but also because it results in fullerenols or metallofullerenols with a narrow range of hydroxyl number distribution. Products resulting from this method were then characterized using the following techniques: FT-IR spectroscopy, elemental analysis (EA), Thermal Gravimetric Analysis (TGA), and Mass Spectroscopy (MS). Characterization of the hydroxylated fullerenes using a variety of techniques was deemed essential for the elucidation of the chemical structure and approximating the number of the hydroxyl groups attached to the fullerene surface.

Materials

Materials used for hydroxylation of fullerenes are C_{60} (MER, 99+%), toluene (Aldrich, 99.9%), potassium hydroxide (Aldrich, 85+%) and sephadex G-25 (Aldrich, dry head diameter of 20-80 μm, and bed volume of 4-6 mL per g.). $Sc_3N@C_{80}$ MNF and an

extract containing 5% $Sc_2LaN@C_{79}N$ MNAF were prepared in the nano-material synthetic labs of Prof. Steven Stevenson (University of Southern Mississippi, USM) via the CAPTEAR approach (Chemically Adjusting Plasma Temperature, Energy, and Reactivity).[49,26, 27] All commercial materials were used as received without further purification.

Method

The hydroxylation of C_{60}, $Sc_3N@C_{80}$ and $Sc_2LaN@C_{79}N$ extract was performed under HSVM conditions in which 0.062 mmol of fullerene and 16 mmol KOH were mixed in a stainless steel capsule together with three stainless steel milling balls. The capsule was vigorously shaken (for 1 h in case of C_{60} and 7 hr in case of $Sc_3N@C_{80}$ and $Sc_2LaN@C_{79}N$) using a milling machine (Spex mixer/miller 8000) at room temperature. The solid reaction mixture was then added to 5mL of deionized water, yielding a brown homogenous solution. To remove any trace amount of unreacted fullerene or MNF, the solution was filtered through 0.5 μm PTFE membrane, and water was partially removed under reduced pressure. The concentrated sample was chromatographated on a Sephadex G-25 size-exclusion gel column with distilled water as the eluent, thereby removing residual salts. Furthermore, to obtain final fullerenols with a narrow range of hydroxyl number distribution, the sample was collected (pH 6–7) as brown solution in a time interval of only several minutes. The sample was then concentrated under reduced pressure, and added dropwise to 100mL of methanol to produce a precipitate of brown solids. The precipitate was separated by filtration through a 47 mm 0.2 μm PTFE membrane, followed by drying at 50 ^{0}C under vacuum to give $C_{60}(OH)_x$ and $Sc_3N@C_{80}(OH)_y$ in a yield of approximately 83% and 65%, respectively. The

hydroxylated 5% $Sc_2LaN@C_{79}N$ extract was also obtained. The hydroxylated fullerenes were then characterized by FT-IR spectroscopy, EA, TGA, and MALDI-MS.

Techniques and Structural Characterization

FT-IR. The infrared spectra of the prepared samples were recorded in the wavenumber range from 400-4000 cm^{-1} using Nicolet nexus 470 FT-IR spectrometer.

Thermal gravimetric analysis (TGA). In this technique, the weight changes in a well dried material are monitored as a function of temperature under a controlled atmosphere. Using a TA instruments Q5000, an average, 10 mg samples were analyzed in platinum pans over the temperature range of 25-1000 ºC at a heating rate of 20 ºC/min. The number of hydroxyl groups attached to the fullerene cage was estimated by calculating the ratio of the weight loss at 250 ^oC, corresponding to the dehydroxylation of hydroxyl group, to the weight loss at a temperature > 300 ^oC, corresponding to the decomposition of the fullerene cage.

Mass spectroscopy (MS). Mass spectrometry (MS) is an analytical tool used not only for measuring the molecular mass of a sample, but also for elucidating its chemical structure, and this can be achieved by fragmenting the sample inside the spectrometer and analyzing the generated ions using suitable detector.

There are many techniques of mass spectroscopy; one of them is Matrix Assisted Laser Desorption/Ionization (MALDI) mass spectroscopy, introduced by Karas et al. in 1985.[106] This technique is based upon an ultraviolet absorbing matrix mix with a sample at a molecular level in an appropriate solvent. The sample/matrix mixture is placed onto a sample probe trip, then under vacuum conditions, the solvent is removed, leaving co-crystallized sample molecules homogenously dispersed within matrix molecules. When

the pulsed laser beam is tuned to the appropriate frequency, the energy is transferred to the matrix which is partially vaporized, carrying sample into the vapor phase and charging it.

To prepare the sample for MALDI mass spectroscopy, 1, 8, 9-Anthracenetriol (M.W of 226.23), dissolved in acetonitrile in a concentration of 5 mg in 500 µL, was used as a matrix. A small amount of the hydroxylated fullerenes, dissolved in water, was mixed with the matrix solution in a suitable ratio, and then a small drop of this mixture was placed on the target plate. The mixture was kept for few minutes to co-crystallize. C_{60} (mol. Wt. 720.67 g/mol) and Sc3N@C80 (mol. Wt. 1109 g/mol) were dissolved, individually, in toluene to be used as a reference. Since the molecular mass of the unhydroxylated fullerene was known, then the number of the hydroxyl groups attached to the fullerene cage can be calculated as follow:

$$\#\ of\ OH = \frac{molar\ mass_{(fullerenol)} - molar\ mass_{(fullerene)}}{17} \quad (1)$$

Data and Discussion

The FT-IR spectra, shown in Figure 3 (a-c), confirmed the attachment of hydroxyl groups (at 3500 cm^{-1}) to the carbon cage of C_{60}, $Sc_3N@C_{80}$, and the 5% $Sc_2LaN@C_{79}N$ extract. Also, the spectra showed three characteristic bands at 1080, 1370, and 1620 cm^{-1} assigned for υC-O, δ_sC-O-H and υC=C absorption. These four broad bands are invariably reported as diagnostic absorptions of various fullerenols.[70, 73,80]

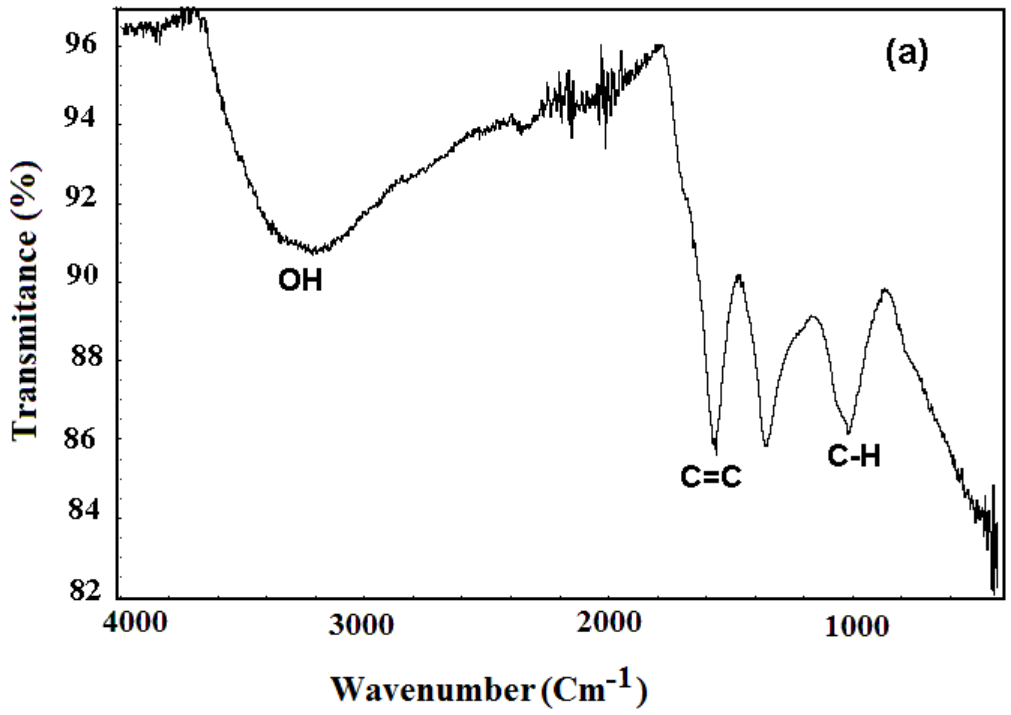

Figure 3a. FT-IR spectra of $C_{60}(OH)_{29}$

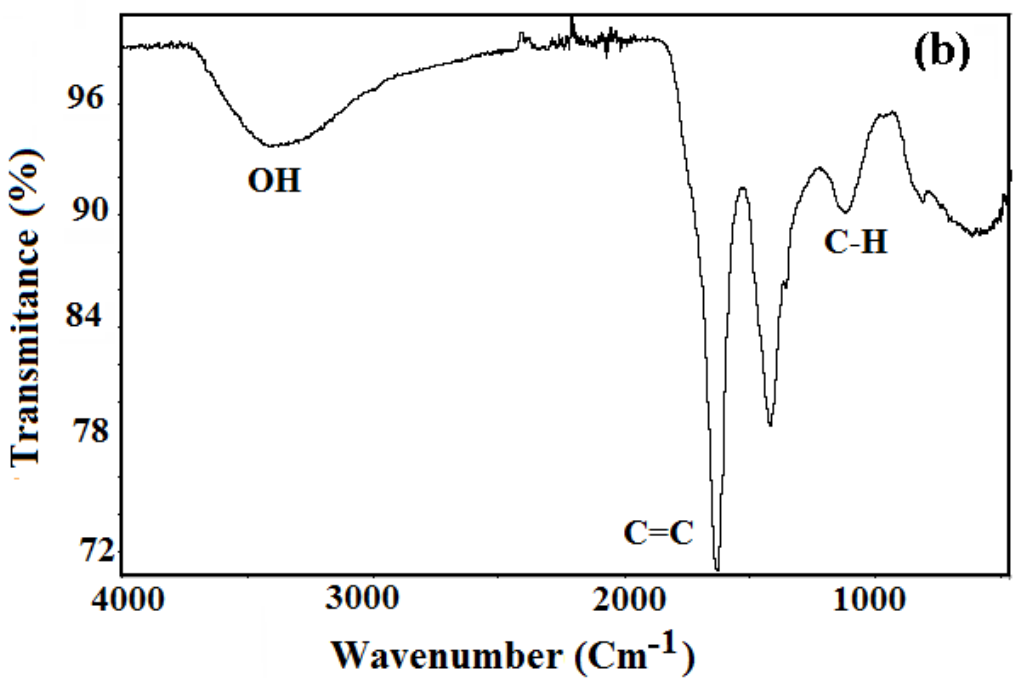

Figure 3b. FT-IR spectra of $Sc_3N@C_{80}(OH)_{18}$

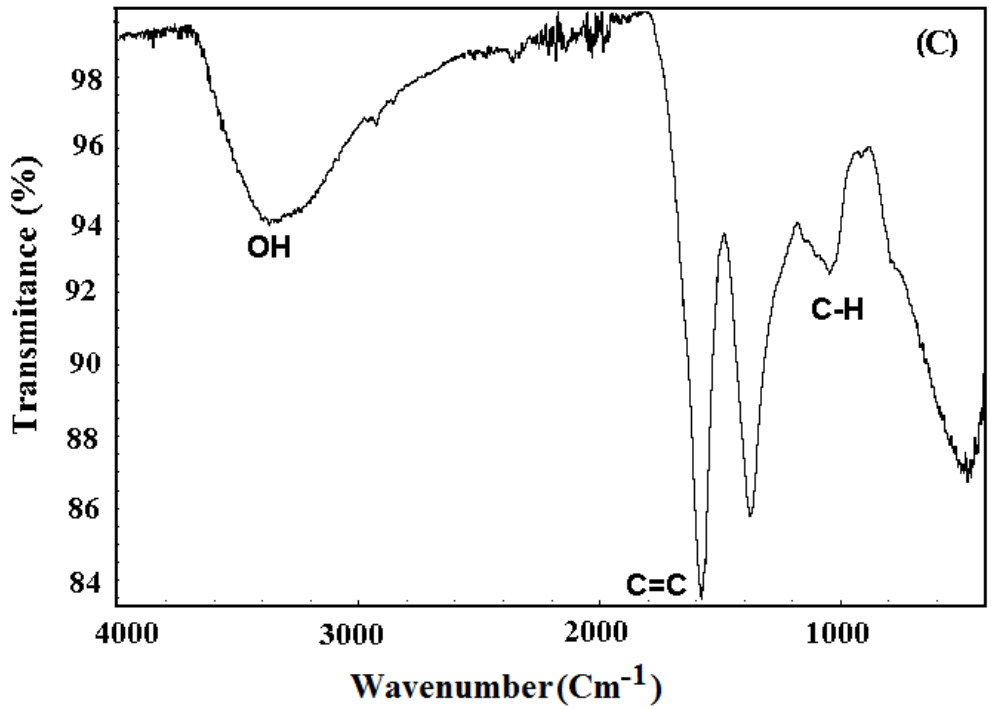

Figure 3c. FT-IR spectra of 5% $Sc_2LaN@C_{79}N(OH)_z$ extract.

The number of hydroxyl groups attached to the surface of C_{60} or $Sc_3N@C_{80}$ was estimated using a combination of EA, MS and TGA. To obtain the elemental analysis data, the prepared samples were sent to a commercial analytical lab, Atlantic Microlab, Inc. (http://www.atlanticmicrolab.com) for C, H, O, and N determination. The data provide is presented here in Table 1.

Table 1

Elemental Analysis of $C_{60}(OH)_x$ and $Sc_3N@C_{80}(OH)_y$

Element	$C_{60}(OH)_x$	$Sc_3N@C_{80}(OH)_y$
C	41.65	26.70
H	2.20	2.82
O	39.13	49.72
N	--	0.36

In most previous studies, the average number of hydroxyl groups attached to the fullerene cage was estimated using only the elemental analysis technique.[69, 70, 73, 79, 80, 107] However, especially for highly hydroxylated fullerenes, a substantial amount of secondary water bound to the multiple hydroxyl groups on a fullerene surface may exist.[73] Therefore, we monitored the weight loss of our hydroxylated fullerenes using the thermal gravimetric analysis technique, TGA. The data obtained from TGA, Figures 4 (a and b), showed that the weight loss for the hydroxylated fullerenes was observed in three temperature ranges: from room temperature to 110 °C which has been assigned to the secondary bound water,[108] from 110–300 °C which corresponds to dehydration of the attached hydroxyl, and >300 °C which has been attributed to the decomposition of the fullerene nucleus. The approximate number of hydroxyl groups attached to C_{60} or $Sc_3N@C_{80}$ MNF cages according to the data obtained from the TGA were 28 and 17 OH groups, respectively.

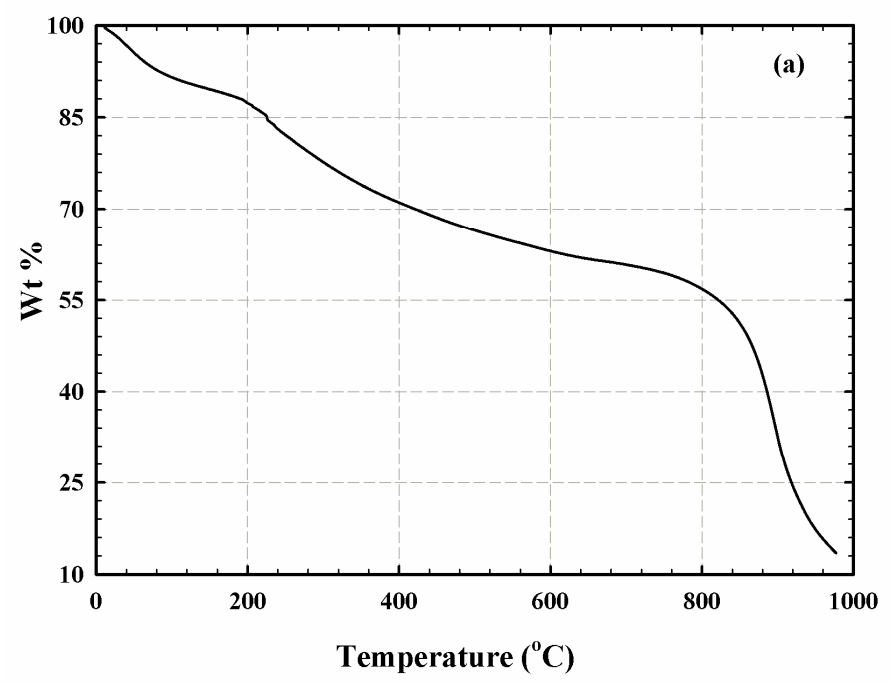

Figure 4a. TGA of $C_{60}(OH)_{29}$

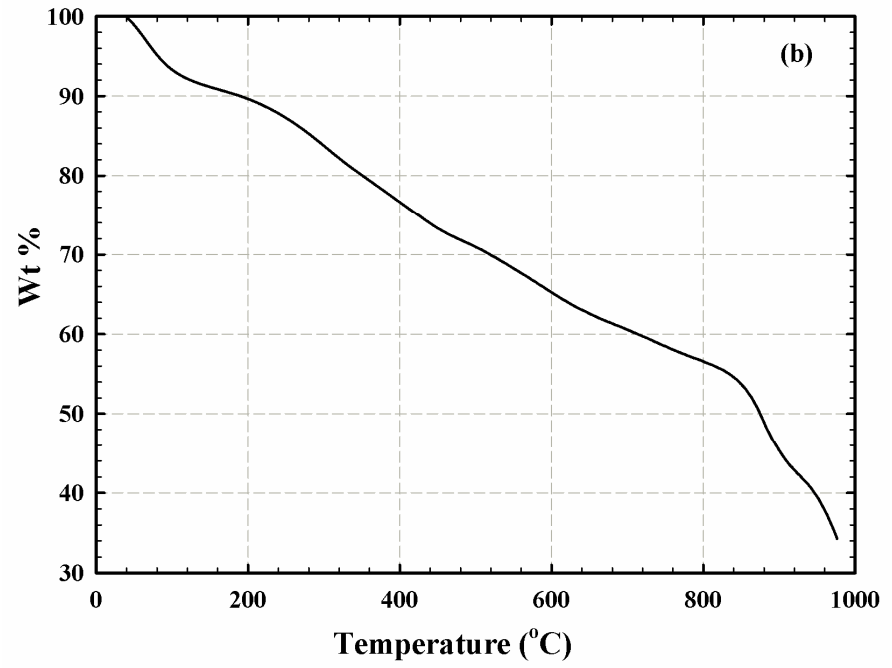

Figure 4b. TGA of $Sc_3N@C_{80}(OH)_{18}$

To confirm the number of hydroxyl groups attached to the fullerene cage, mass spectroscopic studies of the prepared fullerenols were performed using MALDI-MS.

Mass spectrum, Figures 5a and 5b, showed peaks at m/z 720 and 1109 which correspond to the C_{60} and $Sc_3N@C_{80}$. There are also several peaks corresponding to the water-soluble adducts such as the peaks at m/z 1230 and 1725 that correspond to the $C_{60}(OH)_{30}$, and $Sc_3N@C_{80}(O)_{18}(OH)_{19}$.

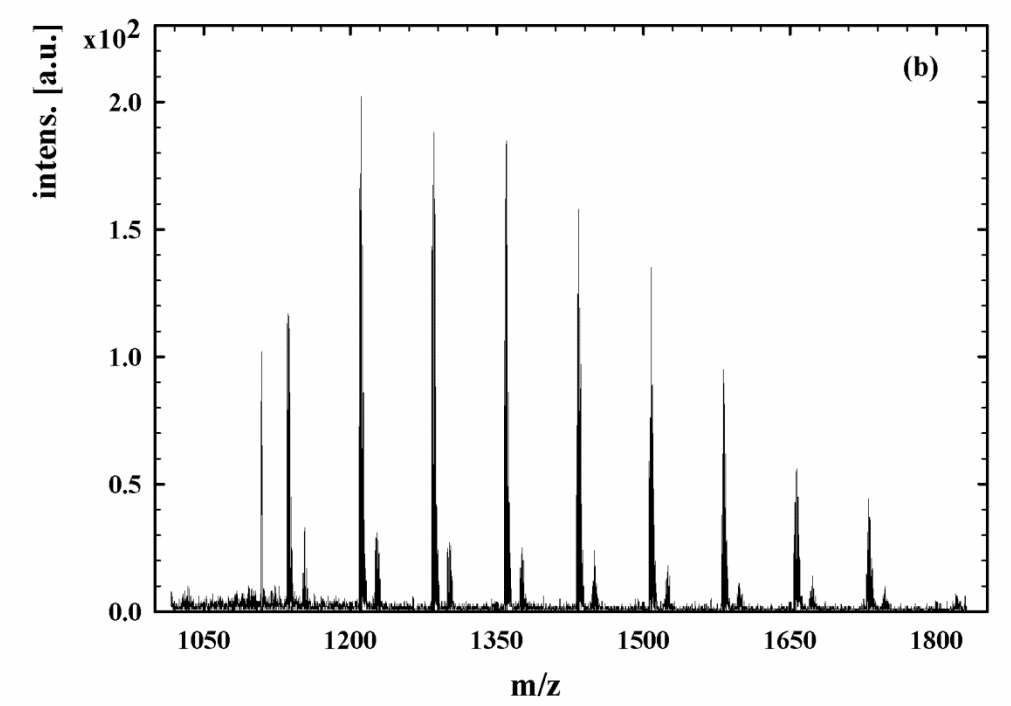

Figure 5a. MALDI-MS of $C_{60}(OH)_x$

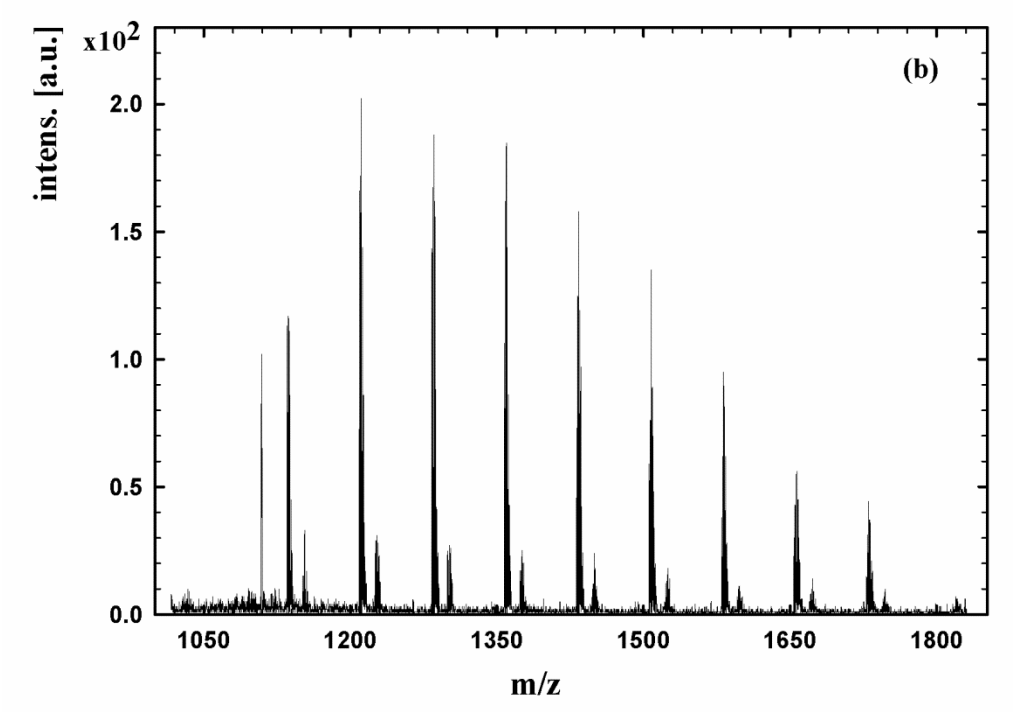

Figure 5b. MALDI-MS of $Sc_3N@C_{80}(OH)_y$

Table 2 summarizes the data obtained from EA, TGA, and MALDI-MS to estimate the number of hydroxyl groups in $C_{60}(OH)_x$, and $Sc_3N@C_{80}(OH)_y$. From this table, it is evident that for both samples, the numbers of OH obtained from EA are not in agreement with that obtained from TGA and MS. This was expected due to EA data providing additional values for H and O of secondary bound water that are bound to the multiple hydroxyl groups on a fullerene surface. The data obtained from TGA and MS are close to each other, thus by averaging the numbers of hydroxyl groups obtained from these two techniques, we can conclude there are, approximately 29 OH groups attached to C_{60} cages, and 18 OH groups attached to $Sc_3N@C_{80}$ cages. This would mean our hydroxylated fullerenes are $C_{60}(OH)_{29}$, and $Sc_3N@C_{80}(OH)_{18}$.

Table 2

Estimated Number of the Hydroxyl Groups in $C_{60}(OH)_x$ and $Sc_3N@C_{80}(OH)_y$.

Sample	EA	TGA	MALDI-MS
$C_{60}(OH)_x$	40	28	29
$Sc_3N@C_{80}(OH)_y$	50	17	19

For the extract containing 5% $Sc_2LaN@C_{79}N$ azafullerene, it is difficult to approximate the number of hydroxyl groups attached to the $C_{79}N$ cage because the sample is not pure.

Preparation of Fullerene-Containing Polyurethane Networks

The preparation of C_{60}- and $Sc_3N@C_{80}$-crosslinked polyurethanes with different loading of fullerenes is also discussed herein. In an attempt to study the effect of the encapsulated metallic nitride on the physical and electronic properties of $Sc_3N@C_{80}$-PU networks, when compared to C_{60}-PU as the reference material, a series of $Sc_3N@C_{80}$-PU and C_{60}-PU networks were prepared based on condensation reactions between the polyhydroxylated $C_{60}(OH)_x$ and $Sc_3N@C_{80}(OH)_y$ and a diisocyanate end-capped oligomer. The resultant networks were characterized using the standard techniques (FT-IR, Gel Fractions, TGA, and dynamic mechanical analysis, DMA), and the results are addressed.

Materials

Materials used for the preparation of the networks are poly(tetramethy1ene oxide) glycol (PTMO) (Monomer-Polymer & Dajac Labs Inc., Mn=2000 and Mw=4500) and

4,4'-methylene diphenyldiisocyanate (MDI) (Aldrich, 98 %). N,N dimethylormamide (DMF) (Fisher, 99.9%) and tetrahydrofuran (THF) (Fisher, 99.9%) and were dried before use. THF was distilled over sodium, and DMF was dried over molecular sieves for more than 2 days. hexylamine (Aldrich, 99%), HCl (Fisher, 99%), and iso-propanol (Fisher, 95%) were used as received.

Method

For the preparation of C_{60}-PU and $Sc_3N@C_{80}$-PU networks, we modified the synthetic methods reported by Chiang et al.[94] Prior to the preparation of the networks, we determined the NCO content of MDI, due to its importance in controlling the quality of the polyurethane products. The determination of the NCO content was carried out by reacting the MDI (dissolved in toluene) with an excess of hexylamine (dissolved in toluene) followed by back-titration with standardized HCl (in iso-propanol) in the presence of bromothymol Blue as indicator. The equivalent volume of HCl was recorded as V_s. The titration was repeated without MDI, and the equivalent volume of HCl was recorded as V_b. The NCO content was calculated from the following equation 2:

$$NCO\% = 4.202\ \frac{(V_b - V_s)N}{W(g)} \qquad (2)$$

where, W is the weight of MDI (in g) and the value of 4.202 is a constant combining the equivalent weight of NCO (42.02) mg/meq, conversion of g to 1000 mg, and conversion to 100%. The NCO% of the MDI used was 32%, the theoretical value is 33.6%.

Preparation of C_{60}-PU and $Sc_3N@C_{80}$-PU networks, were performed in two steps: (1) preparation of the diisocyanate end capped prepolymer, and (2) condensation reaction between the $C_{60}(OH)_{29}$ or $Sc_3N@C_{80}(OH)_{18}$ and the prepared prepolymer. The synthesis routes of C_{60}-PU and $Sc_3N@C_{80}$-PU polymer networks were shown in Scheme

9. The $C_{60}(OH)_{29}$ and $Sc_3N@C_{80}(OH)_{18}$ are used as crosslinkers, and a typical preparation was carried out as follows: In a three-necked reaction vessel (25 mL), a mixture of MDI (2.1 equiv.), PTMO (1 equiv.), and THF was stirred at 60 ^oC under nitrogen for 10 hours to produce diisocyanate end capped prepolymer. At the completion of this step, in the same reaction vessel, an appropriate amount of fullerenol, $C_{60}(OH)_{29}$ or $Sc_3N@C_{80}(OH)_{18}$ was stirred with the prepolymer in a mixture of THF and DMF (3:1) at 60 ^oC under nitrogen for 16 hours. The hydroxylated fullerene was dried under vacuum at 60 ^oC for a one day period and stirred with a small amount of DMF for 1 hour. Within 5 hours the reaction mixture became more viscous. At the end of the reaction, the solution was poured into a teflon mold, and the solvent was allowed to evaporate slowly under N_2 to afford a rubbery film. The resulting film was then suspended in methanol and treated briefly in an ultrasonic bath at room temperature to quench the unreacted prepolymer. Removal of methanol and drying at 60 ^oC under vacuum yielded the fullerene-crosslinked PU network. Two different sets of fullerene-PU networks were prepared: the C_{60}-PU set with five different loadings of C_{60} (0.8 %, 1 %, 2 %, 3%, and 5 % C_{60}/PU (w/w)), and $Sc_3N@C_{80}$-PU set with four different loadings of $Sc_3N@C_{80}$ (0.8 %, 1 % 2 %, 3%, and 5 % $Sc_3N@C_{80}$ /PU (w/w)).

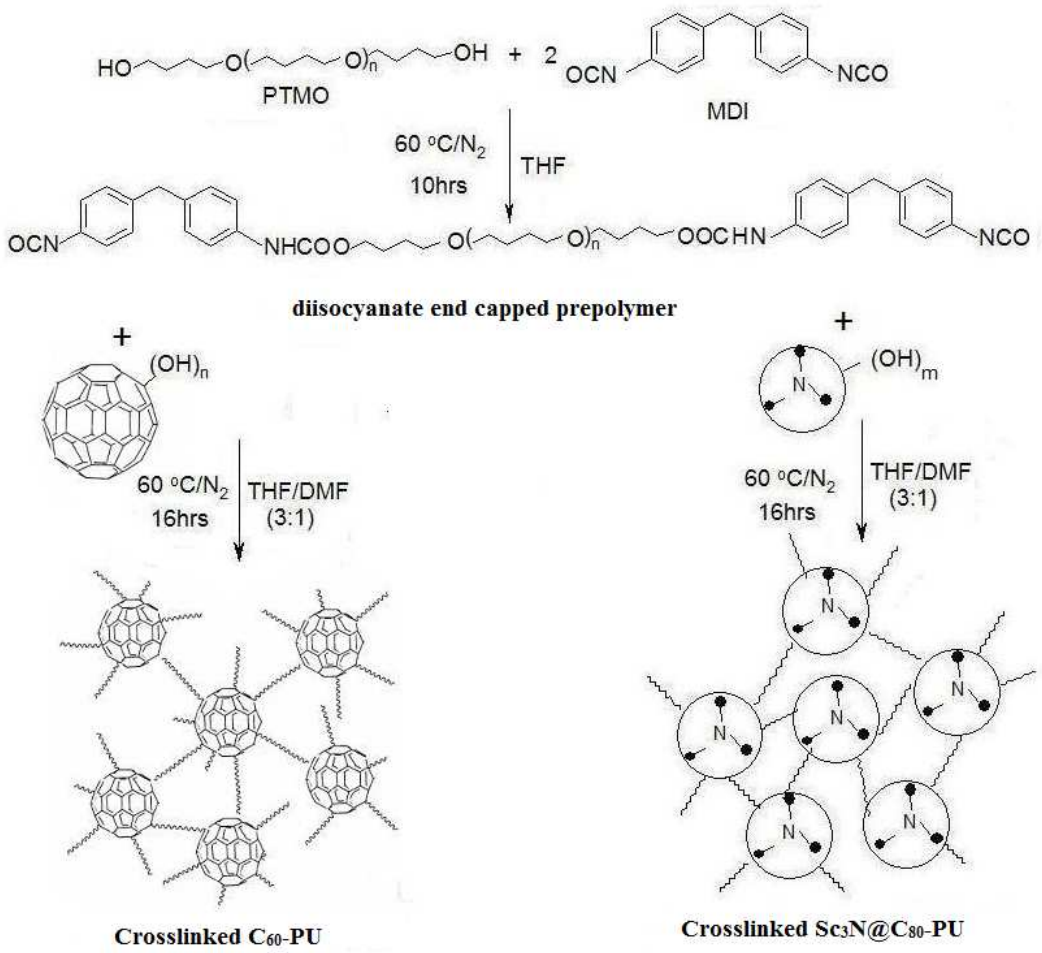

Scheme 9. Preparation steps of fullerene-PU networks.

The fullerenes-containing polyurethane networks obtained through this process were kept dry and under nitrogen for further characterization.

Techniques and Characterization

To elucidate their chemical structure, the prepared fullerene-PU networks were characterized using a variety of techniques, such as FT-IR, TGA, Gel Fraction, and Dynamic Mechanical Analysis (DMA).

In thermal gravimetric analysis (TGA), the thermal stability of the prepared networks was evaluated using a TA instruments Q5000 over the temperature range of 25-700 ºC at a heating rate of 20 ºC/min. The thermal degradation onset temperature of the

prepared networks was determined and reported as the temperature corresponding to 10 % mass loss.

Gel fraction. Gel fractions of the prepared networks were obtained by dissolving a known mass of film in chloroform, resting the sample for 24 hours at room temperature, and recovering the insoluble mass fraction, followed by residual solvent evaporation under reduced pressure.

Dynamic mechanical analysis (DMA). Dynamic Mechanical Analysis is a technique used generally to study the viscoelastic behavior of polymeric materials; which means that these materials exhibit the properties of a glass (high modulus) at low temperatures and the properties of a rubber (low modulus) at higher temperatures.[109] In this technique, a sinusoidal force (stress) is applied to a material and the resulting displacement (strain) in the material is measured, resulting in determining the complex modulus, E*, which is given by equation 3:

$$E^* = E' + iE'' \tag{3}$$

where, E′ and E″ are the storage modulus (real part) and the loss modulus (imaginary part), respectively, and i represents the square root of minus one. The storage modulus is a measure of the energy stored elastically in a substance during deformation under the effect of an applied force, while the loss modulus measures the energy dissipated as heat. E′ and E″ are related to each other as follow:

$$\tan\delta = \frac{E''}{E'} \tag{4}$$

where tan δ is the loss tangent, and δ represents phase lag of strain with respect to the stress. For the perfectly elastic material, the resulting stress and strain are in phase, δ is 0^o, however, for a totally viscous material, there will be a 90^o phase lag of strain with

respect to the stress. Viscoelastic materials exhibit behavior somewhere in between these two extreme; $0 > \delta < 90$ during the mechanical analysis.[110]

Varying the temperature or the frequency of the stress is leading to variation in the complex modulus; thus temperature scanning of the modulus helps to locate the glass transition temperature of the examined material, and the transitions corresponding to other molecular motions can be identified. The transitions related to the glass transition is referred to α transition, and the transition related to other transitions taken place at temperatures below T_g are referred to β, γ, and δ transitions.[109]

The dynamic storage modulus (E') and tan δ ($= E''/E'$) vs. temperature curves for samples were generated using a TA Q800 instrument. Rectangular samples (8 x 12 mm) were run under nitrogen in tensile mode with a frequency of 1 Hz and amplitude of 15 μm. The experiments were performed over the temperature range -150 to 100 ^oC at a heating rate of 2° C/min. These measurements were performed to examine the effect of fullerene (C_{60} and $Sc_3N@C_{80}$) on the mechanical response of the polyurethane as well as to determine the glass transition temperature, T_g, of the resultant fullerene-PU networks.

Data and Discussion

In the preparation of fullerene-PU networks, the MDI and PTMO concentration were held constant at 2.1:1 (MDI:PTMO) molar equivalents to obtain a prepolymer end caped with isocyanate functional group for further reaction with the hydroxylated fullerenes. Two different sets of fullerene-PU network were prepared, each with different loadings of fullerene; 0.8 %, 1 % 2 %, 3%, and 5%, and their identities and their OH: NCO molar ratios were recorded in table 3.

The gel fractions of the prepared fullerene-PU networks are listed in Table 3. It is apparent that the prepared fullerene-PU samples have high gel fractions ranging from 72-97% depending on the percent of the fullerenols added.

Table 3

Characterization of Fullerene-PU Films: Gel Fraction and Thermal Properties.

Sample ID[a]	OH:NCO	Gel fraction %[b]	Thermal degradation onset (°C)[c]
0.8%C_{60}-PU	1:4	72	322
1%C_{60}-PU	1:3	97	330
2%C_{60}-PU	2:3	82	324
3%C_{60}-PU	1:1	83	327
5%C_{60}-PU	3:2	75	322
0.8% $Sc_3N@C_{80}$-PU	1:4	85	343
1% $Sc_3N@C_{80}$-PU	1:3	77	330
2% $Sc_3N@C_{80}$-PU	2:3	80	331
3% $Sc_3N@C_{80}$-PU	1:1	85	332
5% $Sc_3N@C_{80}$-PU	3:2	70	320

[a] wt % of $C_{60}(OH)_{29}$ or $Sc_3N@C_{80}(OH)_{18}$ in films; insoluble mass fraction recovered after 24 h solvent exposure; and [c] calculated from TGA data as the temperature corresponding to 10% mass loss.

FT-IR spectra of the pre-polymer and the prepared networks are shown in Figure 6. In this figure, a band at 2272 cm^{-1}, corresponding to the absorption of NCO group, disappeared from the spectra of both C_{60}-PU and $Sc_3N@C_{80}$-PU networks. Instead, other two bands appeared in the polymer networks at 3311 and 1728 cm^{-1}, corresponding to the

urethanic NH and carbonyl absorptions, respectively, which means that isocyanate functions were converted into urethanes. The broadening in urethanic NH band may be attributed to the hydrogen bonding between urethane groups, NH.

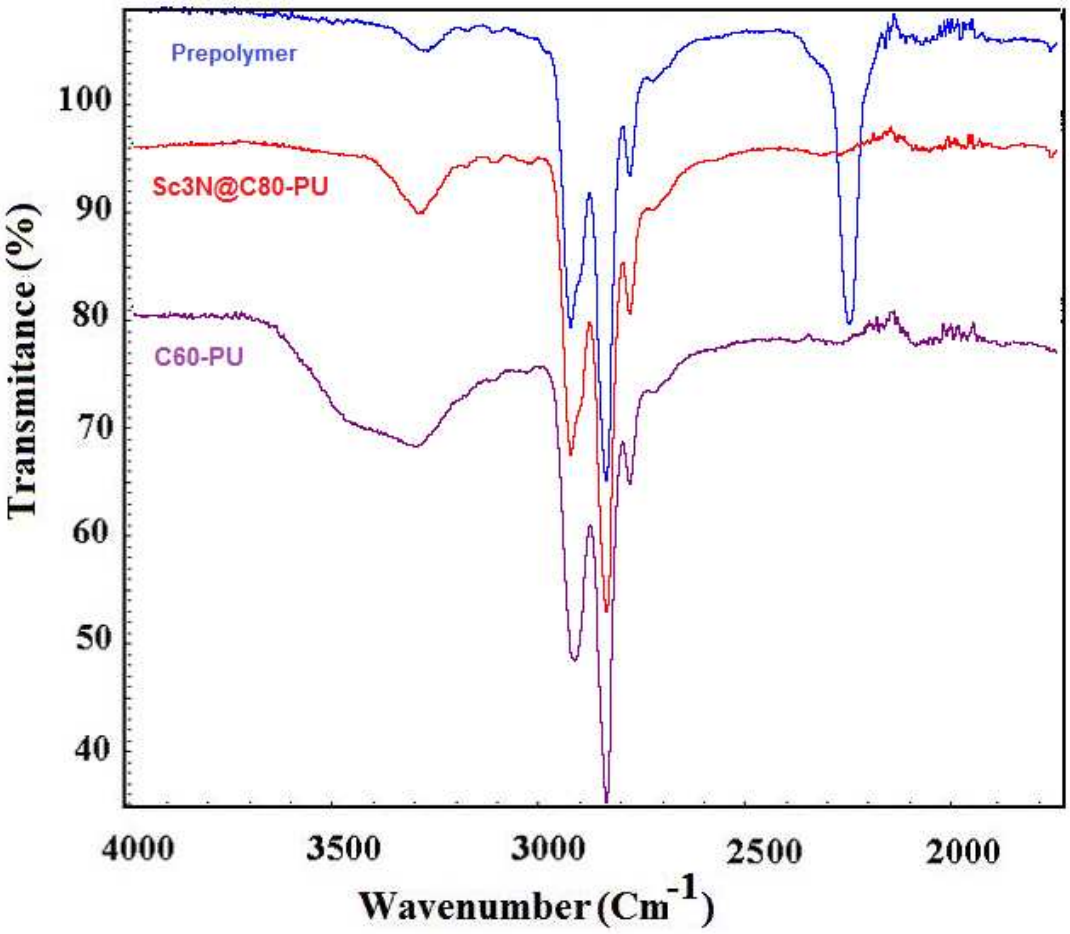

Figure 6. FT-IR spectra of diisocyanate end capped prepolymer, C_{60}-PU and $Sc_3N@C_{80}$-PU

Information about the thermal stability and the thermal degradation processes taken place in the prepared fullerene-PU networks were obtained from TGA plots shown in Figure 7 and Figure 8. It is observed in these figures that there is no mass loss up to 300 °C which reveals the high thermal stability of these samples. Furthermore, two weight loss stages are seen more clearly in the derivative curves; one is observed over the temperature range of 300-340 which corresponds to the decomposition of the urethane

linkage, and the other weight loss occurred in a single process over the temperature range of 430-460 ^{o}C which corresponds to the degradation of polymer chains. For all prepared networks, the thermal degradation onset temperatures were determined for all prepared networks at 10% mass loss and recorded in Table 4. It is found that this temperature increases as the gel fraction of the networks increases.

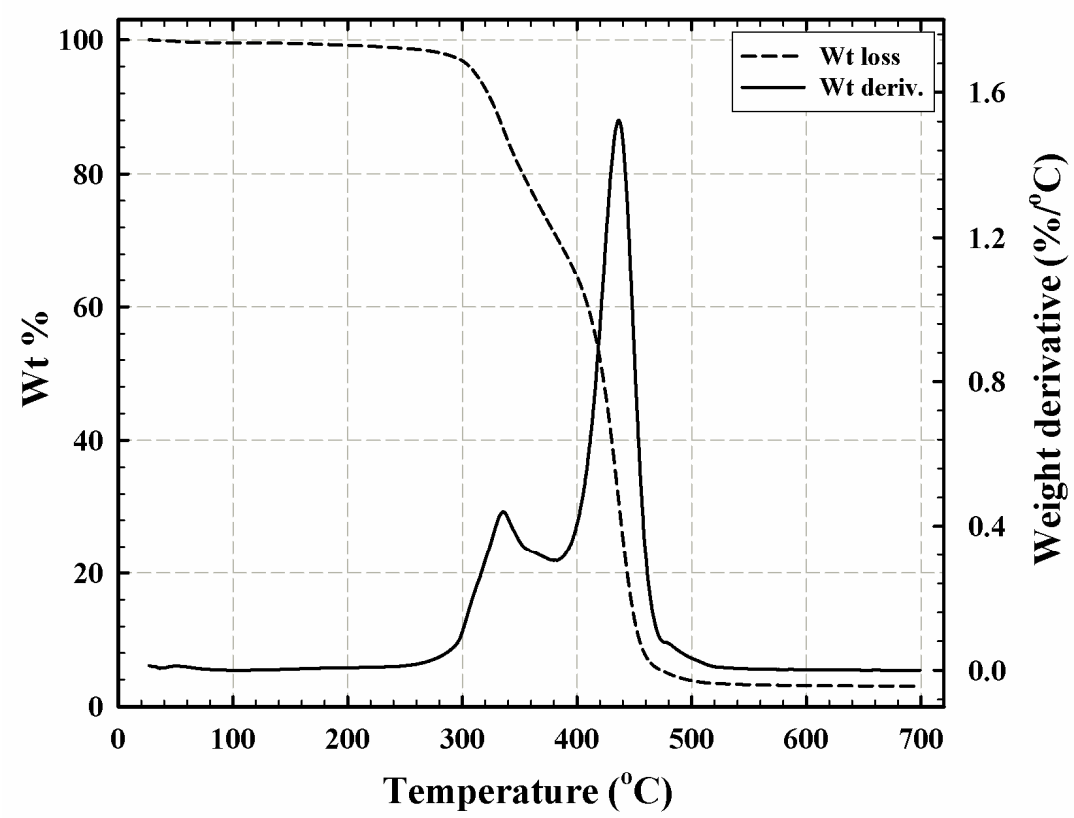

Figure 7. TGA weight loss and weight derivative of 3% C_{60}-PU

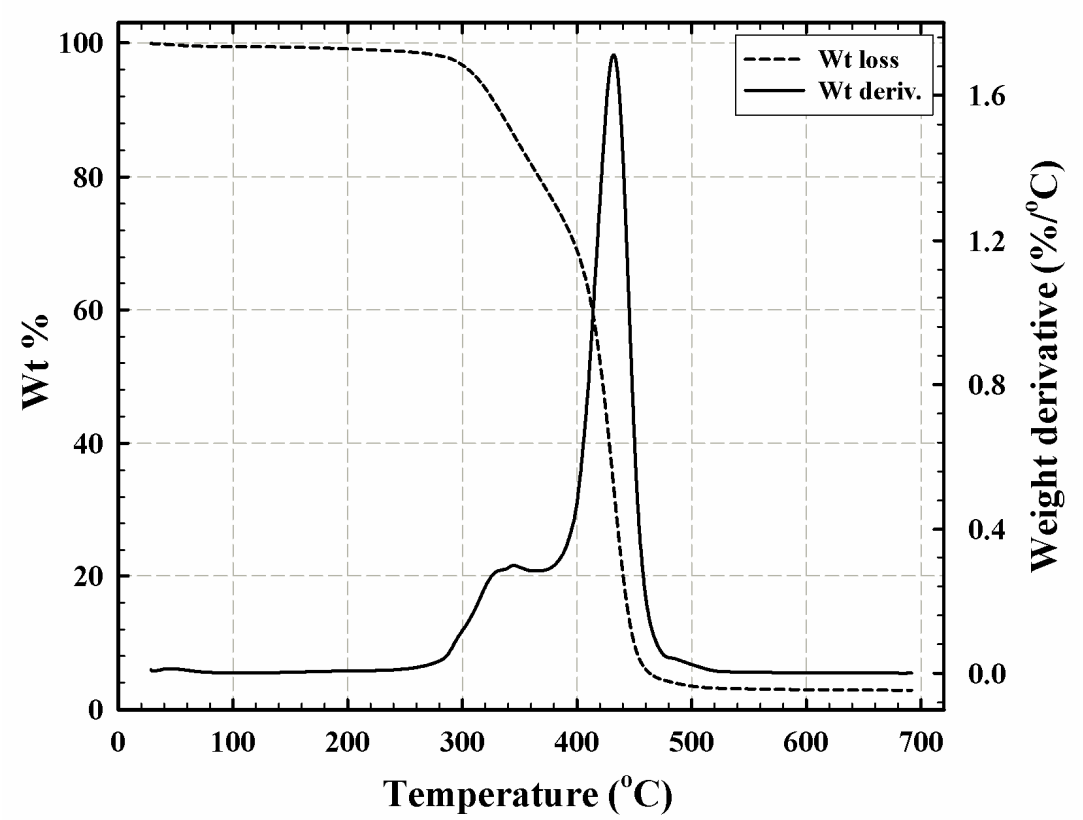

Figure 8. TGA weight loss and weight derivative of 3% $Sc_3N@C_{80}$-PU

The data obtained from dynamic mechanical analysis of the prepared fullerene-PU networks are shown in figures 9 and 10. Tan $\delta = E''/E'$ vs. temperature curves for (C_{60} or $Sc_3N@C_{80}$)-PU networks are shown in Figure 10, with three distinct peaks shown. The origin of the peak in the temperature range of -150 to -110 °C seen for all samples is presently unknown, but must be due to local motions along the PU chains that are not influenced by crosslinking or insertion of Sc_3N molecules in the fullerene cages. The largest peak at around -50 °C corresponds to the glass transition temperature of the fullerene-PU networks, and the high temperature shoulder after the glass transition is due to the thermally-driven reaction between residual OH groups and PU endgroups.

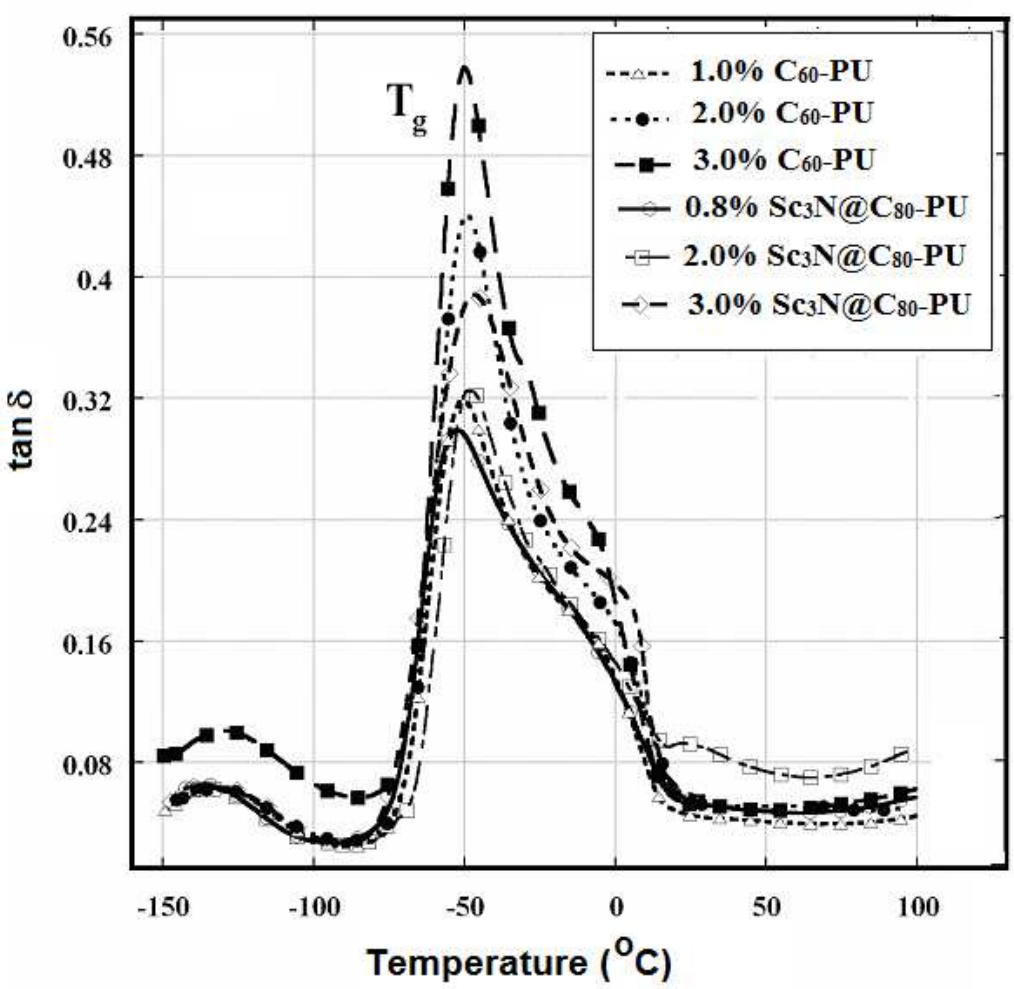

Figure 9. Dynamic mechanical loss tangent, tan δ, vs. temperature for fullerene-PU at different fullerene loadings.

It is known that for any polymer undergoing a crosslinking reaction, there would be a restriction in the polymer chain mobility, and consequently there would be a shift in T_g to higher temperature with increasing the crosslinking content.[109] For our materials, there is unremarkable difference in T_g upon increase of the fullerene loading, and this may be attributed to the low overall fullerene content in this study. Another reason accounted for the unremarkable change of the T_g of our samples with changing the fullerene loadings is the polymer free volume effect caused by the presence of fullerene cages acting as polymer packing defects. This effect would make the polyurethane chains

more flexible, and this would lead to decrease in T_g. In other words, there was a competition between the factors which might increase the T_g, and factors which might lower T_g values, and the net result of this competition is that T_g values of all fullerene-PU networks are close. The T_g of the prepared samples were summarized in Table 4. More details about the molecular dynamic motions and the transition processes taken place in these samples will be discussed in further detail in Chapter 4.

Table 4

Glass Transition Temperature Values, T_g, for the Prepared Fullerene-PU.

Sample ID[a]	T_g from DMA, (°C)
0.8%C_{60}-PU	-52
1%C_{60}-PU	-51
2%C_{60}-PU	-50
3%C_{60}-PU	-48
0.8% Sc3N@C_{80}-PU	-52
1% Sc_3N@C_{80}-PU	-51
2% Sc_3N@C_{80}-PU	-50
3% Sc_3N@C_{80}-PU	-49

Figure 10 shows the dynamic storage modulus (E′) vs. temperature curves for (C_{60} or Sc_3N@C_{80})-PU networks. As seen in this figure, all samples exhibit the behavior of viscoelastic materials (glassy at low temperatures and rubbery at high temperatures) with a glass transition around -50 °C that is associated with the PU fraction. E′ of the samples

in the glassy state, just below the T_g, is constant because the molecular motions in this region are largely restricted to the vibrations and short-range rotational motions.[109,110] After a few degrees of temperature change, and going from the glassy region to the glass transition region, E′ drops due to the long-range molecular motion associated with the progressive material softening taken place in this region. In the plateau region, and after the sharp drop in E′ taken place in glass transition region, E′ should be constant because the materials at this region exhibit long-rang rubber elasticity, which means that these elastomers can be stretched and snap back to the original length upon releasing the applied force. For our materials, there is an increase in modulus with increase in temperature in the rubbery state, and this may be attributed to the thermally driven reactions between the un-reacted hydroxyl groups on the fullerene and the polymer end groups. This increase in degree of cross-linking during the measurements would account for the increase in storage modulus.

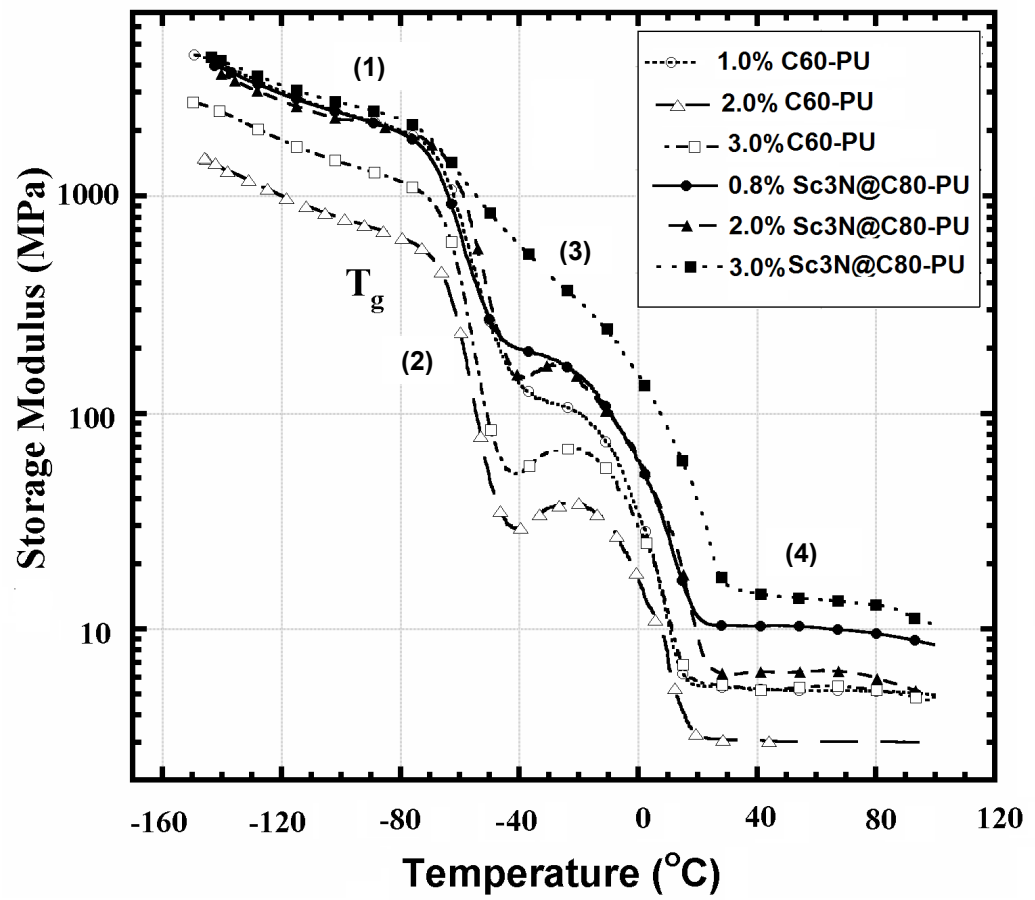

Figure 10. Dynamic storage modulus, E′, vs. temperature for fullerene-PU at different fullerene loadings.

There are several studies interested in the mechanical properties of fullerene containing polymers, and it was noticed from this previous work that varying the composition and the physical properties of the polymers results in a change in their mechanical behavior.[91,111,112] Benzylaminofullerene/low-density polyethylene (BAF/LDPE) composites containing up to 10 wt.% BAF exhibit superior thermal mechanical stability and dramatic increase in their storage and loss moduli compared to their polymeric precursor.[91] Furthermore these moduli increase with BAF loading, while a higher BAF loading has an adverse effect on the mechanical behavior of these composites. A similar result was reported by Ouyang, et al., during the study of the

mechanical properties of a composite material prepared via the side chain carboxylated poly(dimethylsiloxane)/1-(4-methyl)-piperazinylfullerene (PDMS/MPF).[112] The increase of the MPF content in the composites leads to a denser packing of MPF nanodomains, resulting in better thermal, mechanical, and viscoelastic properties.

CHAPTER III

ELECTRICAL PROPERTIES OF FULLERENE-CONTAINING POLYURETHANE NETWORKS

In this chapter, the dielectric properties of fullerene-containing polyurethane networks will be discussed. Surface and volume resistivity measurements as well as the capacitance-voltage characteristics will also be discussed here.

Dielectric Properties Investigate By Broadband Dielectric Spectroscopy

Introduction

A dielectric response is a result of the interaction of matter with an applied electric field that oscillates at different frequencies (*f*) at given temperatures.[109, 113, 114] Understanding the interaction mechanism is critical for the analysis of dielectric properties. Several dielectric mechanisms, depending on the frequency of the applied field, can describe that interaction.[114-118] Dielectric relaxation, as a whole, is the result of the movement of dipoles (dipole relaxation) and electric charges (ionic relaxation), and is usually observed in the frequency range 10^2-10^{10} Hz. Relaxation mechanisms are relatively slow compared to resonant electronic transitions or molecular vibrations, which usually have frequencies above 10^{12} Hz.[115] Figure 11[118] summarized all types of polarizations: Electronic polarization occurs in all materials when the electron cloud was displaced relative to the nucleus under an applied electric field. Atomic polarization is observed when the electronic cloud is deformed under the applied field, so that the negative and positive charges are formed. Dipole relaxation originates from the alignment of permanent or induced dipoles under the force of the applied field. The orientation polarization of these dipoles is disturbed by thermal noise which causes the dipole

relaxation to be strongly dependent on temperature and chemical surrounding. Ionic relaxation, molecular relaxation, comprises ionic conductivity and interfacial and space charge relaxation. Ionic conductivity predominates at low frequencies and introduces only losses to the system. Interfacial relaxation occurs when charge carriers are trapped at interfaces of heterogeneous systems.

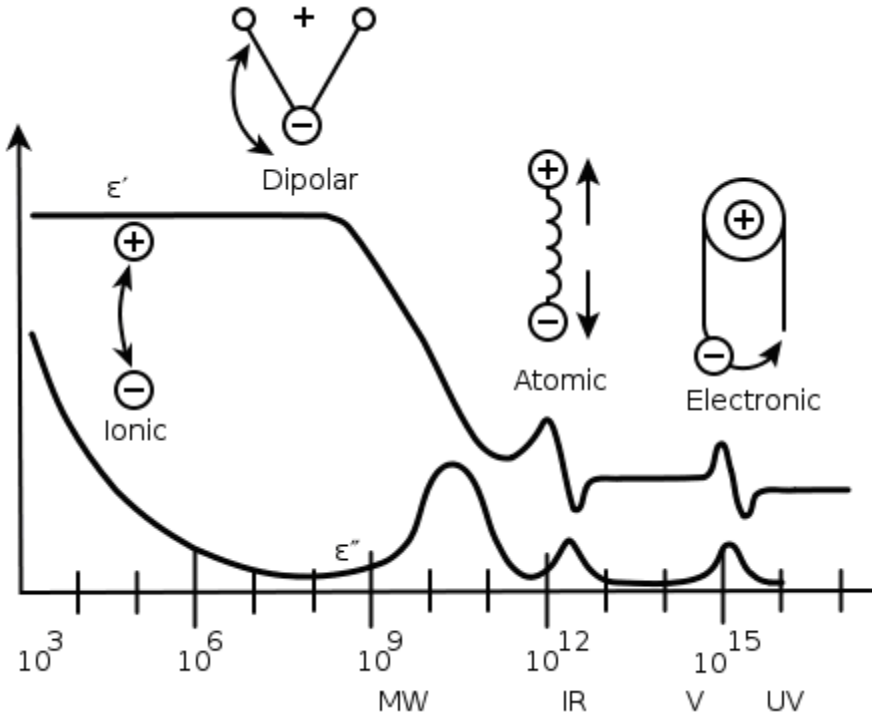

Figure 11. Frequency response of dielectric mechanisms
http://www.psrc.usm.edu/mauritz/dilect.html

The essential quantity measured by dielectric spectroscopy is the complex dielectric permittivity which is given by the following equation:[119]

$$\varepsilon^*(\omega) = \varepsilon'(\omega) - i\varepsilon''(\omega) \quad (5)$$

In this relationship, ω is the angular frequency = $2\pi f$ and i = √-1. ε′, the real permittivity, reflects material polarizability that can be due to dipole reorientation, deformation of delocalized electron distributions, or interfacial polarization (internal material or material in contact with the electrode) relaxation. ε″, the imaginary or loss permittivity is

proportional to the energy dissipated per cycle during any of these processes, termed 'relaxations'. It is known that when an alternating electric field is applied on a material, there is delay between the change in the field and the change in polarization, and this delay was represented by the angle δ. Tan δ, dissipation factor, represents the ratio of the energy dissipated to the energy stored in the dielectric, and tan $\delta = \varepsilon''/\varepsilon'$. [113]

Several studies of the temperature and frequency dependencies of dielectric properties of solid C_{60}[120-124] reveal valuable information about structural changes as well as defect behaviors, so that one can understand the structure of these materials and their physical properties. Although, numerous exciting properties of metallofullerenes have been found to result from the encapsulated metals, e.g., optical (Er), magnetic (Gd), radioactive (Ho); few studies about their dielectric properties are found. Iwasa et al. related the dielectric properties of La@C_{82} solids to their molecular motions, and the temperature dependence of the dielectric properties of these materials revealed that the metallofullerene molecules are dielectrically active due to the mobility of their dipoles.[125]

Polymeric composites are an important class of functional and/or structural polymeric materials formed by incorporating active materials into host polymer matrices. These materials can combine successfully electronic, optical and magnetic properties of inorganic or organic materials with attractive mechanical properties, especially the process-ability of conventional polymers.[82-86] With a view to modify the properties of these polymeric systems for practical applications, many studies concerning the dielectric properties of polymer composites have been reported; however, few studies about the dielectric of C_{60}-containing polymer exist.[91, 126,127] For example, Lu et al.[91] studied the dielectric properties of Benzylaminofullerene (BAF)-Polyethylene (PE) composites as a

function of BAF loading up to 10 wt%, and they found that the PAF-PE composite has dielectric constant higher than that of unloaded PE, and as BAF load increases, the dielectric constant of PAF-PE composites increases due to the presence of amine groups which increase the interfacial, dipole, atomic and electronic polarization. During the study of the dielectric properties of polyimide films with different loadings of C_{60} and/or C_{70} as admixtures, Subocz et al.[126] found that the capacitance of the C_{60}-polyimide is higher than that of the pure polyimide; however, with increasing C_{60} or C_{70}, the dielectric loss of the resultant films decreases due to the restriction of the polymer chain motion. Ouyang et al.[127] studied the effect of the C_{60}-fullerenols density on the dielectric properties of the C_{60}/poly(dimethylsiloxane) nanocomposites, and found that at low density loading of the fullerenols, the dielectric constant of the composite decreases as the loading of the fullerenols increases due to the restriction of motion of polymer chains; however at high density, the dielectric constant increases with increased loading of the fullerenols increases due to the polarizability that arise from unreacted OH groups in the composite.

Measurements

The dielectric measurements of our prepared samples were performed using a Novocontrol GmbH Concept 40 broadband dielectric spectrometer, BDS. The data were collected over the frequency range 0.1Hz - 3MHz at fixed temperatures from - 150 to 230 ^{o}C. Each experiment consisted of *f* sweep iterations at constant temperature, and the temperature stability of the instrument was controlled to within ± 0.2 °C. Before being measured by the dielectric spectrometer, the samples were preconditioned in a moisture chamber with controlled relative humidity < 0.5% for more than a week to decrease the

influence of water on dielectric response. Upon removing the specimens from the chamber, the specimens were immediately loaded into the spectrometer. The loading process took less than 2 minutes. This procedure helps to reproduce data for each sample as the plasticization effect of water is eliminated.

To compare the changes occurring in fullerenes (C_{60} and $Sc_3N@C_{80}$, and Sc_2La $N@C_{79}N$ extract) upon chemical hydroxylation or compatibility with polyurethane to form polymer nanocomposites, the dielectric properties of all these materials have been measured and analyzed using a Novocontrol GmbH Concept 40 broadband dielectric spectrometer. Two different types of measurements will be performed: one for powder samples (fullerenes and the hydroxylated fullerenes), and the other for film-shaped samples (polymer networks). For powder samples, a Novocontrol BDS 1308 liquid/powder parallel plate sample cell was used. Cell capacity is adjusted by variation of electrode spacing using silica or Teflon spacers.[128] For film sample characterization, discs of 2 cm in diameter of the polymer films were sandwiched between two gold-coated copper electrodes of 2 cm diameter inside a controlled humidity chamber and then rapidly transferred to the instrument for testing. To avoid any adhering of polymer to the gold coated electrode surface, the samples were covered with two aluminum sheets on both sides.

Figure 12 shows a schematic view of a typical dielectric spectroscopy experiment in which a dielectric sample of thickness d and area A is subjected to an alternating electric field of angular frequency ω, and the response is then translated into complex permittivity.

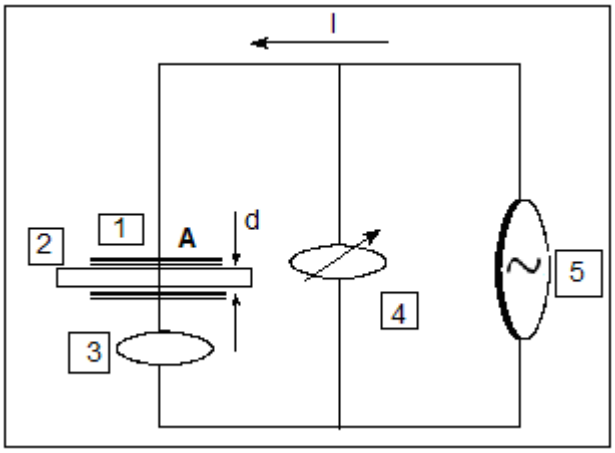

(1) Electrodes of area A
(2) Sample film of thickness d
(3) Current analyzer
(4) Voltage analyzer
(5) Alternating voltage generator.

Figure 12. Schematic draw of a typical dielectric spectroscopy experiment

Results and Discussion

In this section we report for the first time the effect of the encapsulated metallic nitride on the dielectric properties of $Sc_3N@C_{80}$-containing polyurethane nanocomposites, and we compare the obtained data with that of empty C_{60}-PU networks. We also study the dielectric properties of fullerenes (C_{60}, $Sc_3N@C_{80}$ MNF, and 5% $Sc_2LaN@C_{79}N$ aza MNF extract, and their hydroxylate materials). The discussion of the obtained data is divided into two sections; the dielectric data of the powder samples, fullerene and the hydroxylated fullerene, and the dielectric data of the networks.

Dielectric properties of fullerene powder. In this section we will discuss the dielectric permittivity and tan δ behavior of the fullerene and their hydroxylated compounds. The dielectric data of the materials in this part were collected using the sample cell designed for testing powders, since approximately 300 mg of the sample powder was used to fill the cell. The measurements were performed within a frequency range 0.1 Hz to 3.0 MHz, and a temperature range from -150 to 180 ^{o}C with 10 degree increment.

Figure 13 shows the temperature dependence of permittivity, ε′, of C_{60}, $Sc_3N@C_{80}$ and 5% $Sc_2LaN@C_{79}N$ extract powders at different indicated frequencies. For all fullerenes, and after initial flat behavior, ε′ increases with increasing temperature (especially at low frequency). The increase in ε′ with temperature is due to the fact that dipoles have sufficient energy to rotate and the permittivity related to the polarizability of these dipoles increase. In the same plots, and for all fullerenes, ε′ decreases with increasing frequency (especially at high temperature), and this is due to the fact that the time during which the electric field is applied in one direction – that is, one-half the period of oscillation = $1/2f$ - increases with decreasing frequency. The consequence is that slower motions associated with polarizability have more time during which they can be sampled.

The empty cage C_{60} curve lies beneath those for $Sc_3N@C_{80}$ and $Sc_2LaN@C_{79}N$, which may be attributed to C_{60} possessing a spherical symmetry, no polar groups, and the only inherent polarizibility would be due to fluctuations in the distribution of delocalized electrons throughout the cage. The high ε′ values for $Sc_3N@C_{80}$ and $Sc_2LaN@C_{79}N$ reflect their dipole nature. The increase in temperature imparts more rotational freedom to these dipoles thus increasing their polarizability which leads to an increase in ε′ at a given temperature. It is also shown that ε′ for C_{60} begins to rise at a lower temperature than for $Sc_3N@C_{80}$ or $Sc_2LaN@C_{79}N$.

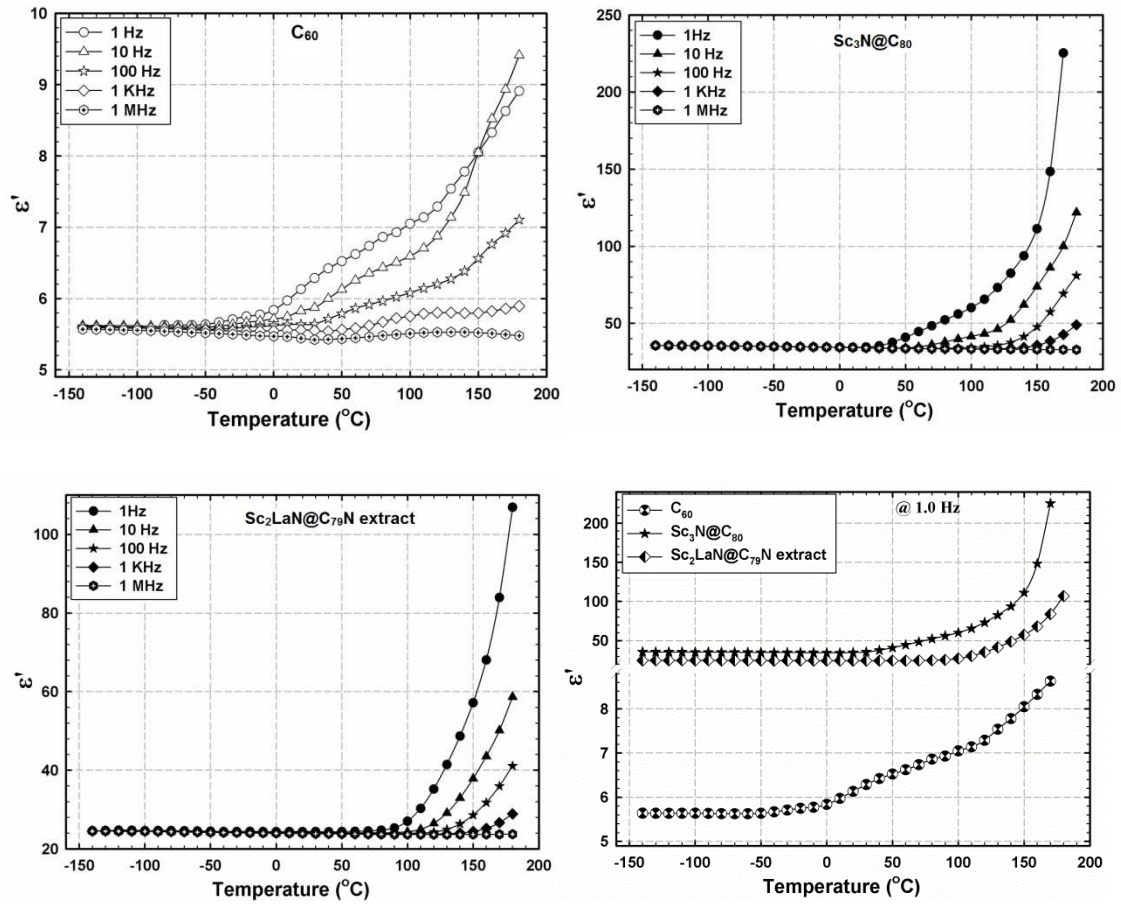

Figure 13. ε′ vs. temperature at different frequencies for all fullerenes.

The presence of different metals (Sc and La) inside the metallic nitride aza fullerene sample results in high polarizability of these dipoles and consequently, should also result in higher ε′ values for $Sc_2LaN@C_{79}N$ than those of $Sc_3N@C_{80}$. However, the aza sample is an extract containing only 5% $Sc_2LaN@C_{79}N$ and the rest, 95%, contains other fullerenes (e.g. empty C_{60} and C_{70}). As such ε′ values are expected to be less than those of $Sc_3N@C_{80}$. Their permittivity values might be higher if a 100% pure aza sample was tested.

Relevant to these results are studies that have shown that the molecules in solid C_{60} arrays rotate almost freely in a rotationally disordered high-temperature face-centered cubic phase (above -260 K at atmospheric pressure). On cooling, this motion slows down

and is transformed into a ratcheting or rocking motion in an orientation ordered simple cubic phase at low temperature or under high pressure.[121-123] Su et.al.[121, 122] demonstrated a structural phase transition at 260 K as well as an anomaly at 90 K resulting from a glass transition. Furthermore, they observed a Debye-like relaxation in the dielectric response which suggests the existence of dipole moments in microcrystalline C_{60} films.

The permittivities (ε′) vs. frequency for all hydroxylated fullerenes at different selected temperatures are shown in Figure 14.

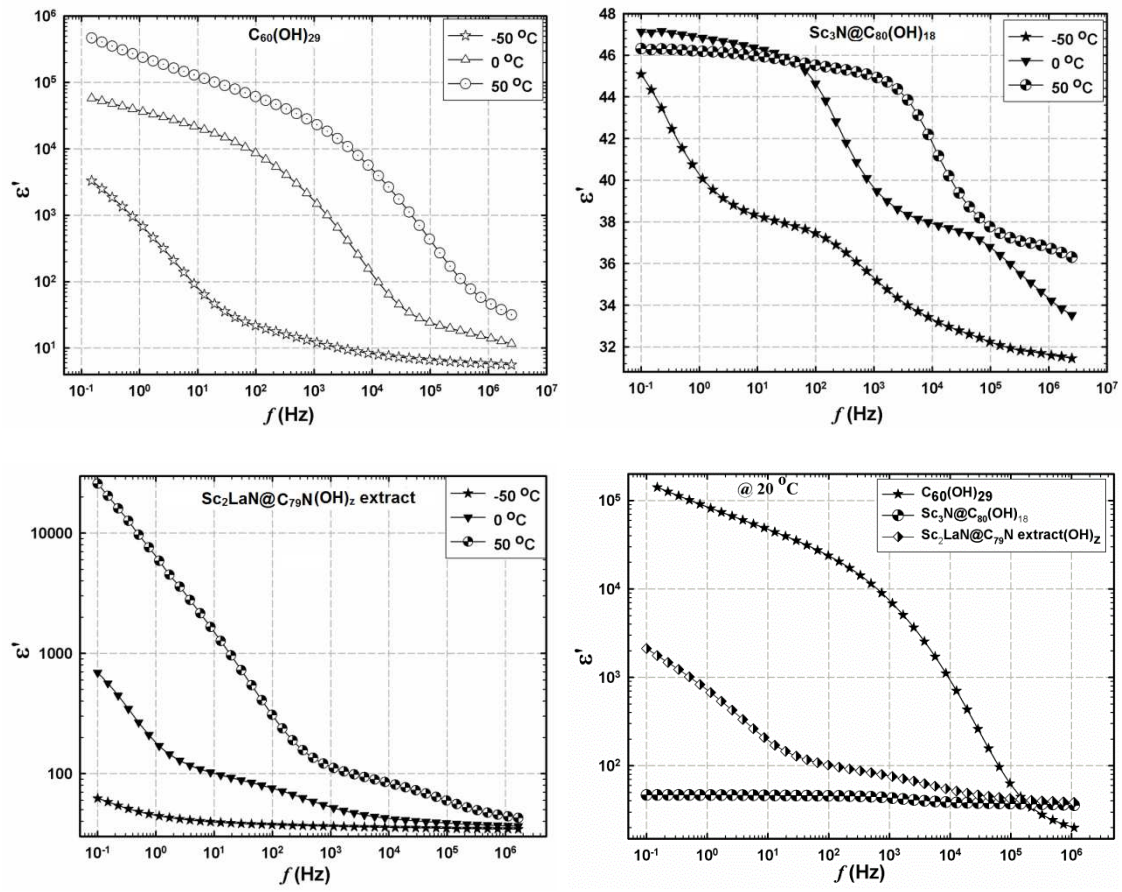

Figure 14. ε′ vs. frequency at different temperatures for all hydroxylated fullerenes.

The monotonically decreasing ε′ behavior in all cases is due, in general terms, to an increasing inability of the natural time scale of the dynamics of polarization to be captured within increasingly smaller signal time scales, i.e., decreasing 1/2*f*. ε′ vs. *f*

curves for $C_{60}(OH)_{29}$ are elevated with increasing temperature and the low frequency limits are rather large in all cases. These large values, compared to the low values for un-hydroxylated C_{60} particles at a given frequency as seen in Figure 13, are attributed to the addition of the polar OH groups to the outside of the cages. It would seem that the only way to achieve these high polarizabilities is for the hydroxylated C_{60} particles to rotate. Also, it is unlikely that the random hydroxylation is uniform across the C_{60} surface so that the dipole moments of all the O-H groups do not cancel each other such that these large molecules have a net dipole moment.

ε' values of hydroxylated C_{60} are much higher than those of hydroxylated $Sc_3N@C_{80}$ MNF and 5% $Sc_2LaN@C_{79}N$ extract, most likely because the former particles, $C_{60}(OH)_{29}$, have more OH groups than hydroxylated $Sc_3N@C_{80}$ MNF and (29 vs. 18, respectively). We were unable to evaluate the number of OH groups attached to the $Sc_2LaN@C_{79}N$ aza MNF cage due to the nature of the sample as a mixture of different fullerenes with only 5% $Sc_2LaN@C_{79}N$.

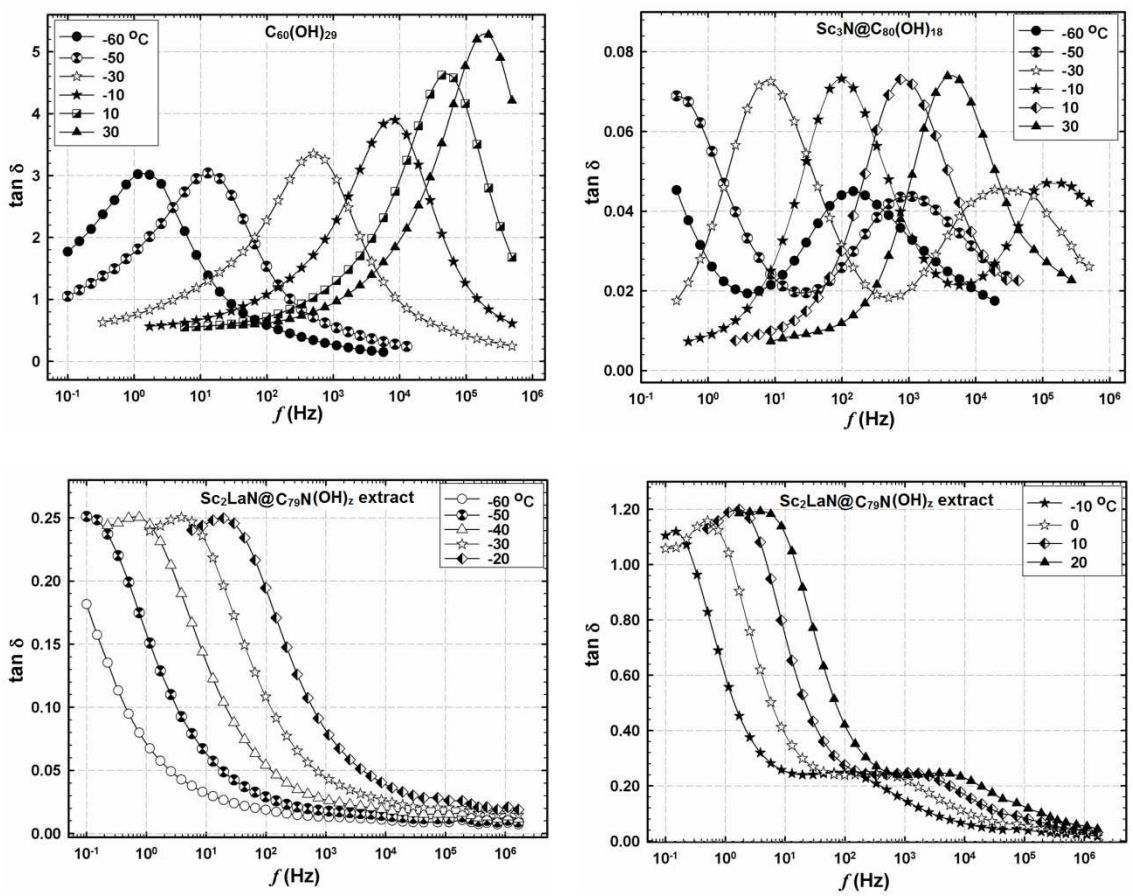

Figure 15. Frequency dependence of tan δ at different temperature for all hydroxylated fullerenes.

Figure 15 shows tan δ vs. *f* curves at different fixed temperatures for hydroxylated $C_{60}(OH)_{29}$, $Sc_3N@C_{80}(OH)_{18}$, and the hydroxylated 5% $Sc_2LaN@C_{79}N$. In all cases, it is seen that as the temperature increases, the tan δ peaks shift to higher frequencies as more thermal kinetic energy is imparted to polar groups causing greater ease of reorientation. Tan δ values for hydroxylated C_{60} are higher than those of hydroxylated $Sc_3N@C_{80}$ and hydroxylated $Sc_2LaN@C_{79}N$ owing to a higher degree of hydroxylation of the former, as mentioned. Interestingly, the curves for hydroxylated $Sc_3N@C_{80}(OH)_{18}$ (at temperatures -60 to -10) and for $Sc_2LaN@C_{79}N$ (at temperatures -10 to 30) are more complex in that there are two relaxation peaks on each spectrum. It is suggested that one peak is due to

cage reorientation while the other is due to tumbling motions of the Sc_3N molecule within the cage.

Dielectric properties of fullerene-PU networks. While the previous discussion dealt with the dielectric properties of individual particles (in packed configuration), the following is a presentation of results for such particles as cross-linking agents in a polymer network.

Figure 16 shows the ε″– f - T surface for C_{60}-PU film with 3% fullerene loading.

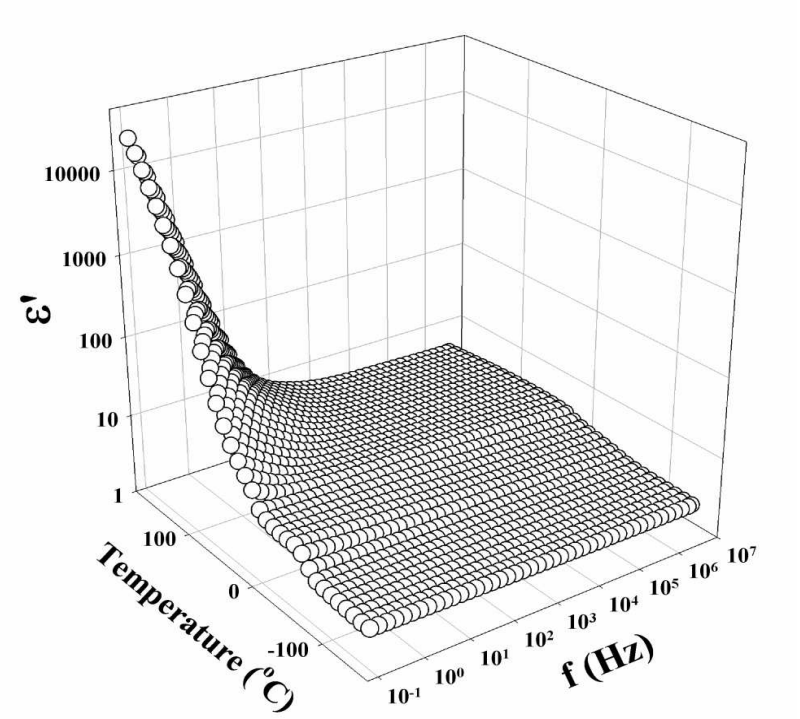

Figure 16. ε′– f - T surface for 3% C_{60}-PU network.

As shown in Figure 16, ε′ decreases with increasing frequency at fixed temperature, and this decrease is very prominent at low frequencies and high temperature. The decrease of ε′ with increasing frequency is the expected behavior in most dielectric materials. As frequency increases the time scale during which the electric field is applied in one direction decreases (*f* is 1/period), and the diploes do not have enough time to get

oriented in the direction of the electric field before it reverses. Therefore, the materials do not build up higher polarizability values. However, as the frequency is decreased, the time scales increased and the most mobile groups begin to orient, resulting in an increase in the observed dielectric constant, ε′.[129-131] Figure 16 shows also a stepwise increase in ε' with increasing temperature at fixed frequency, and this trend is more prominent at lower frequencies. The increase in ε′ with temperature is due to the increase in thermal kinetic energy that facilitate the free movement of polar groups of the polymer network which results in an increase in polarization, and consequently also in dielectric constant.[132] The very high values of ε′ at the highest temperatures might be due to sample-electrode interfacial polarization.

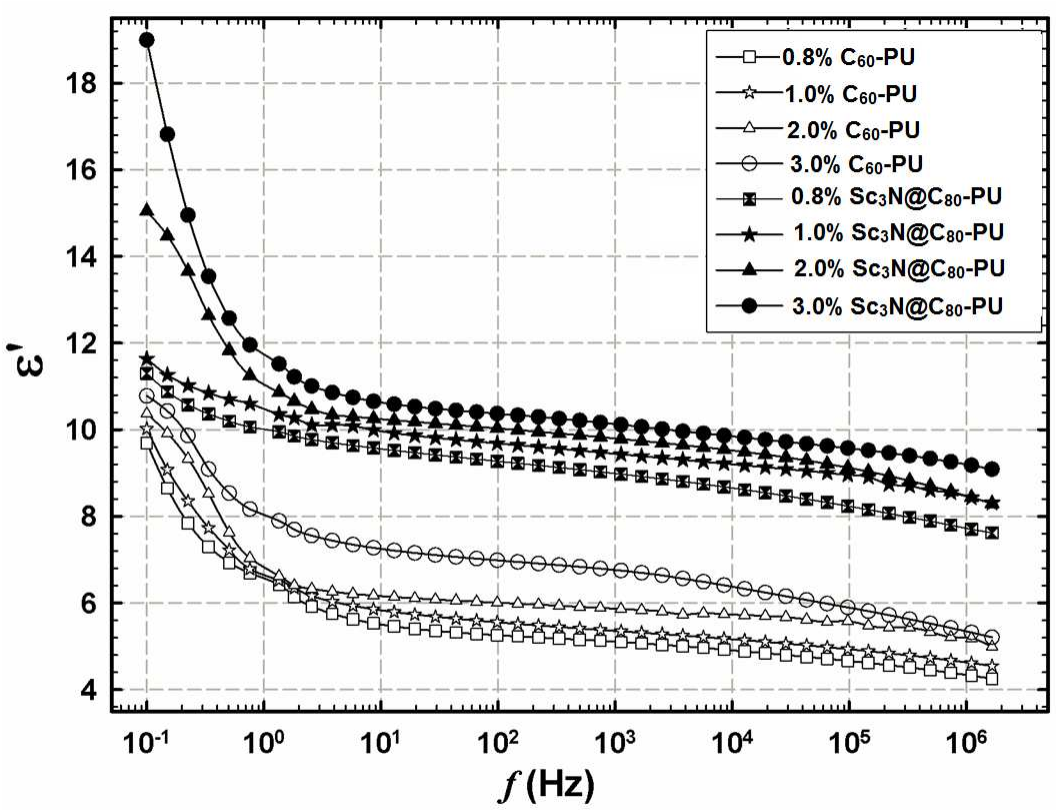

Figure 17. ε′ vs. *f* for fullerene-PU at 20 °C for fullerene-PU with different loadings of fullerene

The effects of particle type (empty vs. MNF) and particle loading on ε′ vs. *f* profiles of fullerene-PU networks are shown in Figure17 at 20 °C. The family of curves for $Sc_3N@C_{80}$-PU lies above the family for the C_{60}-PU networks, presumably due to rotationally-mobile dipoles within the structures of $Sc_3N@C_{80}$. For both C_{60}-PU and $Sc_3N@C_{80}$-PU networks, the curves for the fullerene-PU network elevate as fullerene loading increases due to the simple increase in the number of unreacted -OH groups bonded to the fullerene cages. Perhaps another factor for the upward curve shifts might involve an increase in polymer free volume v_f due to fullerene cages acting as polymer packing defects. Increase in v_f would make the PU chains more mobile, which, in turn, would affect greater ease in dipole reorientation. A similar effect was observed by Lu et al.[91] who studied the dielectric properties of benzylaminofullerene (BAF)-polyethylene composites as a function of BAF loading. However, the study of dielectric properties of polyimide films with different C_{60} and/or C_{70} loadings as admixtures by Subocz et al.[126] showed that as C_{60} or C_{70} concentration increases, the dielectric permittivity of the resultant films decreases due to restriction on polymer chain motions. Ouyang et al.[127] studied the effect of C_{60}-fullerenol density on the dielectric properties of C_{60}/poly(dimethylsiloxane), and found that at low fullerenol density, the real permittivity of the composite decreases as fullerenol loading increases due to restriction of polymer chain motions. However, at high density, the dielectric constant was seen to increase with increasing the fullerenol loading due to polarizability arising from unreacted -OH groups in the composite.

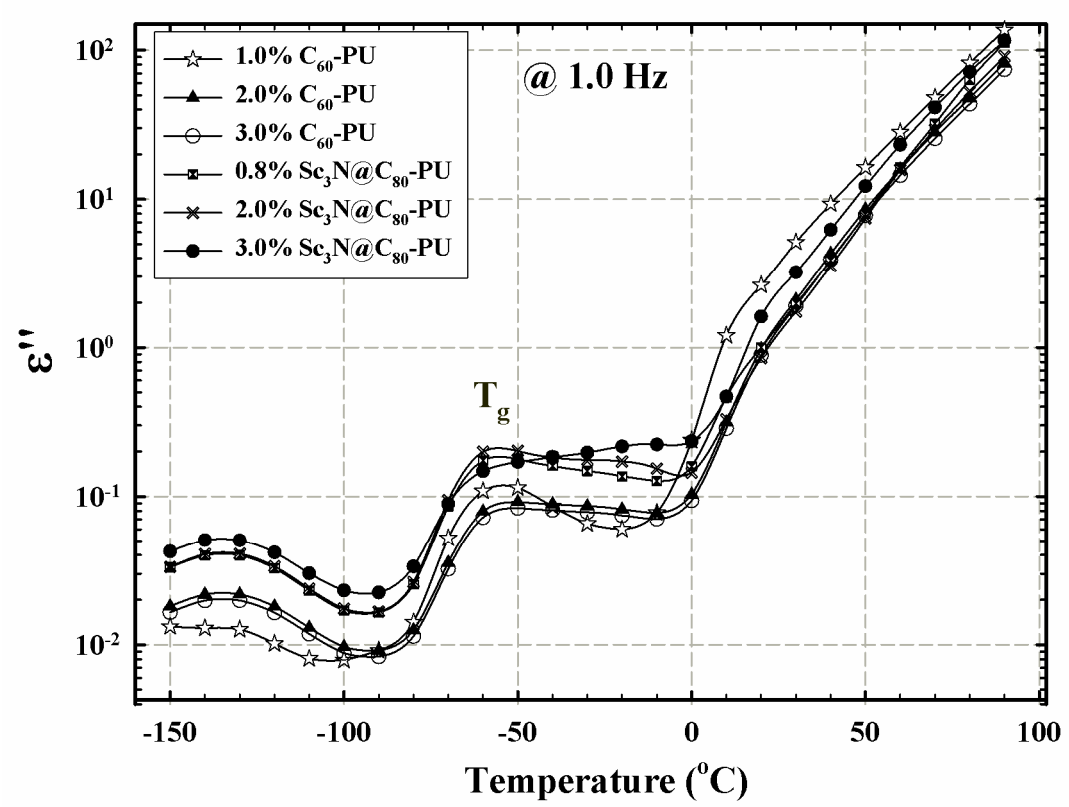

Figure 18. Temperature dependence of ε″ at 1.0 Hz for fullerene-PU at different loadings of fullerene.

ε″ vs. temperature at 1.0 Hz of fullerene-PU networks with different tethered fullerene loadings, some with Sc_3N molecules in cages, is shown in Figure 18. For T < 0 °C, three relaxation features are seen for all networks. After 0 °C, ε″ monotonically rises with increase in temperature and there are no relaxation peaks. Relaxation peaks occur at approximately the same low temperatures for all samples. Comparing these plots with the DMA plots in Figure 9, the peaks at around - 50 °C correspond to the glass transition and the peaks at around - 130 °C are due to short range chain motions in the glassy state. Support for the latter mechanism is that this relaxation appears the same whether or not the fullerene cages contain Sc_3N molecules The weak feature at ~ 25 °C corresponds to the dynamic mechanical feature, seen in figures 9 and 10, that was associated with thermally-driven reactions between un-reacted hydroxyl groups on $C_{60}(OH)_{29}$ and

polymer end groups. The ε″ curve for the lowest cross-linking degree (0.8% C_{60}-PU) is the lowest before T_g but becomes the highest after the glass transition. The curves for Sc3N@C_{80}-PU are above those of C_{60}-PU beneath T_g. Perhaps this is due to the fact that, while the mobility of dielectrically active –OH groups is suppressed beneath T_g, the cage-contained Sc_3N molecules continue to undergo a reorientation process.

To further investigate fullerene-PU network glass transitions, ε″ vs. *f* was plotted at different temperatures for 3% C_{60}-PU and 3% Sc_3@C_{80}-PU, and the results for these variants are seen, respectively in Figures 19 and 20.

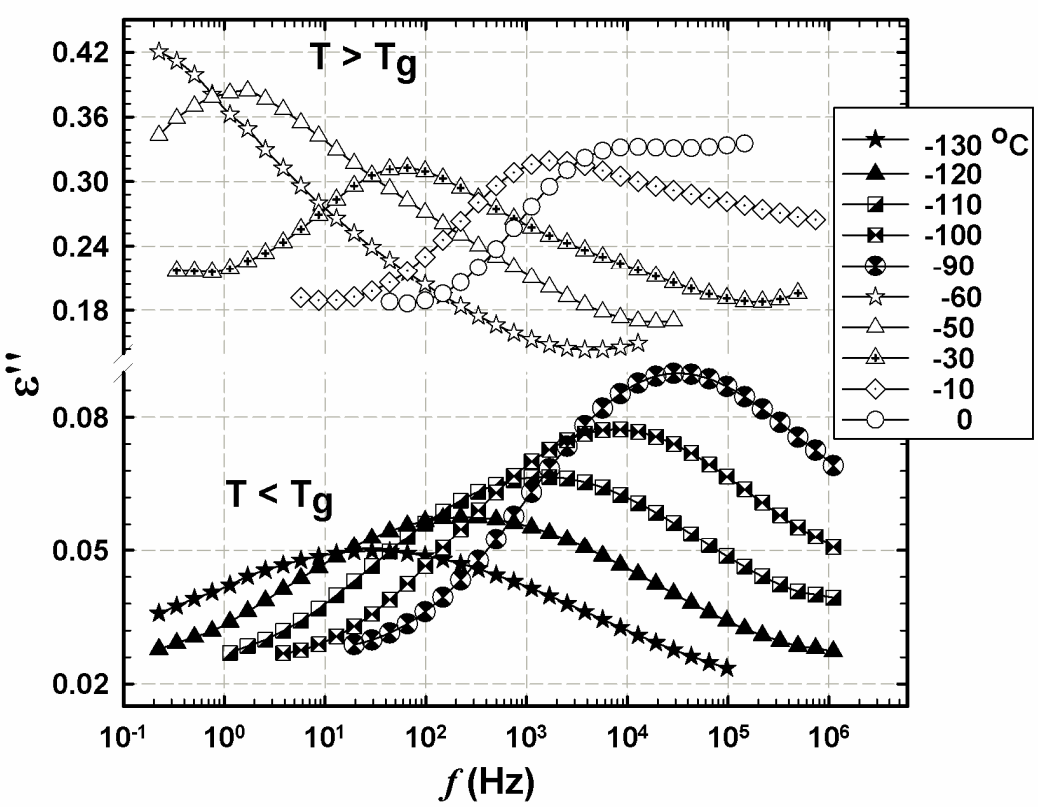

Figure 19. ε″ vs. *f* at different indicated temperatures, above and below the network T_g, for 3.0 % C_{60}-PU.

It is seen in figure 19 that the curves are split into two families: one for data points above, and the other for below the glass transition temperature. ε″ values within the sub-T_g family are considerably lower than those for above T_g. This can be simply

understood in terms of increased dipole reorientation mobility in the rubbery state facilitated by long range chain segmental mobility. As the temperature increases, the single, glass transition-related peak shifts to higher f_{max} as more thermal energy input increases the rate of PU chain segmental motions. However, below T_g the single relaxation must involve local motions along the PU chain and f_{max} for these peaks increases with increasing temperature.

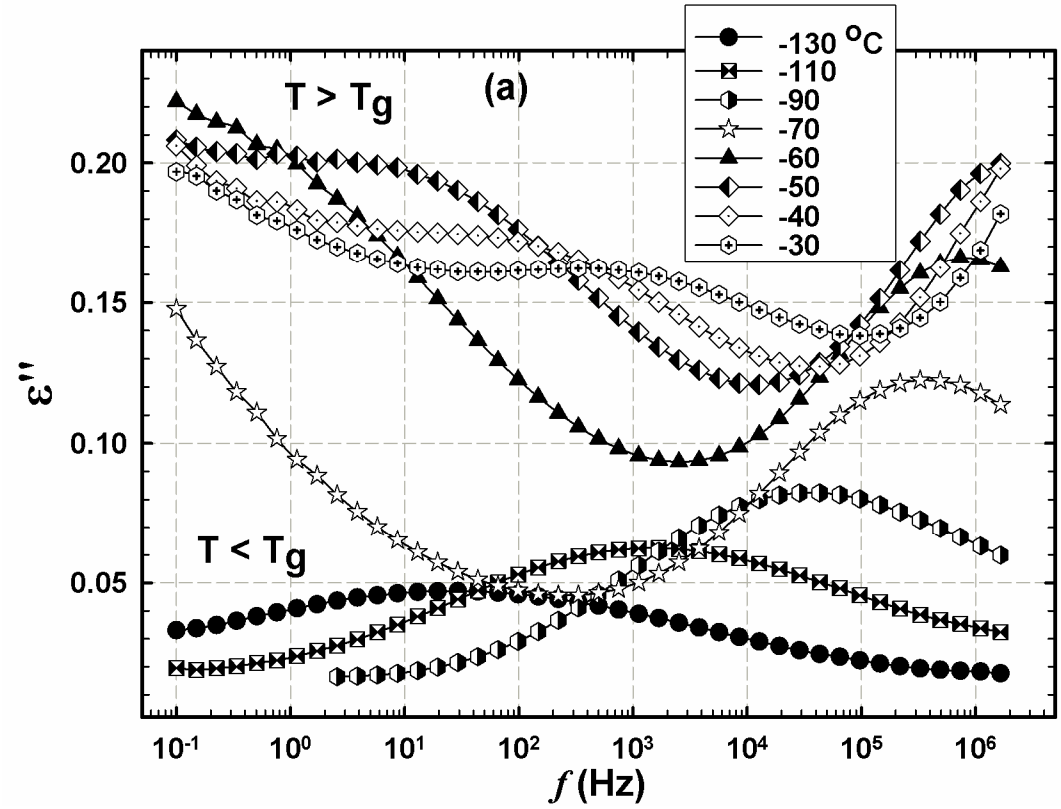

Figure 20a. ε″ vs. frequency at different temperatures for 3.0% $Sc_3N@C_{80}$-PU above and below the T_g.

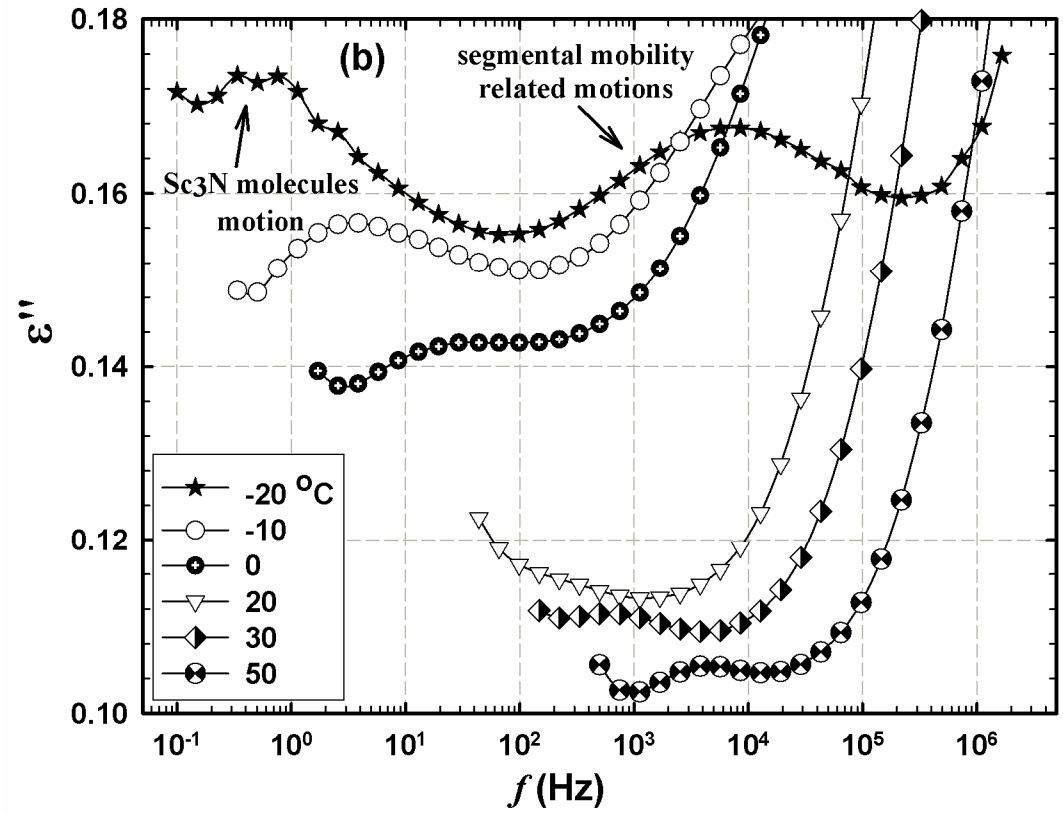

Figure 20b. ε″ vs. frequency at different temperatures for 3.0% $Sc_3N@C_{80}$-PU above the T_g. Tumbling motions of the cage-contained Sc_3N molecules are shown.

The same general comments can be made regarding the data seen in Figure 20a, and Figure 20b collected under similar conditions, except that there are fullerene cages that contain Sc_3N molecules. The curves, as before, are split into two families of curves above and below the glass transition temperature and ε″ values within the above-T_g curves are considerably greater than those in the sub-T_g curves. However, there is a significant difference in that there is an additional relaxation in the curves for $T > T_g$ in Figure 20b. The additional peak is attributed to reorientation motions of Sc_3N molecules in their cages as discussed above for non-PU-tethered pure particles. It is thought that the lowest frequency peak is due to segmental mobility as these long range polymer chain motions would be more sluggish than tumbling motions of the cage-contained Sc_3N molecules. It is seen that the sub-T_g curves in Figures 19 and 20 are essentially

independent of whether or not the cages contain Sc_3N molecules. This is attributed to the fact that the sub-T_g motions are of a local character and therefore not influenced by the nature of the chain ends.

Further details that focus exclusively on dielectric properties will investigate the temperature dependence of f_{max} for these two relaxations, and these details will be discussed in Chapter 4.

Resistivity Measurements

Introduction

Polymeric thin film materials exhibit extreme electrical properties that can be difficult to measure in a repeatable fashion. The primary goal of this research was to establish a reliable method for categorizing the electrical properties of elastomeric thin film materials, including surface and bulk resistivity because of their potential applications as shielding against electromagnetic/radio-frequency interface, electrostatic discharge and as heating elements for moderate temperatures.[133,134]

Polymers, in general, are good insulators with volume resistivity ranging from 10^{15} to 10^{22} Ω cm[135]. High-insulating polymeric insulators are more often used in high voltage equipment due to ease of machining, their excellent dielectric properties and their high volume resistivity. Particularly for use in high voltage equipments, the volume resistivity has to be determined in order to allow a proper choice of different insulating materials. Furthermore, the factors affecting the electrical properties of polymers, such as the humidity content, additives and temperature, have to be known in order to estimate change of volume resistivity which can lead to a distortion of the electric field distribution in high voltage systems during operation.

The resistance measurements of a device can be obtained by applying DC voltage across its terminals, and measuring the DC current through that device. For resistances in the gigohm and higher ranges, an electrometer, that can measure both very low current and high impedance voltage, must be used. Using such performance electrometer, resistances up to 10^{18} Ω can be measured, and special measurement precautions such as shielding and guarding must be applied to minimize leakage current, noise and other undesirable effects that can degrade the accuracy of the measurements.[136] Electronic engineers are interested in these characteristic measurements to determine basic parameters of devices such as those made of polymeric materials and to model their behaviors in an electrical circuit.

Measurements

Current-voltage characteristics, I-V, of the samples were measured using a Keithley multimeter model 2400-SCS equipped with Keithley 8008 stainless steel test fixture using the ASTM D257 standard,[137] Figure 21. It is an extremely versatile system that was also used in this study to measure capacitance vs. applied DC voltage.

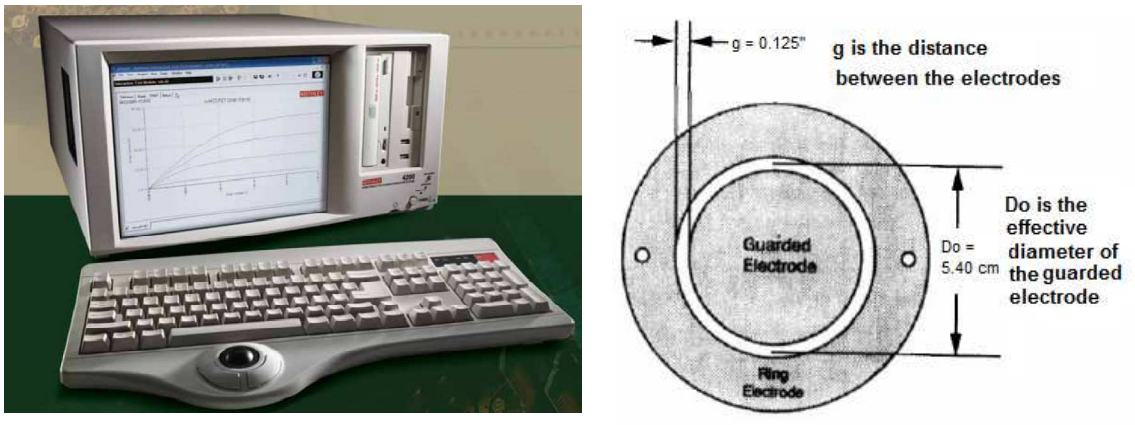

Figure 21. Keithley 4200-SCS multimeter (left) and Keithley 8008 electrode dimensions (right)

The basic measurement connections for the volume and surface resistivity measurements using Keithley 8008 electrode are shown in Figure 22.[136] The volume resistivity is measured by applying a voltage across the sample, ranging from - 210 to + 210 volt, and measuring the resulting current. However, the surface resistivity is measured by applying a voltage across the surface of the sample, between the bottom two electrodes. The resistivity is calculated from the geometry of the electrodes, shown in Figure 21, and the thickness of the sample. The recommended sample size for the 8008 test fixture is 3 to 4 inches in diameter and between 0.001 and 0.125 inch thick.

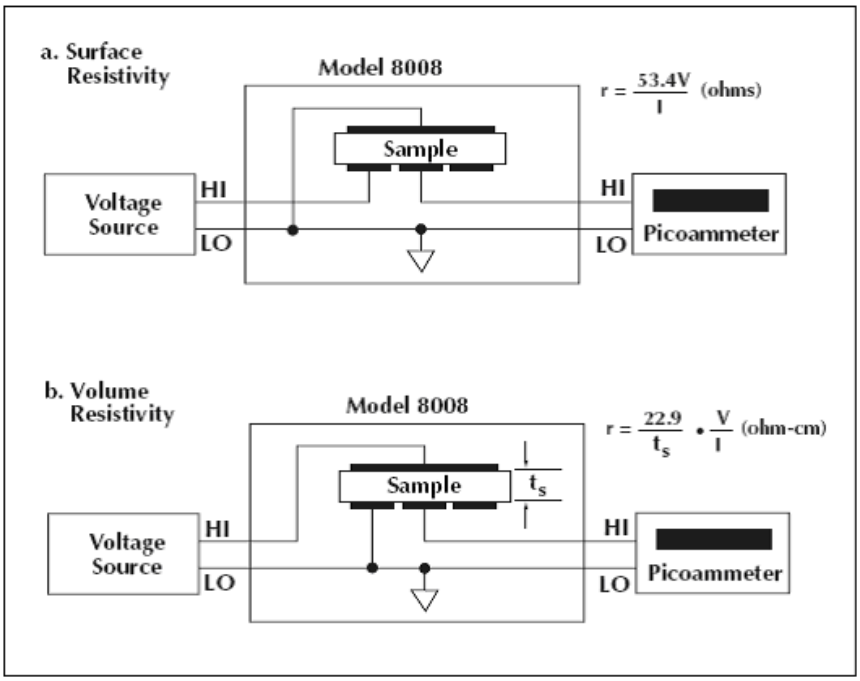

Figure 22. Schematic draw showing the electronic connections for the resistivity measurements.
Keithley Catalog. *Volume and Surface Resistivity Measurements of Insulating Materials;* [Online]; Keithley Instruments, Inc. 2001.

I-V characteristics of three C_{60}-PU films, with 1%, 3%, and 5% C_{60}, were measured at room temperature, 22 ^{o}C, and at different humidity content, 5%, 20% and 50%. The same measurement, under the same conditions, was performed for

5%$Sc_3N@C_{80}$-PU film for comparison. The volume and surface resistivities were, then, calculated from the equations shown in Figure 22.

Data and Discussion

The current-voltage profiles of the prepared fullerene-PU samples were shown in Figure 23. The slopes of the plots on left are the surface resistance from which the surface resistivity, σ, was calculated. However, the volume resistivity, ρ, was calculated from the slopes of the plots on right. The surface and volume resistivities of all samples at different humidity, 5%, 20% and 50%, are summarized in table 5.

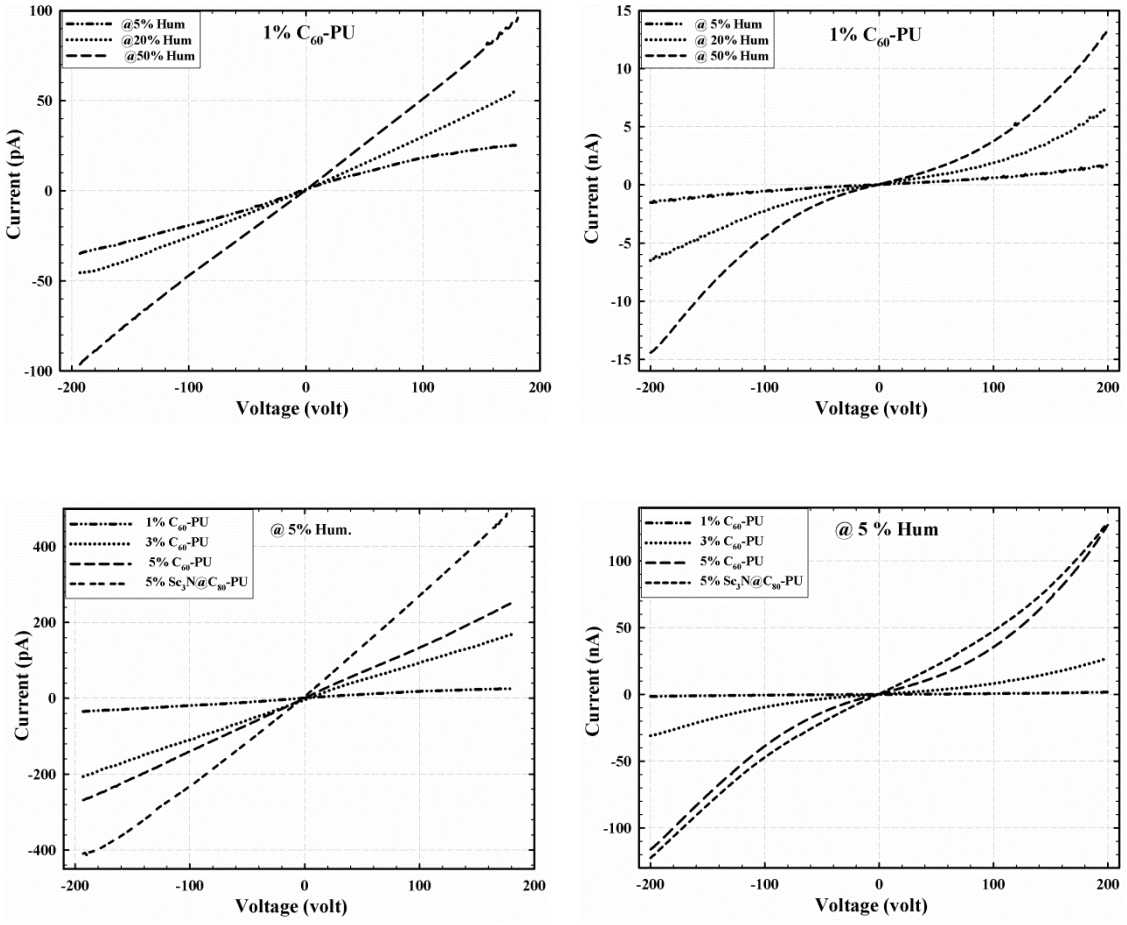

Figure 23. I-V profiles of fullerene-PU samples. Surface resistivities will be calculated from the slopes of plots on left, however, volume resistivities will be calculated from the slopes of plots on right.

The large discrepancy in voltage to current shows that according to Ohm's law, all samples very large volume and surface resistivity, and they demonstrate nonlinear I-V characteristics. The observed nonlinearity can be associated with two factors: (1) specific conductivity mechanism in the samples and (2) humidity in the chamber, and this nonlinearity increases as humidity increases. It is also shown in these plots that surface and the volume resistivities decrease with increasing the humidity content due to the effect of the conductivity arises from the water molecules. The plots show also that the electrical current that is passing through the fullerene-PU samples increases with increasing the fullerene contents. Consequently, both surface and volume resistivities decrease as the fullerene contents increase. By comparing the samples containing 5% C_{60} to that containing 5% $Sc_3N@C_{80}$, it is noticed that the surface and volume resistivity of 5% $Sc_3N@C_{80}$-PU sample is smaller than those of 5% C_{60}-PU. This decrease in resistivity, or increase in conductivity, is attributed to the presence of the metal nitride cluster, Sc_3N, inside the cage of the MNF, which alters the fullerene electronic structure.[21-24]

The values of volume resistivity of our prepared fullerene-networks lie between 10^{12} to 10^{14} Ω cm, and as mentioned above, polymers with volume resistivity ranging from 10^{15} to 10^{22} Ω cm are considered good insulators,[135] thus these materials might not utilized as good insulators. In the following section, we will study the capacitance - voltage characteristics of these samples and ensure their ability to be used in applications of charge separation and storage.

Table 5

Surface and Volume Resistivity of Fullerene-PU Samples at Different Fullerene Contents and at Different Humidity Percentages

Sample / Humidity %	Surface resistivity (Ω)			Volume resistivity (Ω cm)		
	5%	20%	50%	5%	20%	50%
1%C60-PU	2.8E+14	2.2E+14	1.1E+14	3.3E+14	1.0E+14	5.7E+13
3%C60-PU	5.1E+13	3.9E+13	3.3E+13	3.2E+13	1.3E+13	7.2E+12
5%C60-PU	3.8E+13	3.0E+13	2.3E+13	6.2E+12	4.7E+12	2.4E+12
5%Sc3N@C80-PU	2. 5E+13	2.2E+13	2.3E+13	4.58E+12	3.8E+12	4.3E+12

Capacitance-Voltage Measurements

Introduction

Physical characterization of semiconductor device has always been a challenging task for device engineers and researchers. Capacitance-voltage, C-V, measurement refers to a technique used for characterization of semiconductor materials and devices by varying the applied DC voltage and recording the response in the capacitance change. These measurements are extremely important to product and yield enhancement engineers, who are responsible for improving processes and device performance. The fundamental nature of these measurements makes them useful in a wide range of applications and disciplines since they are used to evaluate new materials, processes, devices, and circuits.[138]

For any material to be used as a semiconductor or energy storage, it should be easy to transfer their electrons from the valence band to the conduction band, Figure 24.

Generally, an external bias voltage is required to efficiently separate the electrons and holes and thus prevent their recombination, and the efficiency of the semiconductors can be enhanced by reducing both their band gap and their highest occupied molecular orbital.

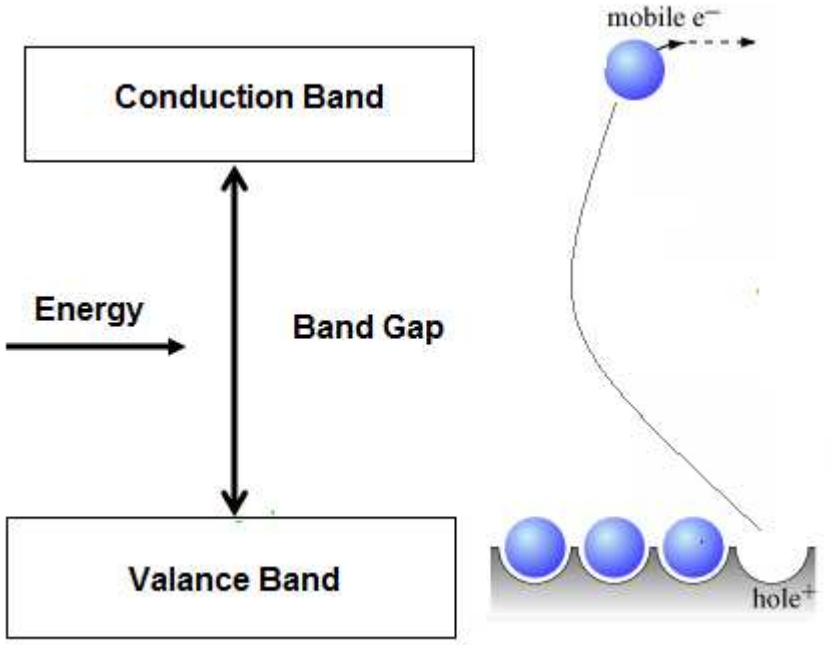

Figure 24. Schematic draw shows the principle of electron-hole separation.

Polymeric organic photovoltaic (OPV) cells with polymer fullerene bulk hetero-junction are promising candidates for future low-cost, high-performance energy sources, owing to their low material and processing costs and mechanical flexibility.[139-141] In many of the most efficient polymer-fullerene OPV devices, 50% or more of the energy loss is caused by the recombination of electrons and holes.[139,142,143]

A new method was reported recently by Yuan et.al to enhance the efficiencies of fullerene-polymer devices by incorporating a ferroelectric polymer layer into these devices which to ensure a large, permanent, internal electric field that can eliminates the need for an external bias. The enhanced efficiencies are 10–20% higher than those

achieved by other methods, such as morphology and electrode work-function optimization.[139] Furthermore, the devices showed the unique characteristics of ferroelectric photovoltaic devices with switchable diode polarity and tunable efficiency.

The most common tunable dielectric materials are ferroelectrics, which are polar materials having at least two equilibrium orientations of a spontaneous polarization vector. However, despite considerable advancements in the application of ferroelectrics to tunable dielectrics in recent years, these materials still possess unacceptable high losses and limited tunability, especially where application to high frequency and room temperature requirements must be met. To be tunable, the direction of polarization must be capable of switching after application of an external electric field.

Encapsulation of metal atoms inside fullerene cages, forming MNF, was found to significantly modify the fullerene electronic structure and produce novel materials, which hold promise in applications of charge separation, transport, and storage.[21-24] Thus, the most valuable goal of our study is to evaluate these unique materials as new low-loss materials for tunable dielectric applications, which are suitable for high-frequency applications and possess significant tunability at low temperatures. For example, in the erbium-scandium family of mixed-metal MNFs, a permanent dipole moment is produced when the three metals are dissimilar, e.g. $Er_2ScN@C_{80}$. Judicious choice of the metal cluster among the available lanthanides will provide a significant permanent electric dipole which may be oriented using an applied electric field, Figure 25.

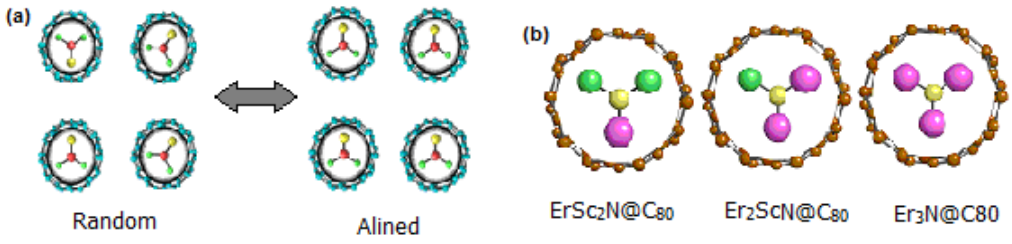

Figure 25. (a) aligned and random orientation extremes of MNFs having electronic or magnetic dipoles resulting from the incorporation of dissimilar metals; (b) example of erbium mixed-metal MNF system.

Measurements

In addition to determining the I-V characteristics of our samples using Keithley 4200-SCS multimeter, capacitance-voltage measurements, and capacitance-frequency measurements can be performed for our prepared networks. Capacitance-Voltage Unit, (CVU) can measure the capacitance as a function of an applied DC voltage (C-V) by connecting the sample under evaluation to the 4200-CVU as shown in Figure 26.[138] The C-V measurement involves a four-wire connection to compensate for lead resistance. The HPOT/HCUR terminals are connected to the anode and the LPOT/LCUR terminals are connected to the cathode. This connects the high DC voltage source terminal of the CVU to the anode.

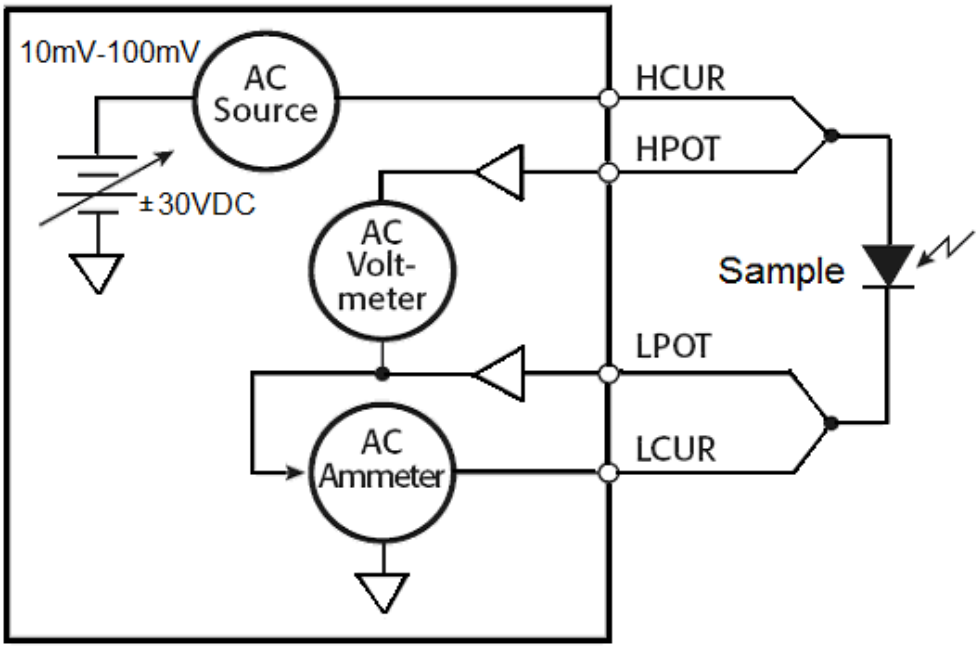

Figure 26. Schematic draw shows the connections in C-V measurements using Keithley 4200-SCS multimeter.
Stauffer, L. *Fundamentals of Semiconductor C-V Measurements*, [Online]; Keithley Instruments, Inc., 2009.

The capacitive chamber, shown in Figure 27 and made by S. Bunkley (R. Buchanan research group, School of Computing, USM), is intended to be an all encompassing enclosure that has the ability to maintain a suitable environment for testing the samples accurately. Prior to the measurements, the samples are allowed to saturate in the dry air for an extended amount of time before performing the measurements, the space below the shelf can be used to store the samples that are not currently being tested. The enclosure is grounded so that it will provide electrical shielding from nearby equipment. The conductive plates are wired to shielded BNC cables that mount to the exterior of the fixture. A digital depth micrometer is connected to one of the conductive plates. This allows for thickness measurements to be taken without disturbing the material before a test. The temperature and humidity sensors along with a Light Emitting Diode (LED) are mounted within the box.

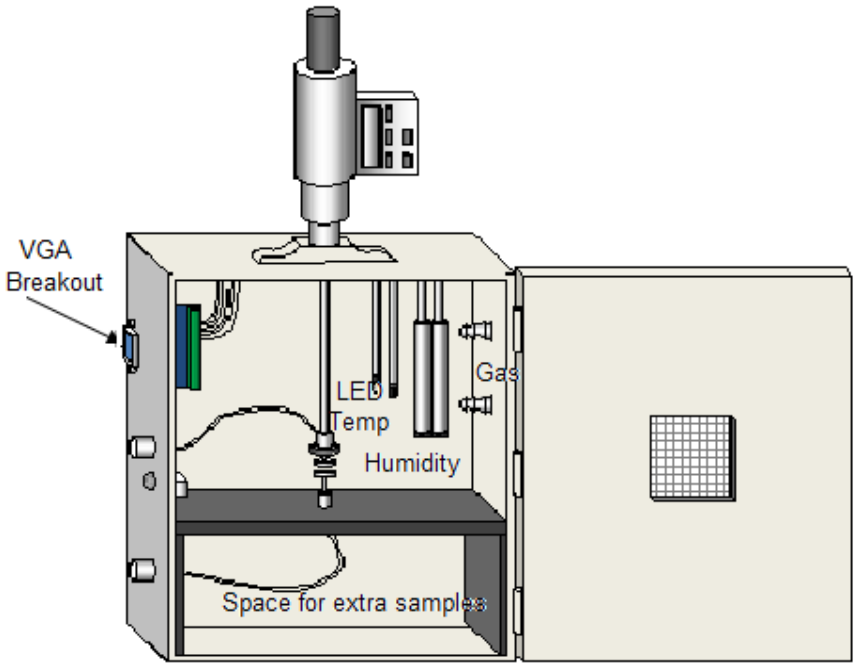

Figure 27. Schematic draw describes the capacitive chamber used for the C-V measurements

The procedure for performing C-V measurements involves the application of DC bias voltages across the sample while making the measurements with an AC signal. Commonly, AC frequencies from 10^3 Hz to 10^7 Hz, and DC bias voltages from -30 to +30 volts are used for these measurements. By comparing the frequency range of this instrument with that of the broadband dielectric spectrometer (Novocontrol spectrometer), it was noticed that we extended the frequency range up to 10 MHz to monitor any other polarization mechanism that might take place within our samples in this frequency range.

Using Keithley 4200-SCS multimeter, all measurements were performed at room temperature (22 ^{o}C), using a sample film sandwiched between two conductive plates of 1.25 cm diameter, and under a controlled humidity (< 1.0% humidity). Because C-V measurements are actually made at AC frequencies, the capacitance for the sample under test is calculated using the following equation:

$$C = \frac{I_{max}}{2\pi f V_{AC}} \quad (6)$$

where, I_{max} is the magnitude of the AC current through the sample, *f* is the test frequency, and V_{AC} is the magnitude and phase angle of the measured AC voltage. In other words, the test measures the AC impedance of the sample by applying an AC voltage and measuring the resulting AC current, AC voltage, and impedance phase angle between them. These measurements take into account series and parallel resistance associated with the capacitance, as well as the dissipation factor (leakage), D. The permittivity, ε', and loss, ε'', were, then, calculated from the following equations:

$$\varepsilon' = \frac{d\ x\ C}{A\ x\ 8.85\ x\ 10^{-12}} \quad (7)$$

$$\varepsilon'' = \varepsilon' x\ D \quad (8)$$

where, A is the area of the sample, and d is its thickness. The value 8.85 x 10^{-12} is the permittivity of vacuum.

Data and Discussion

The frequency dependence of the permittivity of fullerene-PU networks, measured using Keithley 4200-SCS, was shown in Figure 28. The data shown here were close to those shown in Figure 17, within the same frequency range. This observation is very important to ensure our measurements using this new instrument and the handmade test fixture. As explained previously, and up to 3MHz, ε' of all samples decreases with increasing the frequency because at higher frequencies, the dipoles did not have enough time to follow the alteration of the applied electric field. After 3 MHz, ε' started to increase again with increasing the frequency, and this increasing might be due to another

polarization mechanism rather than dipole polarization. Similar observation was seen in Figure 29 which shows the ε″ vs. frequency for fullerene-PU networks.

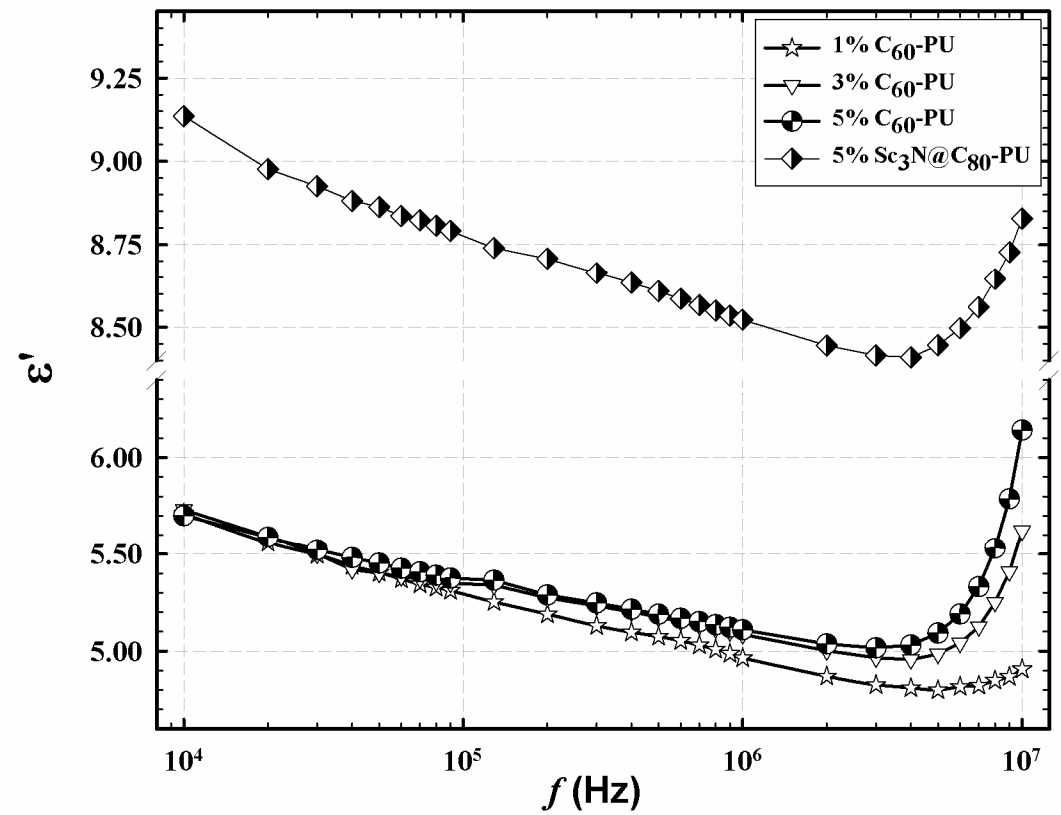

Figure 28. ε′ vs. *f* for fullerene-PU at 22 °C at different fullerene loadings. The data were collected from Keithley 4200-SCS.

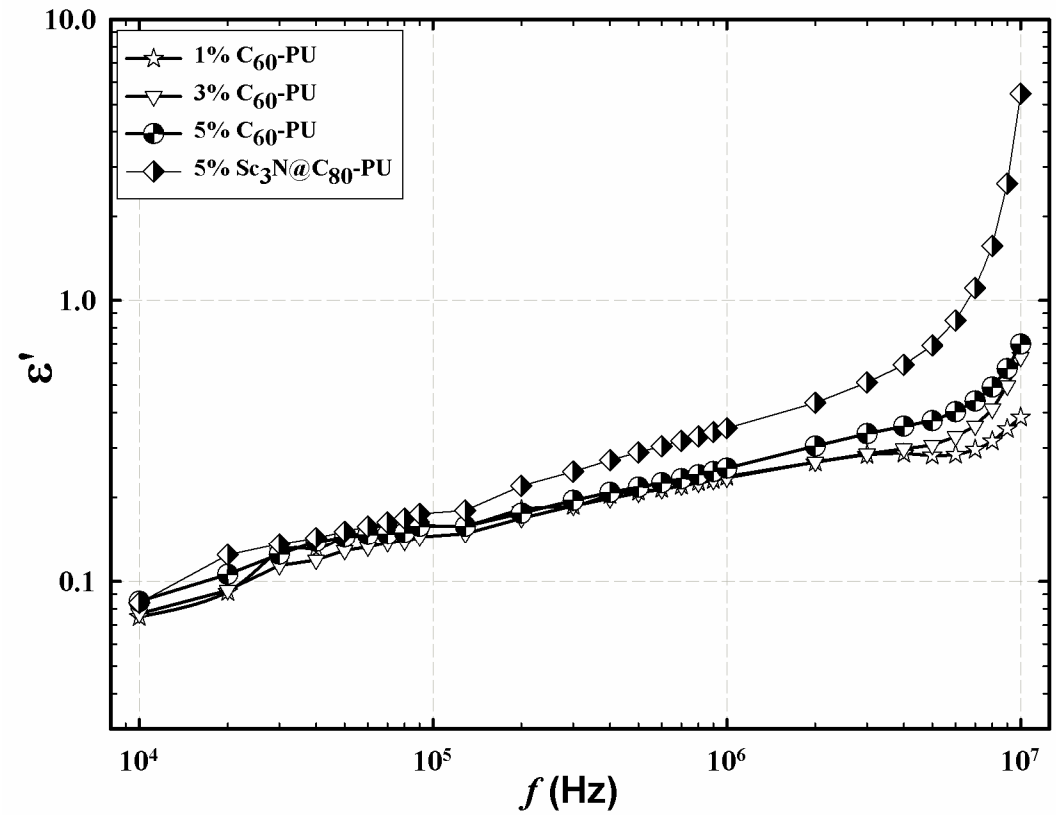

Figure 29. ε″ vs. *f* for fullerene-PU at 22 °C at different fullerene loadings. The data were collected from Keithley 4200-SCS.

The most interesting observation in the dielectric properties of our samples, is the higher values of dielectric permittivity, ε′, over the loss permittivity, ε″, thus these samples might be desirable for many electronic and electric systems provided they are capable of storing and releasing electrical energy.[144] Since the maximum electrical energy storage capacity (U_{max}) of a linear dielectric material is given by $U_{max} = \varepsilon' E_b^2/2$, since E_b is the dielectric breakdown strength (DBS), both large ε′ and high DBS are required for large electric energy storage.[144-147] Consequently, incorporating materials with large ε′ within polymeric matrices of high DBS and excellent mechanical properties might lead to a large energy storage dielectric. [144, 146,147]

Similar conclusion about the importance of our materials (fullerenes and fullerene-PU networks) as energy storage systems can be observed in Figure 30 and

Figure 31 that show the higher ε′ values over the ε″ values for $Sc_3N@C_{80}$ and 3% $Sc_3N@C_{80}$-PU as investigated by the broadband dielectric spectrometer at 20 ^oC.

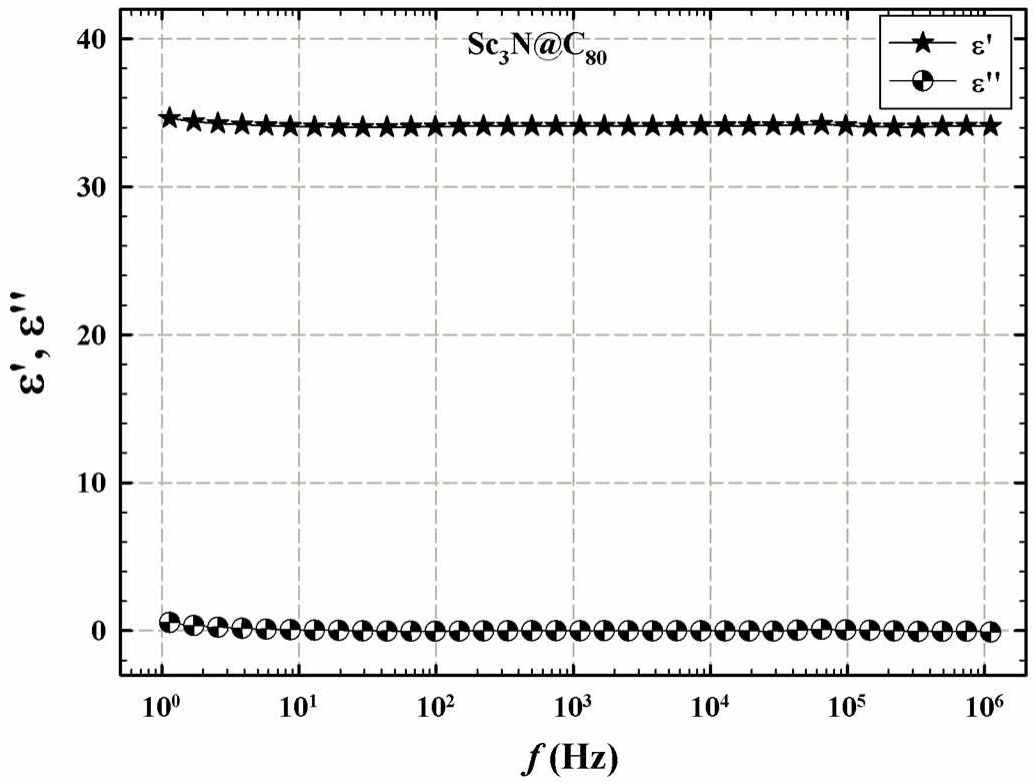

Figure 30. ε′ and ε″ vs. f for $Sc_3N@C_{80}$ at 20 ^oC. The data were collected from Novocontrol dielectric spectrometer.

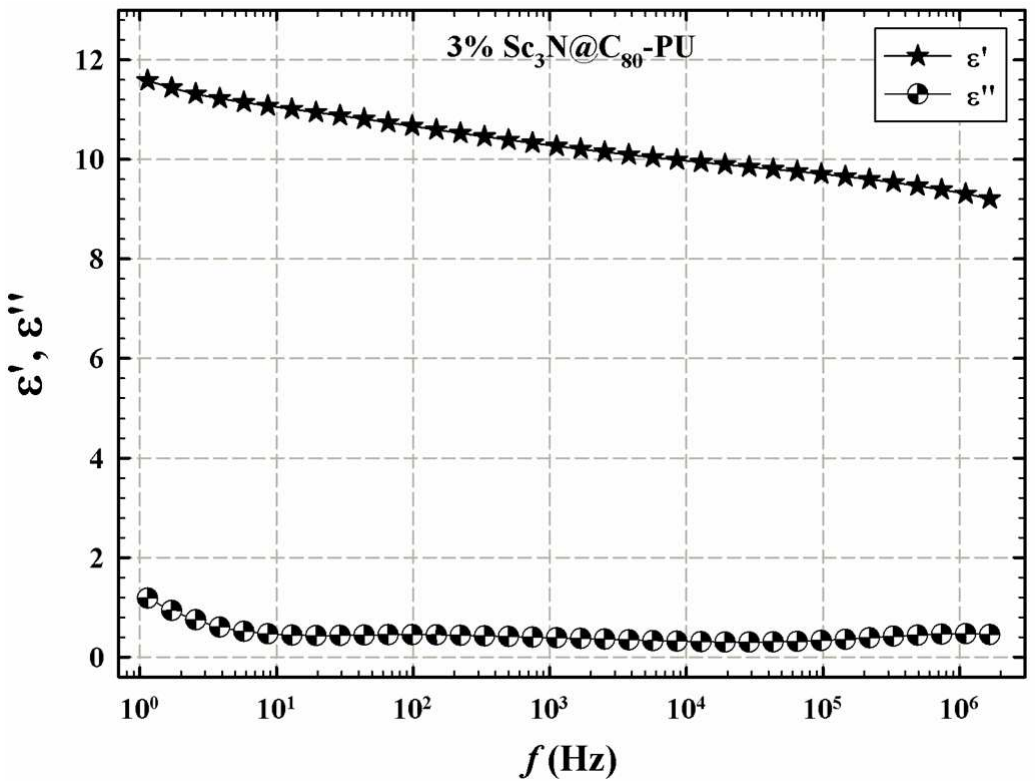

Figure 31. ε′ and ε″ vs. f for 3% $Sc_3N@C_{80}$-PU network at 20 ^oC. The data were collected from Novocontrol dielectric spectrometer.

The permittivity vs. applied DC bias voltage for fullerene-PU samples is shown in Figure 32, and this data was collected at 1MH using Keithley 4200 SCS multimeter. For all samples, and within our voltage range, there is no significance change in permittivity with changing the applied voltage, especially at low loading of fullerene. These samples might need higher voltage to be transferred to their conductive state and to behave nonlinearly with the applied voltage.

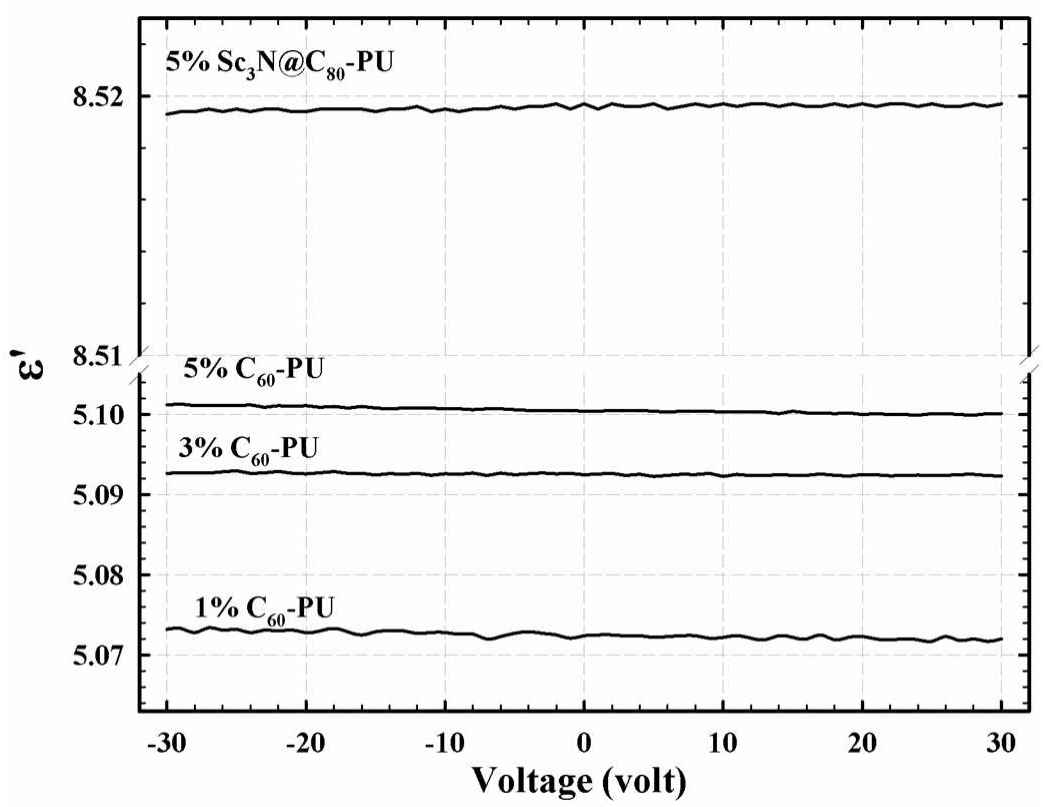

Figure 32. ε′ vs. applied dc. voltage, at 1 MHz, and at 22 ^{o}C for fullerene-PU networks.

CHAPTER IV

MACROMOLECULAR DYNAMIC OF FULLERENES AND FULLERENE-CONTAINING POLYURETHANE NETWORKS

Introduction

Macromolecular dynamic of polymer is of fundamental importance in polymer physics.[110,148] Since many macroscopic properties of polymers, such as mechanical and thermal, are the reflection of microscopic polymer chain motions, it is important to study polymer dynamics. Among all methods that study the viscoelastic transitions in polymers, broadband dielectric spectroscopy is used as a tool for probing the molecular dynamics of polymers over a broad frequency range from the milli- to mega-hertz region.[114] Therefore, motional processes which take place in polymers on extremely different time scales, or relaxation times, can be investigated versus temperature. The relaxation time (τ) is frequency dependent given by $\tau = 1/(2\pi f_{max})$, where f_{max} is the frequency corresponding to the loss peak.

In polymers, the observable polarization results mainly from the orientation or alignment of dipoles of polymer molecules, and macromolecular motions in polymers result in multiple relaxation behaviors where each process is indicated by a peak in ε'' and a step-like decrease in ε' versus frequency at a fixed temperature.[113] in analyzing dielectric spectra, the relaxation time corresponding to each type of molecular motions are extracted from model functions. Although polymers do not show pure Debye, but modified Debye behavior, the Havriliak-Negami (HN) equation shows strong adaptability to polymers and complex systems.[114, 149,150]

The HN equation, below, is fitted to the experimental data obtained from the broadband dielectric spectroscopy to extract useful parameters that give more information about the relaxation processes taken place in our prepared samples. This equation represents dielectric spectra with an additional term to account for possible dc conductivity at low f [114, 149]

$$\varepsilon^*(\omega) = \varepsilon' - i\varepsilon'' = -i\left(\frac{\sigma_0}{\varepsilon_0 \omega}\right)^N + \sum_{k=1}^{n}\left[\frac{\Delta\varepsilon}{\left(1+(i\omega\tau_{HN})^{\alpha_{HN}}\right)^{\beta_{HN}}} + \varepsilon_{\infty k}\right] \tag{9}$$

Each term in the sum represents a different relaxation process. Parameter values result from fitting this equation to experimental data. $\Delta\varepsilon = \varepsilon_o - \varepsilon_\infty$ is the difference between the low and high frequency limits of ε' for a given process. τ_{HN} is a time related to the actual relaxation time, τ_{max}, associated with the frequency at peak maximum, f_{max}. α_{HN} and β_{HN} are measures of the breadth and symmetry, respectively, of the given relaxation such that $\alpha_{HN} < 0 \leq 1$ and $0 < \beta_{HN} \leq 1$. α_{HN}, β_{HN} and τ_{HN} are used to determine τ_{max} using equation 10: [151]

$$\tau_{\max} = \tau_{HN}\left[\frac{\sin\left(\frac{\pi\alpha_{HN}\beta_{HN}}{2(\beta_{HN}+1)}\right)}{\sin\left(\frac{\pi\alpha_{HN}}{2(\beta_{HN}+1)}\right)}\right]^{\frac{1}{\alpha}} \tag{10}$$

When present, dc conductivity can obscure polymer relaxations that occur at low frequencies resulting in a superposition with the α relaxation. This superposition is removed once N (≤ 1) and the dc conductivity σ_0 are determined by curve fitting in the low f regime so that this term is subtracted point-by-point from ε″ curves to reveal un-obscured relaxation peaks.

Isothermal dielectric permittivity data were fitted to the HN equation including the dc term to obtain τ_{HN}.[149] The d.c. term accounts for inherent or unintended (impurity) charge migration that is often subtracted to uncover loss peaks corresponding to macromolecular motions. It is especially necessary to resolve relaxation peaks at temperatures above T_g at which d.c. conduction becomes stronger.[152] As the experimental time scale, that is, one half the period of electric field oscillation = $(2f)^{-1}$, increases, mobile charges can execute more elementary hops before the applied field reverses. In the low *f* region, ε'' is directly proportional to σ_{dc} according to the equation:

$$\varepsilon'' \approx \sigma_{dc}/2\pi f \varepsilon_0 \tag{11}$$

Loss-frequency spectra can also be analyzed via the Kramers-Krönig transformation, K-K transformation, equation 12. ε_0 is the vacuum permittivity, and the second term on the right, labeled ε''_{kk}, is an integral transformation from the real to the imaginary permittivity evaluated at a particular frequency ω_0[153,154]

$$\varepsilon''(\omega_0) = \frac{\sigma_0}{\varepsilon_0\,\omega_0} + \frac{2}{\pi}\int_0^\infty \varepsilon'(\omega)\frac{\omega}{\omega^2-\omega_0^2}d\omega = \frac{\sigma_0}{\varepsilon_0\omega_0} + \varepsilon''_{kk} \tag{12}$$

As in the HN equation, experimental values of $\varepsilon''(\omega_0)$, on the left side of equation 8, include resistive losses. The relaxation terms in the sum in equation 5 become more distinct after subtraction of the obscuring d.c. conduction term $\sigma_0/\varepsilon_0\omega_0$ from measured values of $\varepsilon''(\omega_0)$ point-by-point, over the frequency range. Equation 12 offers an alternative route whereby this subtraction is not necessary because ε''_{kk} involves the real permittivity in the integral that does not involve resistive losses so that it is not necessary to deal with the conductivity term. Therefore, pure relaxations can be extracted knowing

experimental $\varepsilon'(\omega)$ values over a broad frequency range and performing a numerical integration that yields ε''_{kk}.

Data Analysis

As mentioned above, to obtain parameters that quantify the nature of relaxations taken place in our prepared samples (hydroxylated fullerenes and fullerene-PUs networks), curve fitting to dielectric permittivity data was performed by two ways; (1) the Novocontrol Winfit program by which the HN was best-fitted to the loss (ε'' vs. f) spectra, and (2) K-K transformation by which the Ohmic conduction loss-free data were obtained.

To calculate K-K transformations, software which adopted the K-K transformation algorithm developed by Steeman and van Turnhout[153,154] was constructed in C programming language under the Linux operating system. This software was written by Dr. A. Abukmail, School of Computing, USM.

Results and Discussion

In this section we will discuss the analyzed data investigated by the broad band dielectric spectroscopy and fitted by both HN equation and Kramer-Kronig transform.

Analyzed Data Using Kramer-Kronig Transform

Dielectric loss spectra of polymers that incorporate intended or impurity charge carriers can show high dc conductivity at low f and high T which can obscure relaxation peaks[155-158] ε''_{kk} in equation 12 does not involve this contribution because it is derived from the real permittivity that does not involve dc conduction.[153,154] for these reason, more resolved relaxations might be appeared in ε''_{kk} vs. f plots.

It should be mentioned that the Kramers-Krönig transformation is model-independent, and, as such, is not linked to the dipole rotation mechanism as it is in the Debye model and its subsequent improvements and variations; in short, it does not require a molecular underpinning.[158]

Figure 33a shows the original losses vs. frequency data for $C_{60}(OH)_{29}$, at different temperatures, and the high values of ε'' at low frequency and high temperatures is a contribution of the dc conductivity. Thus, ε''_{kk} vs. f was calculated from experimental $\varepsilon'(\omega)$ data using K-K transform software to observe conductivity-free relaxations and the results are displayed in Figure 33b.

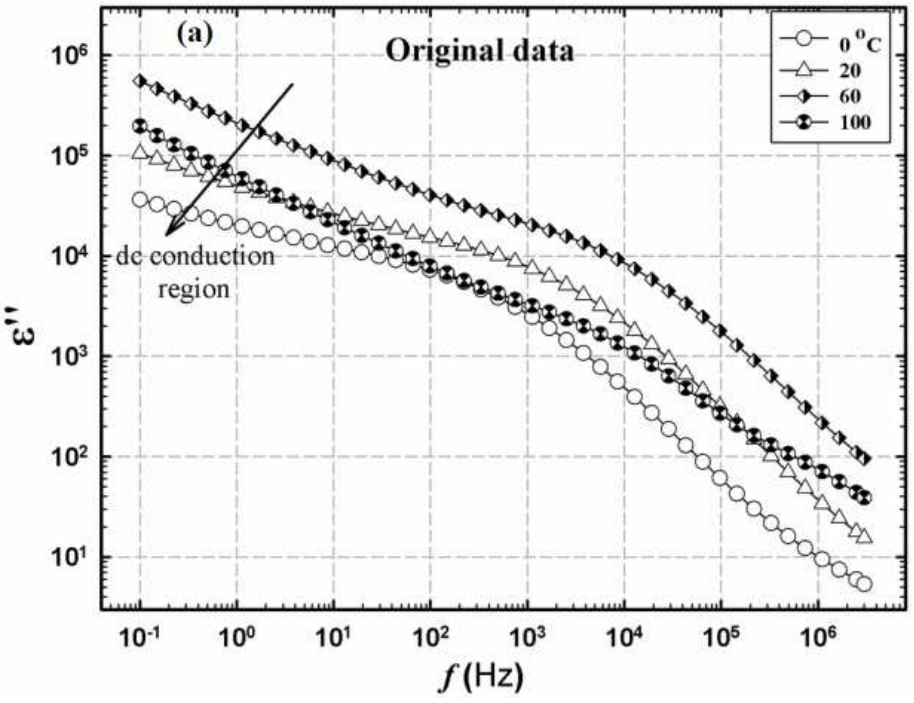

Figure 33a. Frequency dependence of ε″ of $C_{60}(OH)_{29}$ at different temperatures. The original data obtained from Novocontrol dielectric spectrometer.

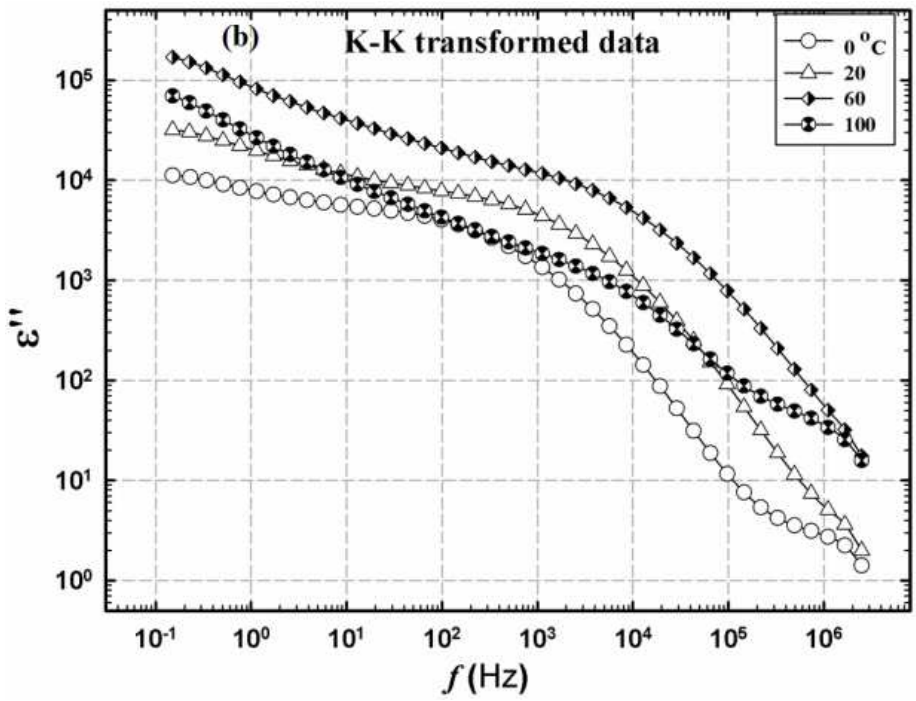

Figure 33b. Frequency dependence of ε″ of $C_{60}(OH)_{29}$ at different temperatures. The analyzed data, using the K-K transformation, based on data shown in Figure 33a.

In the same way, Figure 34a shows the frequency dependence of ε″ of $Sc_3N@C_{80}(OH)_{18}$ at different selected temperatures, and the fitted data, using the K-K transform, were shown in Figure 34b. Comparing the resolved and fitted data of these two hydroxylated fullerenes, it is noticed that subtracting the dc conductivity from the original data of $C_{60}(OH)_{29}$ does not affect the behavior of the loss vs. frequency spectra, especially at high temperatures. However, significant changes in the dc-conduction free losses for the hydroxylated $Sc_3N@C_{80}(OH)_{18}$ were observed.

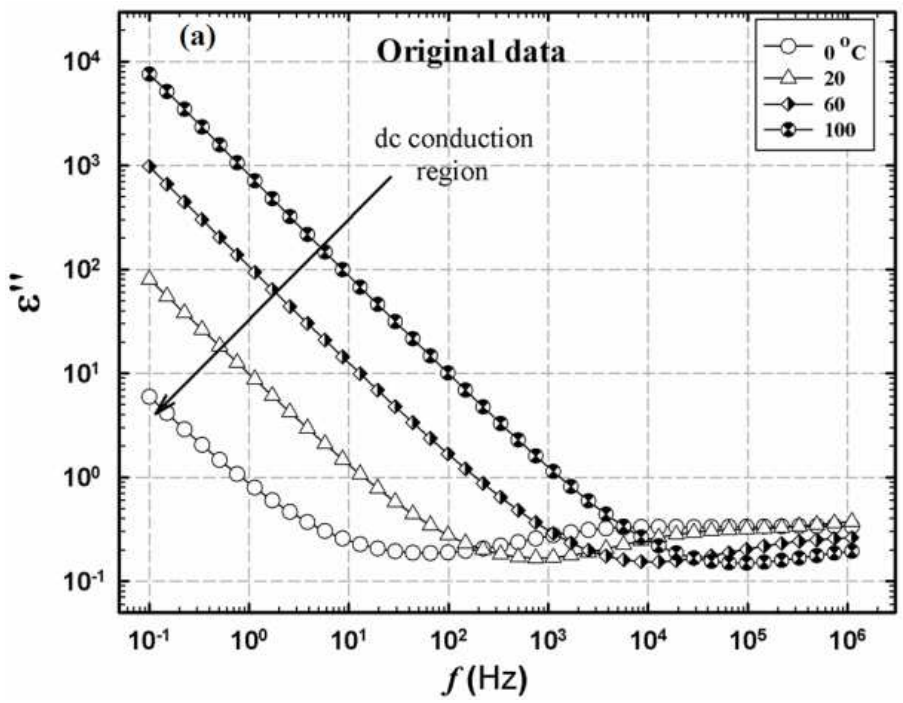

Figure 34a. Frequency dependence of ε″ for $Sc_3N@C_{80}(OH)_{18}$ at different temperatures. The original data obtained from Novocontrol dielectric spectrometer.

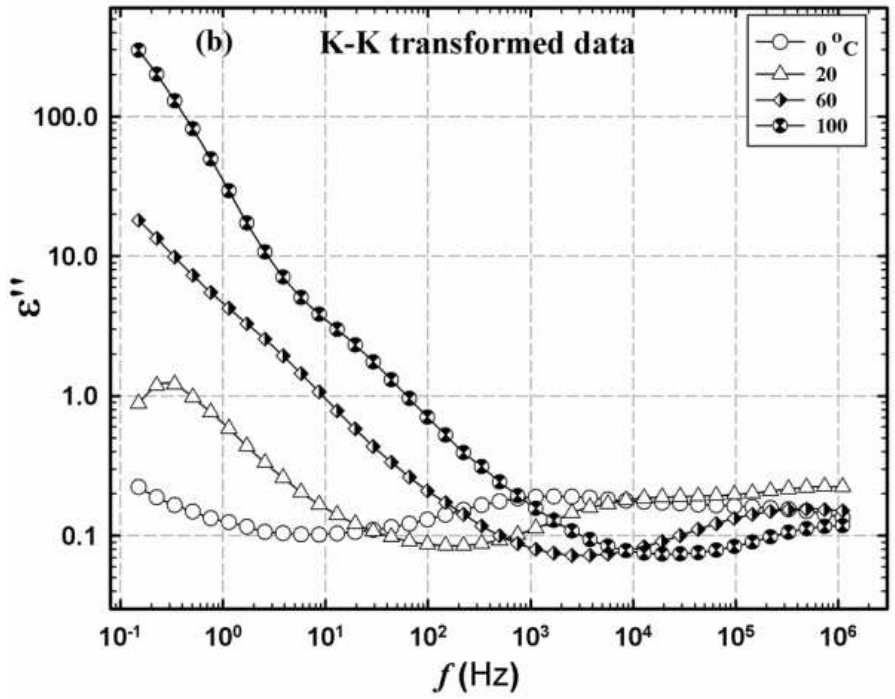

Figure 34b. Frequency dependence of ε″ for $Sc_3N@C_{80}(OH)_{18}$ at different temperatures. The analyzed data, using the K-K transformation, based on data shown in Figure 34a.

Figure 35 shows the analyzed data of $Sc_3N@C_{80}(OH)_{18}$ versus that of $C_{60}(OH)_{29}$ at one selected temperature, 20 ^oC, to see the effect of encapsulation of metal cluster, Sc_3N, on the behavior of the dielectric properties of these hydroxylated fullerenes after resolving their original loss data. The arrows pointed at the resolved loss maxima that were not shown clearly on the original data. The transition shown at high frequency might be due to certain molecular motions taken place in these samples. The peak shown in the low *f* is referred to sample-electrode interfacial polarization peak which is attributed to accumulation/dissipation of charge at the sample | electrode interface.[158-160]

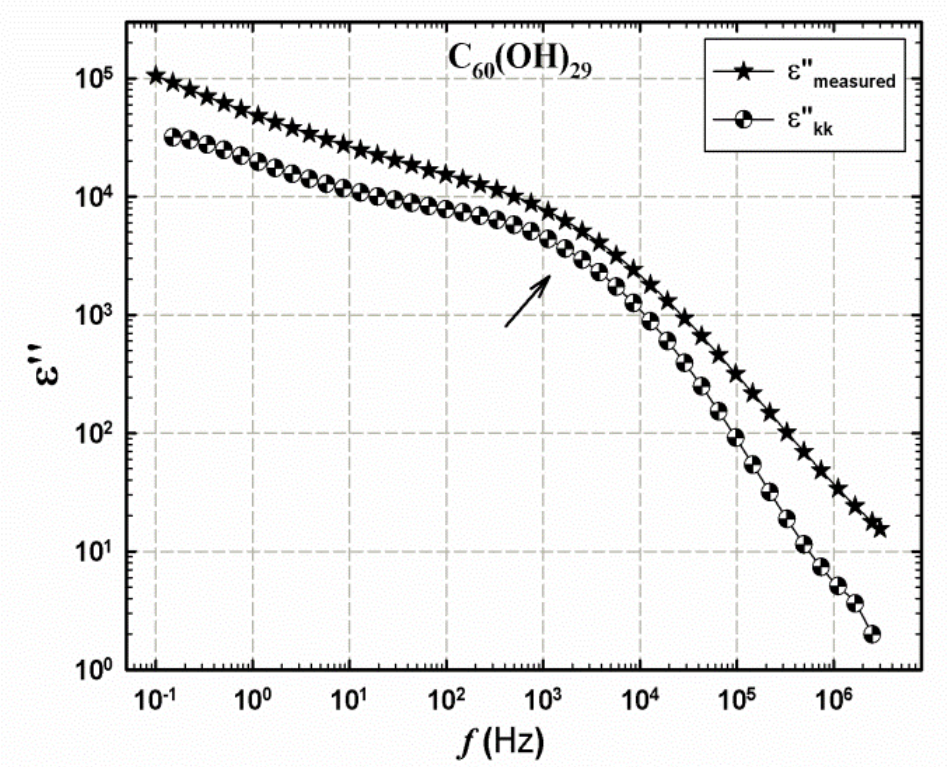

Figure 35a. Frequency dependence of measured and K-K transformed losses for hydroxylated C_{60} at 20 ^oC.

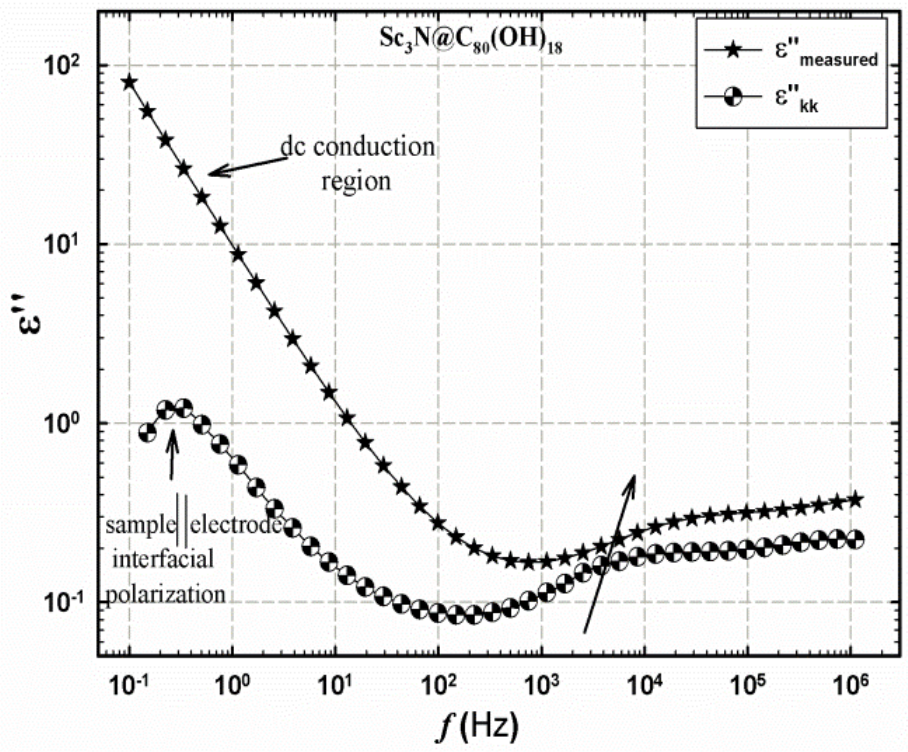

Figure 35b. Frequency dependence of measured and K-K transformed losses for hydroxylated C_{60} $Sc_3N@C_{80}$ at 20 ^oC.

In the same manner, Figure 36 shows the analyzed data of 3% $Sc_3N@C_{80}$-PU versus that of 3% C_{60}-PU networks at one selected temperature, 40 ^oC. As mentioned above, the first relaxation, at low frequency, is due to sample electrode polarization, however, the other relaxations appeared at high frequency might be due to certain transition or any segmental motions taken place in these networks. The resolved loss for $Sc_3N@C_{80}$-PU showed two more relaxations, other than the interfacial polarization, compared to one relaxation in case of C_{60}-PU, and this might be due to the orientation of the Sc_3N cluster inside the C_{80} fullerene cage.

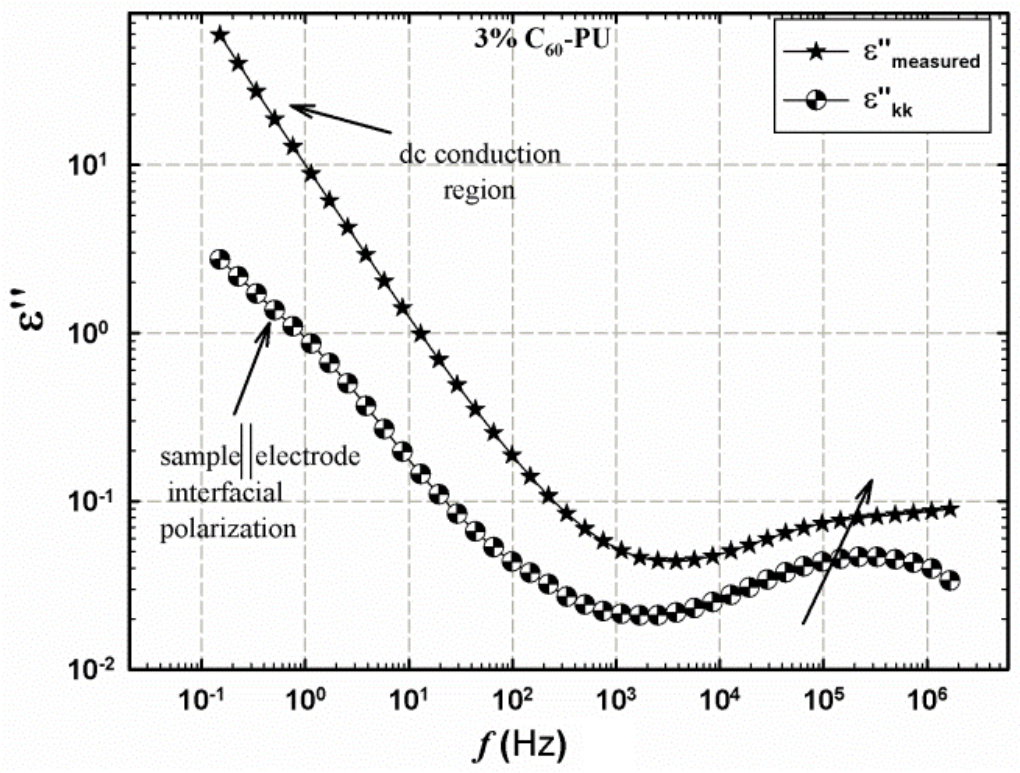

Figure 36a. ε″ vs. frequency (original and K-K transformed) for 3% C_{60}-PU at 40 ^{o}C.

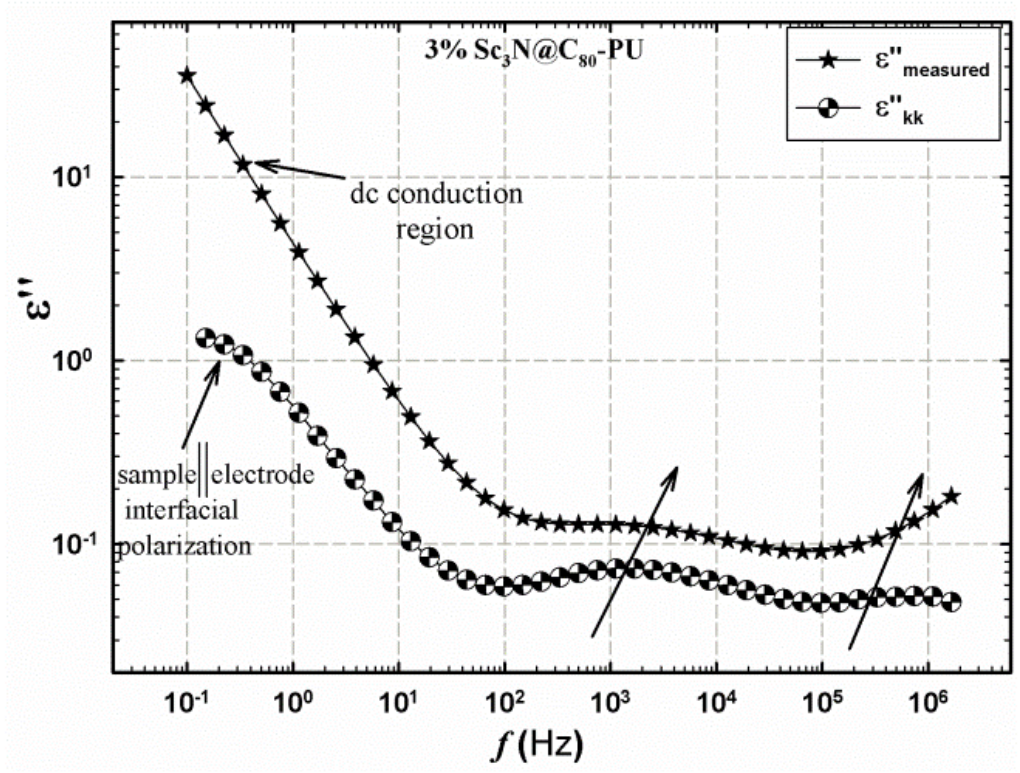

Figure 36. ε″ vs. frequency (original and K-K transformed) for 3% $Sc_3N@C_{80}$-PU at 40 ^{o}C.

More details about these proposed molecular motions and their activation energies were obtained by analyzing ε″ vs. frequency spectra for the same materials using the Novocontrol Winfit program, and the results will be discussed in the following section.

Analyzed Data Using HN Equation

For all samples presented here, the low *f* dc contribution from all ε″ vs. *f* spectra, and the Havriliak-Negami equation can be fitted to these data very well. From this fitting, and for any relaxation taken place in these samples, relaxation times (τ) were determined in the appropriate frequency regions at different temperatures.

For hydroxylated fullerenes, $C_{60}(OH)_{29}$ and $Sc_3N@C_{80}(OH)_{18}$, the dc conductivity free losses and their fitted data were plotted vs. frequency at 20 ^{o}C, and the plots were shown in Figure 37 (a and b). As seen in this figure, there are two resolved peaks for $C_{60}(OH)_{29}$ compared to three peaks for $Sc_3N@C_{80}(OH)_{18}$, and the additional peak appeared for the later material might be due to the presence of Sc_3N cluster inside C_{80} cage. Each peak represents a certain type of relaxation taken place in these samples.

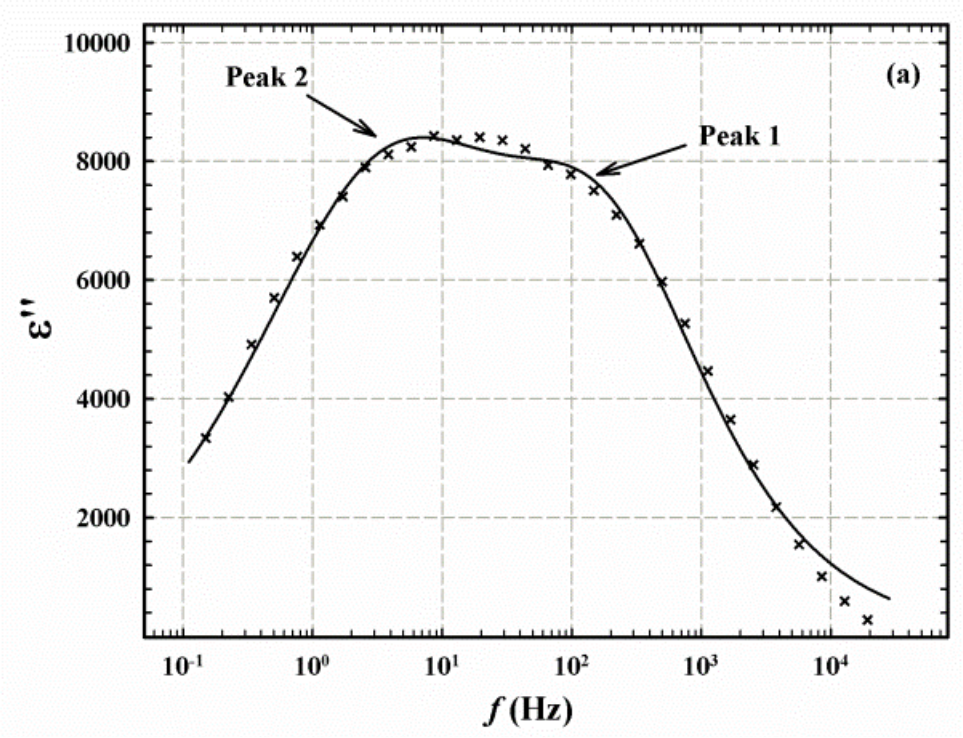

Figure 37a. ε″ vs. frequency at 20 °C for $C_{60}(OH)_{29}$. The scatters are the dc conductivity free data and the solid lines are the HN fitted data.

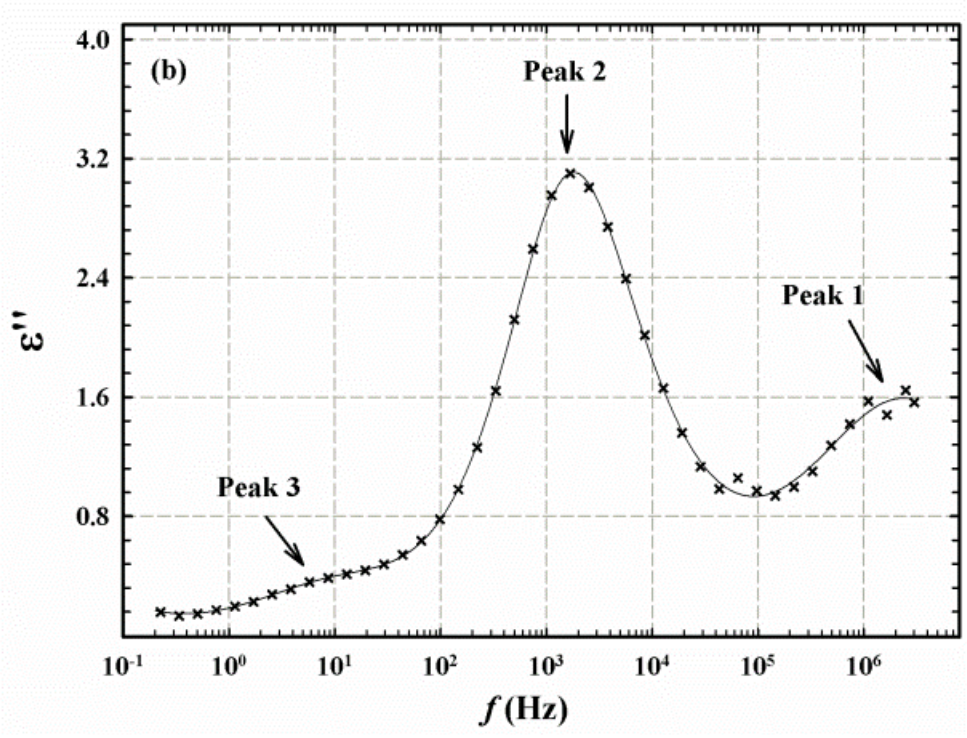

Figure 37b. ε″ vs. frequency at 20 °C for $Sc_3N@C_{80}(OH)_{18}$. The scatters are the dc conductivity free data and the solid lines are the HN fitted data.

Using the Novocontrol Winfit program, and by monitoring each peak from its beginning to its end, it was noticed that each peak started and ended within certain temperature range, thus, relaxation times at different temperatures were extracted from the fitted data of each peak. Plots of log τ_{max} vs. 1000/T, shown in Figure 38, were linear, and the activation energies, E_a, were derived from the slopes of the fitted lines of these plots according to Arrhenius equation as follow:

$$\tau_{max} = \tau_0 e^{(\frac{E}{RT})} \tag{13}$$

$$\log \tau_{max} = \log \tau_0 + \frac{E}{2.303\, RT} \tag{14}$$

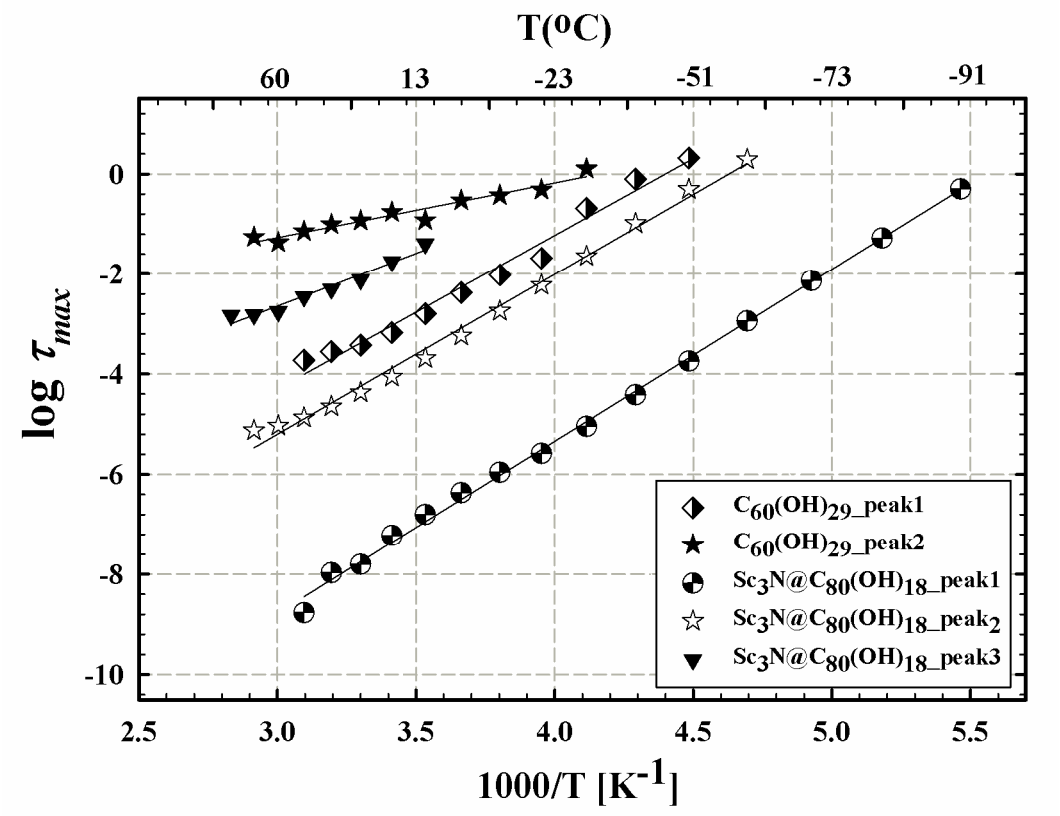

Figure 38. Relaxation time, log τ_{max}, vs. 1000/K for different relaxations taken place in $C_{60}(OH)_{29}$, and $Sc_3N@C_{80}(OH)_{18}$. The scatters are the calculated values, and the solid lines are the fitted lines.

The values of activation energies for all relaxations taken place in hydroxylated samples were recorded in Table 6. The higher E_a values for these relaxations, 58.8 KJ/mol and 61.0KJ/mol might be for the motion of the fullerene cages, C_{60} and C_{80}, respectively, however, the additional Ea value, 65.8 KJ/mol, for $Sc_3N@C_{80}(OH)_{18}$ might be for the rotation of the tri metallic cluster, Sc_3N, inside C_{80} cage. The smaller Ea values, 20.8 KJ/mol and 40.4 KJ/mol, were predicted to be for the molecular motion of the hydroxyl groups attached to the fullerene cages of $C_{60}(OH)_{29}$ and $Sc_3N@C_{80}(OH)_{18}$, respectively. It was noticed that, despite these two E_a values were predicted to be for the motion of same molecule, OH, they are not close to each other, and this is due to the fact that these hydroxyl groups are subjected to different electronic environment, and consequently, they should have different activation energies.

Table 6

Activation Energies for all Peaks Observed for the Selected Sample

Peak / Sample	Activation energy Ea (KJ/mol)			
	$C_{60}(OH)_{29}$	$Sc_3N@C_{80}(OH)_{18}$	3% C_{60}-PU	3% $Sc_3N@C_{80}$-PU
Peak 1	58.8	65.7	37.3	31.4
Peak 2	20.8	61.0	49.5	96.9
Peak 3		40.4	80.5	60.8
Peak 4			38.3	56.1

In the same manner and for fullerene-PU samples, 3% C_{60}–PU and 3% $Sc_3N@C_{80}$–PU, the dc conduction free losses and their HN fitted data were plotted vs.

frequency at different temperatures, and the results were displayed in Figure 39. Multiple relaxations were clearly observed for both samples, and their signatures appeared as peaks in losses vs. frequency spectra. Relaxations appeared at low temperatures, as also seen in Figure 18, in Chapter 3, were predicted to be for any local motion such as the molecular motion of unreacted hydroxyl groups. However, relaxations appeared in a temperature range of -70 to -40 were predicted to be for the segmental motion of the polymeric chains in their glass transition state. Other relaxations appeared at higher temperatures might be for sub T_g or any other molecular motions taken place in these networks.

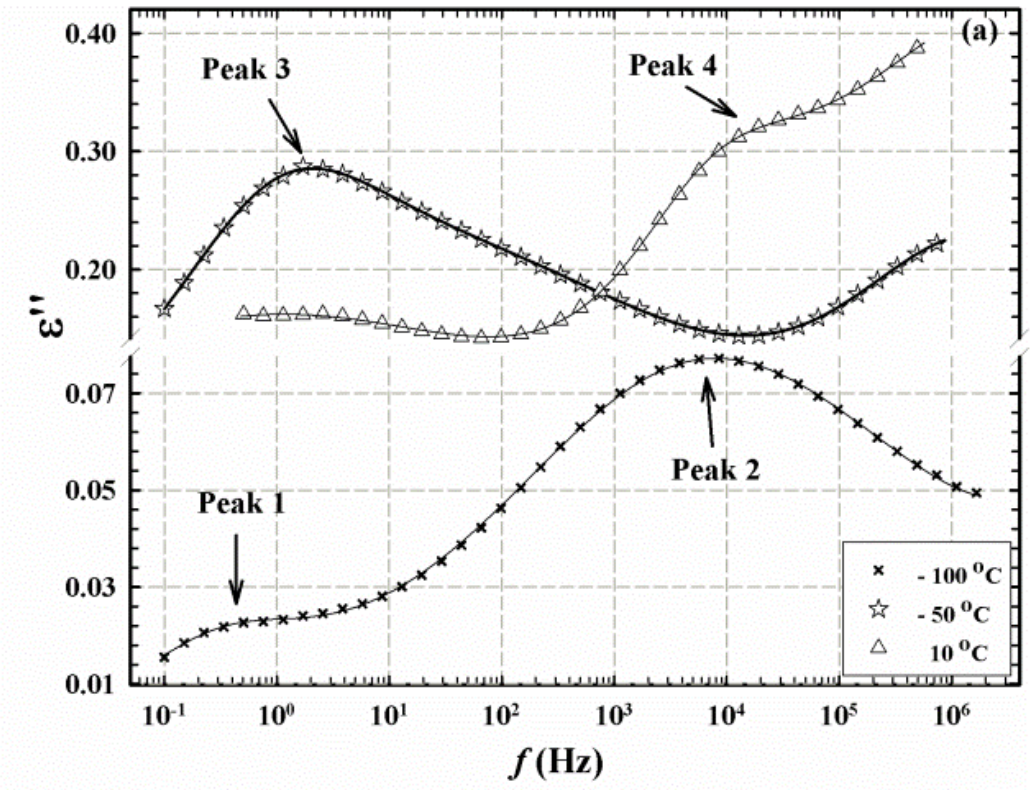

Figure 39a. ε″ vs. frequency at different temperatures for 3% C_{60}-PU. The scatters are the dc conductivity free data, and the solid lines are the HN fitted data.

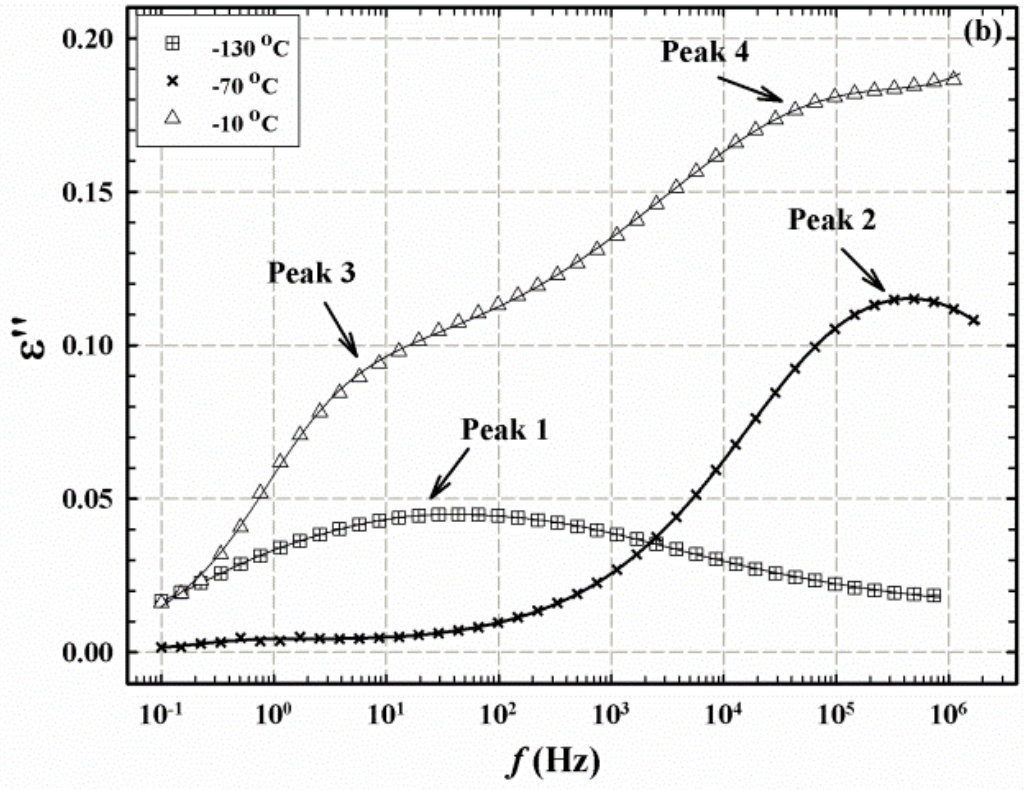

Figure 39a. ε″ vs. frequency at different temperatures for 3% $Sc_3N@C_{80}$-PU. The scatters are the dc conductivity free data, and the solid lines are the HN fitted data.

Relaxation times at different temperatures were determined from the HN fitted data of these fullerene-PU samples, and plots of log τ_{max} vs. the inverse of T were shown in Figure 39. From the slopes of the fitted lines of these plots, the activation energies were derived, and their values were recorded in Table 6.

The values of activation energies for peak 3 and peak 2 of C60-PU and Sc3@C80-PU, respectively, are close and they for the segmental motions in the glass transition regions. Other E_a values are predicted to be for any local motion taken place in these networks. Another technique such as solid state NMR should be used to characterize these samples to confirm the values of activation energy.

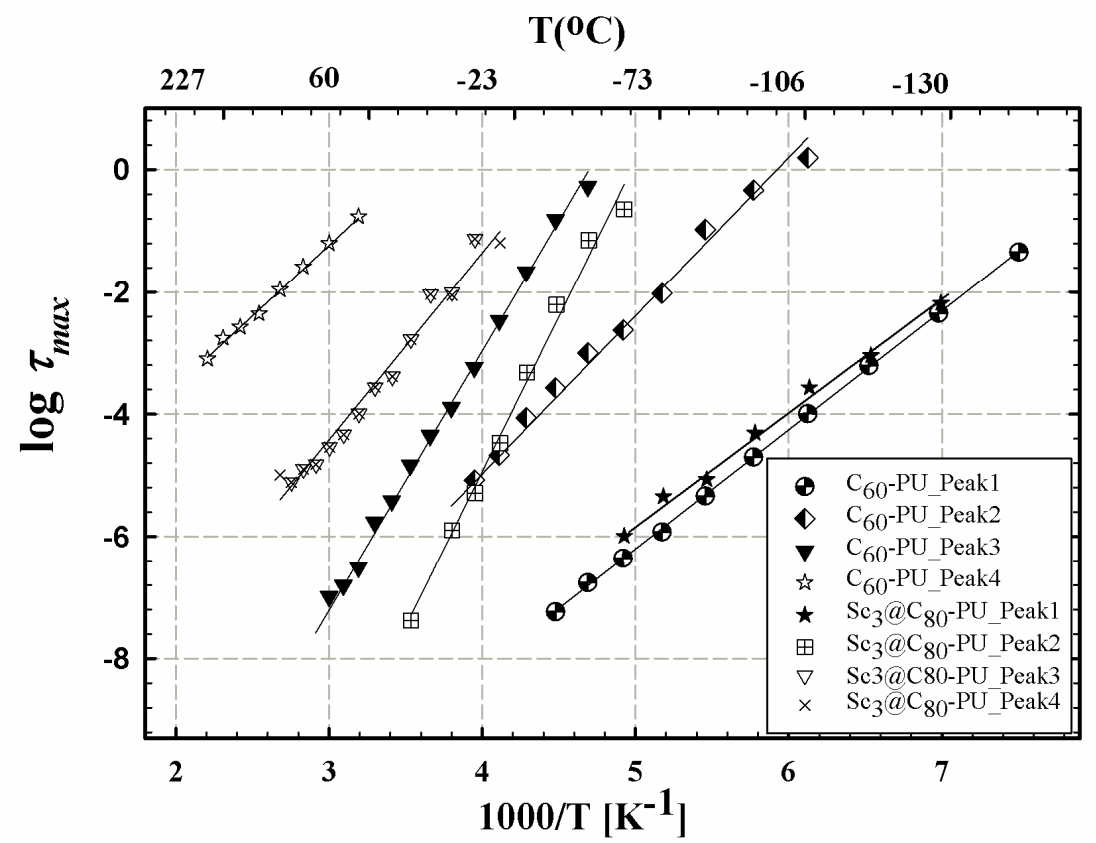

Figure 40. Relaxation time, log τ_{max}, vs. 1000/K for different relaxations taken place in 3% C_{60}-PU and 3% $Sc_3N@C_{80}$-PU networks. The scatters are the calculated values, and the solid lines are the fitted lines.

Summary

$C_{60}(OH)_{29}$ and $Sc_3N@C_{80}(OH)_{18}$ were synthesized via a modified method based on HSVM technique in a yield of 83% and 65%, respectively, and their approximate average number of hydroxyl groups attached to their cages was obtained using TGA and MALDI-MS. Hydroxylation of 5% $Sc_2LaN@C_{79}N$ extract was also achieved by the same method with a difficulty to approximate the number of hydroxyl groups attached to the $C_{79}N$ cage because the sample is not pure. Nanocomposites composed of polyurethane molecules end-linked by polyhydroxylated fullerenes (C_{60} and $Sc_3N@C_{80}$) were prepared via condensation reactions between the hydroxyl groups on the fullerene cages and the NCO groups on an end capped diisocyanate prepolymer. FT-IR spectra confirmed the

attachment of hydroxyl groups to the carbon cages of both C_{60} and $Sc_3N@C_{80}$. The gel fractions of the fullerene-PU networks are high, ranging from 72-97% depending on percent fullerenol added. TGA indicated high thermal stability of these networks up to 300 °C .

Dynamic mechanical analyses of (C_{60} or $Sc_3N@C_{80}$)-PU networks indicate a glassy material at low temperatures and rubbery material at high temperatures with T_g around -50 °C. There is a relaxation in the glassy state in the temperature range of -150 to -110 °C for all samples that is assigned to local motions along the PU chains that are not influenced by crosslinks or by insertion of Sc_3N molecules in the fullerene cages. Above the glass transition is a high temperature feature due to the thermally-driven reactions between residual OH groups on the C_{60} cages and PU end groups.

Dielectric spectroscopic examination of separate non-PU-attached particles revealed large ε' values of hydroxylated, relative to unhydroxylated, fullerenes, attributed to polar OH groups on cage surfaces in the former. In all cases there is one dielectric relaxation but there are two relaxations for hydroxylated $Sc_3N@C_{80}$ and Sc2LaN@C_{79}N which are suggested to be due to (1) reorientation of hydroxylated cages and (2) reorientations of the encapsulated cluster.

Values of ε' for $Sc_3N@C_{80}$-PU are higher than those for C_{60}-PU more likely because of the extra feature of rotationally mobile Sc_3N dipoles inside hydroxylated C_{60} cages. For $T < 0$ °C three relaxations are seen at approximately the same temperatures for all samples. One peak corresponds to the glass transition and another, at lower temperature is due to short range chain motions in the glassy state, in harmony with the DMA results. A weak feature at ~25 °C was associated with thermally-driven reactions

between un-reacted hydroxyl groups on $C_{60}(OH)_{29}$ nanoparticles and polymer end groups; these post-reactions must be considered when processing these nanocomposite materials. For $T < T_g$, the ε'' curves for $Sc_3N@C_{80}$-PU lie above those for C_{60}-PU. Perhaps this is due to the fact that, while the mobility of dielectrically active –OH groups is suppressed in the glassy state in which there is frozen segmental mobility, the cage-contained Sc_3N molecules continue to undergo a more facile reorientation process. To be sure, this hypothesis needs to be confirmed using another technique.

To obtain parameters that quantify the nature of relaxations taken place in our prepared samples (hydroxylated fullerenes and fullerene-Pus networks), curve fitting to dielectric permittivity data was performed using the Novocontrol Winfit program (by which the HN was best-fitted to the loss (ε'' vs. f) spectra) and K-K transformation (by which the Ohmic conduction loss-free data were obtained). More significant changes in the dc-conduction free losses for the hydroxylated $Sc_3N@C_{80}$ were observed compared to those for $C_{60}(OH)_{29}$, especially at high temperatures. The resolved losses for $Sc_3N@C_{80}(OH)_{18}$ and $Sc_3N@C_{80}$-PU showed one additional relaxation compared to one relaxation in case of C_{60}-PU, and this might be due to the orientation of the Sc_3N cluster inside the C_{80} fullerene cage. The activation energies for all proposed relaxations taken place in these samples were calculated from plotting relaxation time vs. inverse of absolute temperature. The numerical values for the calculated activation energy suggest that there are two different motions in the fullerene-PU networks; one local and the other is for the polymeric chains.

Surface and bulk resistivities of fullerene-PU networks were measured at different humidities, and their values increase with increasing the humidity due to the effect of

water conductivity. Capacitance as a function of the applied dc bias voltage was measured for these samples and the data obtained did not show a significant change in capacitance with the applied voltage in the range of our instrument (-30 to +30 volts). A general conclusion is that this class of materials can be rendered quite polarizable, and their higher ε' values over their ε'' revealed that they might be utilized as super capacitors in energy storage systems.

REFERENCES

1) Kroto, H. W.; Health, J. R.; O'Brien, S. C.; Curl, R. F.; Smalley, R. E. *Nature* **1985**, *318*, 162.
2) Krätschmera, W.; Fostiropoulosa, K.; Huffman, D. R. *Chem. Phys. Lett.* **1990**, *170*, 167.
3) Kroto, H. W. Nature **1987**, *329*, 529.
4) Schmalz, T. G.; Seitz, W. A.; Klein, D. J.; Hite, G. E. *J. Am. Chem. Soc.* **1988**, *110*, 1113.
5) Fagan, P. J.; Calabrese, J. C.; Malone, B. J. Am. Chem. Soc. **1991**, *113*, 9408.
6) Olah, G. A.; Bucsi, I. Lambert, C.; Aniszfeld, R.; Trivedi, N. J.; Sensharma, D. K., Prakash, G. K. S. *J. Am. Chem. Soc.* **1991**, *113*, 9385.
7) Wudl, F. *Acc. Chem. Res.* **1992**, *25*, 157.
8) Shinohara H. Rep. *Prog. Phys.* **2000**, *63*, 843.
9) Chai, Y.; Guo, T.; Jin, C.; Haufler, R. E.; Chibante, L. P.; Fure, J.; Wang, L.; Alford, J. M.; Smalley, R. E. *J. Phys. Chem.* **1991**, *95*, 7564.
10) Heath, J.; O'Brien, S. C.; Zhang, Q.; Liu, Y.; Curl, R. F.; Kroto, H. W.; Tittel, F. K.; Smalley, R. E. *J. Am. Chem. Soc.* **1985**, *107*, 7779.
11) Weiss, F. D.; Elkind, J. L.; O'Brien, S. C.; Curl, R. F.; Smalley, R. E. *J. Am. Chem. Soc.* **1988**, *110*, 4464.
12) Nagase, S.; Kobayashi, K.; Akasaka, T. *Fullerene: Chem. Phys. Technol.* **2000**, 293.
13) Shinohara, H. *Fullerene: Chem. Phys. Technol.* **2000**, 357.
14) Bethune, D. S.; Johnson, R. D.; Salem, J. R.; Vries, M. S.; Yannoni, C. S. *Nature* **1993**, *366*, 123.
15) Nagano, T.; Kuwahara, E.; Takayanagi, T.; Kubozono, Y.; Fujiwara, *A. Chem. Phys. Lett.* **2005**, *409*, 187.
16) Sun, D.; Huang, H.; Yang, S. *Chem. Mater.* **1999**, *11*, 1003.
17) Okumura, M.; Mikawa, M.; Yokawa, T.; Kanazawa, Y.; Kato, H.; Shinohara, H. *Acad. Radiol.* **2002**, *9*, S495.
18) Aime, S.; Fasno, M.; Terreno, E. *Chem. Soc. Rev.* **1998**, *27*, 19**.**
19) Wilson, L. J.; Cagle, D. W.; Thrash, T. P.; Kennel, S. J.; Mirzadeh, S. J.; Alford, M.; Ehrhardt, G. J. *Coord. Chem. Rev.* **1999**, *192*, 199.
20) Mikawa, M.; Kato, H.; Okumura, M.; Narazaki, M.; Kanazawa, Y.; Miwa, N.; Shinohara, H. *Bioconjug. Chem.* **2001**, *12*, 510.
21) Suzuki, T.; Maruyama, Y.; Kato, T.; Kikuchi, K.; Achiba, Y. *J. Am. Chem. Soc.* **1993**, *115*, 11006.
22) Yamamoto, K.; Funasaka, H.; Takahashi, T.; Akasaka, T. *J. Phys. Chem.* **1994**, *98*, 12831.
23) Akasaka, T.; Okubo, S.; Kondo, M.; Maeda, Y.; Wakahara, T.; Kato, T.; Suzuki, T.; Yamamoto, K.; Kobayashi, K.; Nagase, S. *Chem. Phys. Lett.* **2000**, *319*, 153.
24) Anderson, M.R.; Dorn, H. C.; Stevenson, S.A. *Carbon* **2000**, *38*, 1663.
25) Stevenson, S.; Rice, G.; Glass, T.; Harich, K.; Cromer, F.; Jordan, M. R.; Craft, J.; Hadju, E.; Bible, R.; Olmstead, M. M.; Maltra, K.; Fisher, A. J.; Balch, A. L.; Dorn, H. C. *Nature* **1999**, *401*, 55.

26) Stevenson, S.; Mackey, M. A.; Coumbe, C. E.; Phillips, J. P.; Elliott, B.; Echegoyen, L. *J. Am. Chem. Soc.*, **2007**, *129*, 6072.
27) Stevenson, S.; Harich, K.; Yu, H.; Stephen R. R.; Heaps, D.; Coumbe, C. E.; Phillips, J. P. *J. Am. Chem. Soc.* **2006**, *128*, 8829.
28) Wang, X.; Zuo, T. M.; Olmstead, M. M.; Duchamp, J. C.; Glass, T. E.; Cromer, F.; Balch, A. L.; Dorn, H. C. *J. Am. Chem. Soc.* **2006**, *128*, 8884.
29) Dunsch, L.; Krause, M.; Noack, J.; Georgi, P. *J. Phys.Chem. Solids* **2004**, *65*, 309.
30) Olmstead, M. M; Bettencounrt, D. A.; Duchamp, J. C.; Stevenson, S.; Dorn, H. C; Balch, A. L. J. Am. Chem. Soc. **2000**, *112*, 12220.
31) Stevenson, S.; fowler, P. W.; Heine, T.; Duchamp, J. C.; Rice, G.; Glass, T.; Harich, K.; Hajdu, E.; Bible, R.; Dorn, H. C. *Nature* **2000**, *408*, 427.
32) Olmstead, M. M; Bettencounrt, A.; Duchamp, J. C.; Stevenson, S.; Marciu, D.; Dorn, H. C; Balch, A.L. *Angew. Chem. Int. Ed.* **2001**, *40*, 1223.
33) Stevenson, S.; Philips, J. P.; Reid, J. E.; Olmstead, M. M.; Rath, S. P.; Balch, A. L. Chem. Commun. **2004**, 2814.
34) Yang, S. F.; Troyanov, S.; Popov, A.; Krause, M.; Dunsch, L. *J. Am. Chem. Soc.,* **2006**, *128*, 16733.
35) Krause, M.; Kuzmany H.; Georgi P.; Dunsch L.; Vietze K. Seifert G. *J. Chem. Phys.* **2001**, *115*, 6596.
36) Liu, S.; Sun, S. *J. Organomet. Chem.* **2000**, *599*, 74.
37) Dunsch, L.; Yang, S. *Electrochem. Soc. Interface* **2006**, *15*, 34.
38) Akasaka, T; Nagase S. *Endofullerene: a new family of carbon clusters;* Kluwer academic Publishers: Dordrecht, 2002.
39) Guha, S.; Nkamoto, K. *Coord. Chem. Rev.* **2005**, *249*, 1111.
40) Dunsch, L.; Yang, S. *Small* **2007**, *3*, 1298.
41) Kuran, P.; Krause, M.; Dunsch, L. *Chem. Phys. Lett.* **1998**, *292*, 580.
42) Wang, C. R.; Kai, T.; Tomiyama, T.; Yoshida, T.; Kobayashi, Y.; Takata, M.; Sakata, M.; Shinohara, H. *Nature* **2000**, *408*, 426.
43) Kashtanov, S; Rubio-Pons, O.; Luo, Y.; Ågren, H.; Stafström, S.; Csillag, S., *Chem. Phys. Lett.*, **2003**, *371*, 98.
44) Chaur, M. N.; Melin, F.; Ashby, J.; Elliott, B.; Kumbhar, A.; Rao, A. M.;
45) Echegoyen, L. *Chem. Eur. J.* **2008**, *14*, 8213.
46) Stevenson, S.; Ling, Y.; Coumbe, C. E.; Mackey, M. A.; Confait, B. S.; Phillips, J. P.; Dorn, H. C.; Zhang, Y. *J. Am. Chem. Soc.* **2009**, *131*, 17780.
47) Hou, J. Q.; Kang, H. S. *Chem. Phys.* **2007**, *334*, 29.
48) Zuo, T. M.; Xu, L. S.; Beavers, C. M.; Olmstead, M. M.; Fu, W. J.; Crawford, D.; Balch, A. L.; Dorn, H. C. *J. Am. Chem. Soc.* **2008**, *130*, 12992.
49) Stevenson, S.; Thompson, M. C.; Coumbe, H. L.; Mackey, M. A.; Coumbe, C. E.; Phillips, J. P. *J. Am. Chem. Soc.* **2007**, *129*, 16257.
50) Chaur, M. N.; Frederic, M.; Bevan, E.; Andreas, A. J; Kenneth., W.; Brian, H. C; Luis, E. *J. Am. Chem. Soc.* **2007**, *129*, 14826.
51) Chaur, M. N., Athans, A. J.; Echegoyen, L. *Tetrahedron* **2008**, *66*, 11387.
52) Fatouros, P. P.; Corwin, F. D.; Chen, Z.; Broaddus, W. C.; Tatum, J. L.; Kettenmann, B.; Ge, Z; Gibson, H. W; Russ, J. L.; Leonard, A. P.; Duchamp, J. C.; Dorn, H. C. *Radiology* **2006**, *240*, 756.

53) Zhang, J.; Fatouros, P. P.; Shu, C.; Reid, J.; Owens, L.S.; Cai, T.; Gibson, H. W.; Long, G. L.; Corwin, F. D.; Chen, Z.; Dorn, H. C., Bioconj. Chem. **2010**, 21, 610.
54) Xie, Q.; P erez-Cordero, E.; Echegoyen, L. *J. Am. Chem. Soc.* **1992**, *114*, 3978.
55) Wudl, F.; Hirsch, A,; Khemani, K.; Suzuki, T.; Allemand, P. M.; Koch, A.; Eckert, H.; Srdanov, G.; Webb, H. *ACS Symp. Ser.* **1992**, *481*, 161.
56) Elliott, B.; Yu, L.; Echegoyen, L. *J. Am. Chem. Soc.* **2005**, *127*, 10885.
57) Iiduka, Y.; Ikenaga, O.; Sakuraba, A.; Wakahara, T.; Tsuchiya, T.; Maeda, Y.; Nakahodo, T.; Akasaka, T.; Kako, M.; Mizorogi, N.; Nagase, S. *J. Am. Chem. Soc.* **2005**, *127*, 9956.
58) Iezzi, E. B.; Cromer, F.; Stevenson (Phillips), P.; Dorn, H. C. *Synth. Met.* **2002**, *128*, 289.
59) Cardona, C. M.; Kitaygorodskiy, A.; Echegoyen, L. *J. Am. Chem. Soc.* **2005**, *127*, 10448.
60) Echegoyen, L.; Chancellor, C. J.; Cardona, C. M.; Elliott, B.; Rivera, J.; Olmstead, M. M.; Balch, A. L. *Chem. Commun.* **2006**, 2653.
61) Cardona, C. M.; Kitaygorodskiy, A.; Ortiz, A.; Herranz, M. A.; Echegoyen, L. *J. Org. Chem.* **2005**, *70*, 5092.
62) Wakahara, T.; Iiduka, Y.; Ikenaga, O.; Nakahodo, T.; Sakuraba, A.; Tsuchiya, T.; Maeda, Y.; Kako, M.; Akasaka, T.; Yoza, K.; Horn, E.; Mizorogi, N.; Nagase, S. *J. Am. Chem. Soc.* **2006**, *128*, 9919.
63) Iezzi, E. B.; Duchamp, J. C.; Harich, K.; Glass, T. E.; Lee, H. M.; Olmstead, M. M.; Balch, A. L.; Dorn, H. C. *J. Am. Chem. Soc.* **2002**, *124*, 524.
64) Lee, H. M.; Olmstead, M. M.; Iezzi, E.; Duchamp, J. C.; Dorn, H. C.; Balch, A. L. *J. Am. Chem. Soc.* **2002**, *124*, 3494.
65) Stevenson, S.; Stephen, R. R.; Amos, T. M.; Cadorette, V. R.; Reid, J. E.; Phillips, J. P. *J. Am. Chem. Soc.* **2005**, *127*, 12776.
66) Cardona, C. M.; Elliott, B.; Echegoyen, L. *J. Am. Chem. Soc.* **2006**, *128*, 6480.
67) Zhang, S. R.; Sun, D. Y.; Li, X. Y.; Pei, F. K.; Liu, S. Y. *Full. Sci. Techol.* **1997**, *5*, 1635.
68) Sun, D. Y.; Liu, Z. Y.; Guo, X. H.; Liu, S. Y. *Chin. Univ. Chem. Res.* **1996**, *1*, 23.
69) Li, J.; Takeuchi, A.; Ozawa, M.; Li, X.; Saigo, K.; Kitazawa, K. *J. Chem. Soc. Chem. Commun.* **1993**, 1784.
70) Cagle, D. W.; Thrash, T. P.; Alford, M.; Chibante, L. P. F.; Ehrhardt, G. J. & Wilson, L. J. *J. Am. Chem. Soc.* **1996**, *118,* 8043.
71) Thrash, T. P., Cagle, D. W., Alford, J. M., Ehrhardt, G. J., Wright, K.; Mirzadeh, S.; Wilson, L. J. *Chem. Phys. Lett.* **1999**, *308*, 329.
72) Cagle, D. W.; Kennel, S. J.; Mirzadeh, S.; Alford, J.M.; Wilson, L. J. *Proc. Natl. Acad. Sci.* **1999**, *96*, 5182.
73) Chiang, L. Y.; Upasani, R. B.; Swirczewski, J. W.; Soled, S. *J. Am. Chem. Soc.* **1993**, *115*, 5453.
74) Kato, H.; Suenaga, K.; Mikawa, M.; Okumura, M.; Miwa. N.; Yashiro, A.; Fujimura, H.; Mizuno, A.; Nishihiro, Y.; Kobayashi, K.; Shinohara, H., *Chem. Phys. Lett.* **2000**, *324*, 255.
75) Mikawa, M.; Kato, H.; Okumura, M; Narazaki, M.; Kanazawa, Y.; Miwa, N.; Shinohara, H. *Bioconjug. Chem.* **2001**, *12*, 510.

76) Kato, H.; Kanazawa, Y.; Okumura, M.; Taninaka, A.; Yokawa, T.; Shinohara, H. *J. Am. Chem. Soc.* **2003**, *125*, 4391.
77) Koltover, V. K. *J. Molecu. Liq.* **2006**, *127*, 139
78) Chen, C.; Xing, G.; Wang, J.; Zhao, Y.; Li, B.; Tang, J.; Jia, G.; Wang, T.; Sun, J.; Xing, L.; Yuan, H.; Gao, X.; Meng, H.; Chen, Z.; Zhao, F.; Chai, Z.; Fang, X. *Nano Lett.* **2005**, *5*, 10.
79) Zhang, P.; Pan, H.; Liu, D.; Guo, Z. X.; Zhang, F.; Zhu, D. *Synth. Commun.* **2003**, *33*, 2469.
80) Wang, X. *Thesis*; Virginia Polytechnic Institute and State University: Blacksburg, 2006, 41.
81) Wang, G. W. *Encyclopedia of Nanoscience and Nanotechnology* **2003**, *3*, 557.
82) Terekhov, I.; Terekhov, A. A. *Ross. Khim. Zh.* **2006**, *50*, 114.
83) Chiang, Y.; Wang, L. Y. *Trends Polym. Sci.* **1996**, *4*, 298.
84) Giacalone, F.; Martin, N. *Chem. Rev.* **2006**, *106*, 5136.
85) Badamshina, E. R.; Gafurova, M. P. *Polym. Sci. Ser. B* **2007**, *49*, 182.
86) Wang, C.; Guo, Z. X.; Fu, S.; Wu, W.; Zhu, D. *Prog. Polym. Sci.* **2004**, *29*, 1079.
87) Lavrenko, P. N.; Evlampieva, N. P.; Leshner, M. D. *Polym. Sci. Ser. A* **2004**, *46*, 1072.
88) Hawker, C. J. *Macromolecules* **1994**, *27*, 4836.
89) Li, F.; Li, Y.; Guo, Z.; Mo, L.; Fan, L.; Bai, F.; Zhu, D. *Solid State Commun.* **1998**, *107*, 189.
90) Pasimeni, L.; Franco, L.; Ruzzi, M.; Mucci, A.; Schenetti, L.; Luo, C.; Guldi, D. M.; Kordatos, K.; Prato, M. *J. Mater. Chem.* 2001, *11*, 981.
91) Lu, Z.; He, C.; Chung, T.S. *Polymer* **2001**, *42*, 5233.
92) Ouyang, J. Y.; Goh, S.H.; Li, Y. *Chem. Phys. Letts.* **2001**, *347*, 344.
93) Ouyang, J.Y.; Goh, S.H. Fullerenes, *Nanotubes Carbon Nanostruct.* **2002**, *10* 183.
94) Chiang, L. Y.; Wang, L. Y.; Kuo, C.S. *Macromolecules* **1995**, *28*, 7574.
95) Chiang, L. Y.; Wang, L. Y.; Tseng, S.M.; Wu, J. S. *J. Chem. Soc. Chem. Commun.* **1994**, 2675.
96) Kyokane, J.; Ishimoto, H.; Yugen, H.; Hirai, T.; Ueda, T.; Yoshino, K. *Synth. Met.* **1999**, *103*, 2366.
97) Bayer, O. *Polyurethanes Modern Plastics* **1947**, *24*, 149.
98) Marchant, R.E., Biodegradability of biomedical polymers. In *Polymer Degradation;* Hamid, S. H., Amin, M. B., Maadhah, A. G.; Marcel Dekker, Inc.: New York, 1992, 617.
99) Saunders, J. H., Frisch, K.C., *Polyurethanes: Chemistry and Technology, Part II: Technology;* Interscience Publishers: New York, 1964.
100) Dombrow, B. A., *Polyurethanes*; Reinhold Publishing Corporation: New York, 1957.
101) Howard, G. T. *International Biodeterioration & Biodegradation* **2002**, *49*, 245.
102) Kaplan, A. M., Darby, R.T., Greenberger, M., Rodgers, M.R. Microbial deterioration of polyurethane systems. In *Developments in Industrial Microbiology*, **1968**, *82*, 362.
103) Urbanski, J., Czerwinski, W., Janicka, K., Majewska, F., Zowall, H. *Analysis of Synthetic Polymers and Plastics*; Ellis Horwood Limited, Chichester: UK, ***1977***.

104) Fried, J.R. *Polymer Science and Technology;* Prentice-Hall, PTR: Englewood CliHs: NJ, 1995.
105) Oertel, G. *Polyurethane: Chemistry –Raw materials –Processing –Application – Properties*, 2nd ed.; Carl Hanser Verlag: Munich, 1993.
106) Karas, S. K.; Hillenkamp, M. F., Anal. Chem., **1985**, *57* (14), 2935.
107) Wang, S.; He, P.; Zhang, J.; Hiang, H. *Synth. Commun,* **2005**, *35*, 1803.
108) Yannoni, C.S.; Hoinkis, M.; Vries, M. S.; Bethune, D.S.; Salem, J. R.; Crowder, M.S.; Johnson, R.D. *Science* **1992**, *256*, 1191.
109) Sperling, L. H. *Introduction to Physical Polymer Science*, 4th ed.; Wiley Interscience: New Jersey, 2006.
110) Meyers, M. A.; Chawla K. K. *Mechanical Behavior of Materials*, Prentice-Hall., 1999.
111) Zhang, W.; Sprafke, J. K.; Ma, M.; Emily, Y. T.; Sydlik, S. A.; Rutledge, G. C.; Swager, T. M. *J. Am. Chem. Soc.*, **2009**, *131*, 8446.
112) Ouyang, J.; Zhou, S.; Goh, S. H. *Polymer*, **2006**, *47*, 6140.
113) Runt, J. P.; Fitzgerald, J. J. Dielectric spectroscopy of polymeric materials: fundamentals and applications; American Chemical Society: Washington, DC, 1997.
114) Kremer, F.; Schonhals, A.; Luck, W. *Broadband Dielectric Spectroscopy*; Springer: Heidelberg, Germany, 2003.
115) Sidorovich, A. M. *Ukrainian Physical Journal,* **1984**, *29*, 1175.
116) Hippel, A. R. Dielectrics and Waves; John Willey & Sons: New York, 1954.
117) Volkov, A. A.; Prokhorov, A. S. *Radiophysics and Quantum Electronics* **2003**, *46*, 657.
118) http://www.psrc.usm.edu/mauritz/dilect.html
119) Havriliak, S.; Negami, S. *J. Polym. Sci. Polym. Sympo.* **1966**, *14*, 99.
120) Bulusheva, L. G.; Okotrub, A. V. *Physics of the Solid State* **2006**, *48*, 185.
121) Heiney, A.; Fischer, J. E.; McGhie, A. R.; Romanow, W. J.; Denenstein, A. M.; McCauley, J. P.; Smith, A. B. *Phys. Rev. Lett.* **1991**, *66*, 2911.
122) Su, J. S.; Chen, Y. F. K.; Chiu, C. *Appl. phys. Lett.* **1999**, *74*, 439.
123) Su, J. S.; Chen, Y. F. K.; Chiu, C. *Appl. Phys. Lett.* **1999**, *75*, 1607.
124) Sundqvist, B.; Persson, N. *J. Phys. Condens. Matter.* **2002**, *14*, 10437.
125) Iwasa, Y.; Nuttall, C. *J. Synth. Met.* **2003**, *135–136*, 773.
126) Subocz J., Valozhyn, A.; Zenker, M. *Rev. Adv. Mater. Sci.* **2007**, *14*, 193.
127) Ouyang, J.; Zhou, S.; Wang, F.; Goh, S. H. *J. Phys. Chem. B* **2004**, *108*, 5937.
128) Sheppard, N. F. Jr., Senturia, S. D. *Adv. Polym. Sci.* **1986**, *80*, 1.
129) Smyth, C. P. *Dielectric Behavior and Structure;* McGraw Hill: New York, 1955, 53.
130) Akram, M.; Javed, A.; Rizvi, T. Z. *Turk. J. Phys.* **2005**, *29*, 355.
131) Kannurpatti, A. R.; Bowman, C. N. *Macromolecules* **1998**, *31*, 3311
132) Frohlick, H., *Theory of Dielectrics;* Oxford University press: Oxford, 1956, 13.
133) Ponomarenko, A. T; Schevchenko, V. G.; Enikolopyan, N. S. *Adv. in Polym. Sci.* **1990**, *96*, 125.
134) Crossman, R. A. *Polym. Eng. Sci.* **1985**, *25*, 507.
135) Brydson, *Plastic Materials*, 5th Ed.; Butterworth: Boston, 1990.
136) Keithley Catalog. *Volume and Surface Resistivity Measurements of Insulating Materials;* [Online]; Keithley Instruments, Inc. 2001.

137) ASTM Standard D 257-99. Standard test methods for D-C resistance or conductance of insulating materials, 1999.
138) Stauffer, L. *Fundamentals of Semiconductor C-V Measurements*, [Online]; Keithley Instruments, Inc., 2009.
139) Yuan, Y.; Reece, T. J.; Sharma, P.; Poddar, S.; Ducharme, S.; Gruverman, A.; Yang, Y.; Huang, J. *Nature Materials*, **2011**, *xx*, xx.
140) Yu, G., Gao, J., Hummelen, J. C., Wudl, F. & Heeger, A. *J. Polymer photovoltaic cells* **1995**, *270*, 1789.
141) Sariciftci, N. S., Smilowitz, L., Heeger, A. J. & Wudl, F. *Science* **1992**, *258*, 1474.
142) Kirchartz, T., Taretto, K. & Rau, U. *J. Phys. Chem. C* **2009**, *113*, 17958.
143) Belmonte, C. G.; Boix,P.P; Bisquert, J.; Lenes, M.; Bolink, H.J; Rosa, A.L; Filippone, S; Mart, N., J *Phys. Chem. Lett.* **2010**, *1,* 2566.
144) Siddabattuni, S.; Schuman, T. P.; Dogan, F. *Polymer Preprints*, 2011, *52*, 45.
145) Siddabattuni, S.; Schuman, T. P.; Dogan, F. *Polymer Preprints*, 2011, *52*, 92
146) Xiaojun, Y.; Zhimin, Y.; Changhui, M.; Jun, D. *Rare Metals* **2006**, *25*, 250.
147) Li, J. Y.; Zhang, L.; Ducharme, S. *Appl. Phys. Lett.* **2007**, *90*, 132901.
148) Doi, M; Edward, S. F. The theory of Polymer Dynamics; Oxford Univrrsity Pres: New York, **1986**.
149) Havriliak, S.; Negami, S. *Polym. J.* **1967**, *8*, 161.
150) Negami, S.; Ruch, R. J.; Myers, R. R. *J. Colloid Interface Sci.* **1982**, *90*, 117.
151) Diaz-Calleja, R. *Macromolecules* **2000**, *33*, 8924.
152) Zhang, S.; Painter, P. C.; Runt, J. P. *Macromolecules* **2004**, *37*, 2636.
153) Steeman, P. A.M,; Turnhout, J. V. *Colloid Polym. Sci.* **1997**, *275*, 106.
154) Wübbenhorst, M.; Turnhout, J. V. *J. Non-Cryst. Solids* **2002**, *305*, 40.
155) Tuncer, E.; Wegener, M.; Frübing, P.; Gerhard-Multhaupt, R. *J Chem Phys* **2005**, *122*, 4901.
156) Bielowka, S.H.; Psurek, T.; Ziolo, J.; Paluch, M. *Phys. Rev. E* **2001**, *63*, 62301.
157) Corezzi, S.; Capaccioli, S.; Gallone, G.; Lucchesi, M.; Rolla, P.A., *J. Phys. Condens. Matter.* **1999**, *11*, 10297.
158) Chen, H.; Hassan, M. K.; Peddini, S. K.; Mauritz, K. A. *Eur. Polym. J.* **2011**, *7,* 5.
159) Klein, R.J.; Zhang, S.; Dou, S.; Jones, B.H.; Colby, R.H.; Runt, J. *J. Chem. Phys.* **2006**, *124*, 144903.
160) Atorngitjawat, P.; Runt, J. *Macromolecules* **2007**, *40*, 991.